

Review

## Trapping (*capture*) into resonance and scattering on resonance: Summary of results for space plasma systems



A.V. Artemyev<sup>a,b</sup>, A.I. Neishtadt<sup>a,c</sup>, D.L. Vainchtein<sup>a,d,\*</sup>, A.A. Vasiliev<sup>a</sup>,  
I.Y. Vasko<sup>a,e</sup>, L.M. Zelenyi<sup>a,f</sup>

<sup>a</sup> Space Research Institute, Moscow, 117997, Russia

<sup>b</sup> Department of Earth, Planetary, and Space Sciences, University of California, Los Angeles, CA 90095, USA

<sup>c</sup> Department of Mathematical Sciences, Loughborough University, Loughborough LE11 3TU, United Kingdom

<sup>d</sup> Nyheim Plasma Institute, Drexel University, Camden, NJ 08103, USA

<sup>e</sup> Space Sciences Laboratory, University of California, Berkeley, CA 94720, USA

<sup>f</sup> Moscow Institute of Physics and Technology, Dolgoprudny, Moscow Region, 141700, Russia

---

### ARTICLE INFO

**Article history:**

Received 25 April 2017

Revised 19 April 2018

Accepted 8 May 2018

Available online 9 May 2018

---

**Keywords:**

Wave-particle resonant interaction

Charged particle acceleration and transport

Nonlinear waves

Adiabatic invariant

Probability of trapping

---

### ABSTRACT

In the present review we survey space plasma systems where the nonlinear resonant interaction between charged particles and electromagnetic waves plays an important role. We focus on particle acceleration by strong electromagnetic waves. We start with presenting a general description of nonlinear resonant interaction based on the theory of slow-fast Hamiltonian systems with resonances. Then we turn to several manifestations of the resonance effects in various space plasma systems. We describe a universal approach for evaluating main characteristics of the resonant particle dynamics: probability of trapping into resonance, energy change due to scattering and trapping. Then we demonstrate how effects of nonlinear resonant trapping and scattering can be combined in a generalized kinetic equation. We also discuss the stability of trapped motion and evolution of particle ensemble in systems with trapping. The main objective of this review is to provide a general approach for characterizing plasma systems with nonlinear resonant interactions.

© 2018 Elsevier B.V. All rights reserved.

---

## 1. Introduction

### 1.1. Collisionless plasma and electromagnetic waves

Plasma is a gas of ionized particles. In sufficiently dense plasma, particle collisions control the energy and momentum exchange between particles and transformation of energy from kinetic to thermal. A characteristic distance between two consecutive collisions, called mean free path, determines spatial scales of the energy dissipation, e.g. shock wave scales and boundary scale between two gas populations [e.g. 1]. In rarefied plasma the mean free path may be very large, even larger than the scale of the entire system. Such plasma systems are effectively collisionless, and in them other kinetic processes control the energy exchange and dissipation. Plasma particles, being charged and affected by electromagnetic fields, can interact with electromagnetic waves. Such waves, generated by one population of particles, can travel in space and interact with another, possible quite distant, particle population. This interaction effectively connects particles which never

---

\* Corresponding author.

E-mail addresses: [aartemyev@igpp.ucla.edu](mailto:aartemyev@igpp.ucla.edu) (A.V. Artemyev), [dlv36@drexel.edu](mailto:dlv36@drexel.edu) (D.L. Vainchtein).

physically collide with each other, and provides a collisionless momentum exchange. Therefore, wave-particle interaction is a crucial component of any detailed picture of energetic processes in collisionless plasma [e.g., 2,3].

Electromagnetic waves are periodic (or quasi-periodic) variations of electromagnetic field. For sufficiently smooth fields, change of phase  $\phi$  in time equals minus the wave frequency,  $\partial\phi/\partial t = -\omega$ , and the gradient equals the wavenumber vector,  $\nabla\phi = \mathbf{k}$ . There are two main regimes of the wave-particle interaction: nonresonant and resonant. If  $d\phi/dt = 0$  somewhere along a particle trajectory, the wave-particle interaction is resonant. This regime is especially important because the slowed phase represents stationary electromagnetic fields, which act on particles much more effectively than nonresonant fields fluctuating around zero. Systems with the resonant wave-particle interaction can be roughly further divided into two groups depending on character of this interaction.

### 1.2. Quasi-linear theory and nonlinear resonant interaction

In the first group are the systems where the wave-particle resonant interaction can be considered as a stochastic process. Such an interaction lasts a short time and its characteristics (e.g., particle shift in phase space due to the wave action) are randomly distributed in the phase space of the initial particle position and velocity. Due to the shortness of resonant interaction, the particle position change during a given interaction is usually small. This allows us to consider the wave-particle interaction in a framework of the perturbation theory. When averaged over unperturbed particle trajectory, oscillating wave field causes a random change of the particle characteristics. These changes have zero mean and their variance is responsible for the diffusion in the phase space. Weakness of wave-particle stochastic interaction and the random nature of this interaction provide a foundation for application of the classical Fokker–Plank equation for description of charged particle evolution [e.g., 4]. Different plasma systems provide different origins of stochasticization of charged particle motion, and thus require individual approaches for derivation of coefficients (diffusion coefficients) of the Fokker–Plank equation.

The stochasticity of charged particle resonance with an electromagnetic field is caused by a broadness of wave spectrum: the duration of the wave-particle resonant interaction is mediated by nonresonant waves with frequencies near the resonant one. This effect is a foundation for the quasi-linear theory of wave-particle resonant interaction [5–9]. However, even in systems with a narrow wave spectrum (or even with a single coherent wave), there may be an effective stochasticity. One the natural source of such a stochasticity is an inhomogeneity of the background magnetic field/plasma density, [see discussion in [10–12]] as gradients of system's characteristics destroy the long-term correlations between the wave and particles [see, e.g., example in 13,14]. Another source of particle stochasticity is an external nonresonant noise (random fluctuations of the background system parameters), which can also significantly limit the duration of the resonant wave-particle interaction [e.g., 15,16]. Finally, the internal instability of waves may also result in the wave spectrum spreading and resonance destruction [17,18]. All these processes justify the applicability of the Fokker–Plank equation (or the quasi-linear theory) for many, but not all, space plasma systems where the wave-particle interactions are crucial for energy transformation and dissipation [e.g., [19–21]]. The main property of this, first, group of systems is the weakness of wave-particle interaction allowing using unperturbed trajectories for calculation the cumulative wave effect on particles.

The second group consists of various systems where wave field is sufficiently strong to change particle dynamics and wave effect should be included for calculation of the resonant particle trajectories. Thus, the perturbation theory is no more applicable for investigation of the wave-particle resonant interaction, and this interaction is called *nonlinear*. In this interaction changes of the resonant particle characteristics due to interaction with waves may have finite (non-zero) mean. Therefore, the resonant wave-particle interaction in systems of the second group may be not diffusive. Such changes essentially depend on the initial particle positions in the phase space. As we usually do not have a detailed information about particle initial distributions with the infinite high accuracy, and thus cannot predict the effect of the nonlinear wave-particle interaction for each particle, we average this effect for large particle ensemble. Such averaging leads to a kinetic equation for particle distribution function, but this equation may differ from the diffusion Fokker–Plank equation because it takes into account significantly nondiffusive effects.

Acceleration/deceleration of particles is closely related to amplification/damping of waves due to the conservation of energy. In many systems the wave energy does not represent a significant energy storage and waves rather play a role of mediator of energy exchange between different particle populations [22,23]. Thus, an accurate modeling of wave evolution requires calculation of inputs of different particle populations [24–29]. Moreover, wave dynamics can be even more complex due to the contribution of trapped particles to the wave dispersion [e.g. 22]. A sufficiently large population of trapped particles may change wave frequency, making it dependent on wave amplitude [e.g., [29–33]]. Such a complicated dynamics of waves requires comprehensive models of wave generation/amplification, but simultaneously significantly simplifies the description of resonant acceleration/deceleration of small particle populations. Indeed, feedback of these acceleration/deceleration to waves can be omitted in the leading approximation, because waves do not provide their own energy to particle acceleration. Thus, consideration of the nonlinear charged particle resonances is often limited to the case of prescribed wave amplitudes and frequencies.

### 1.3. Nonlinear resonant interaction: Some examples

Let us start our discussion of nonlinear resonant interactions by introducing three examples that cover a wide range of the resonant effects in plasma systems.

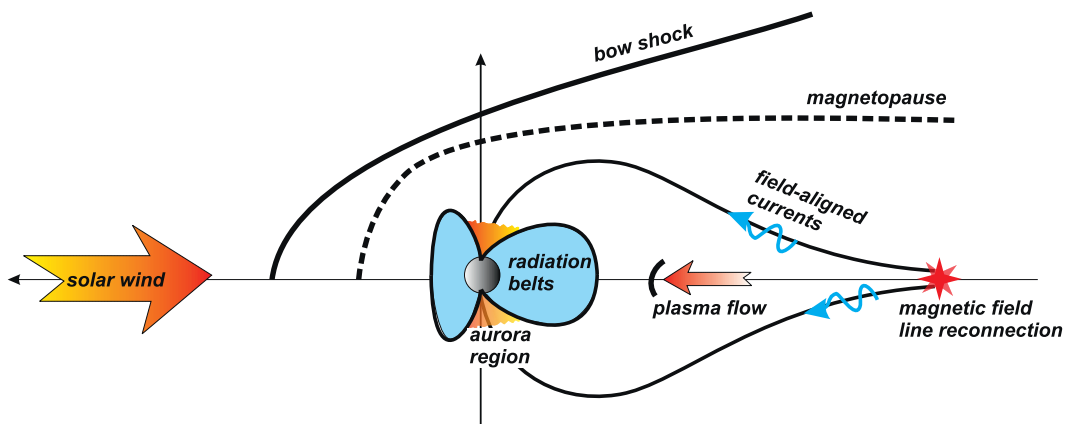


Fig. 1. Schematic view of the near-Earth plasma systems.

For the nonlinear resonant interaction to occur, the wave electromagnetic fields,  $\mathbf{B}_w$  and  $\mathbf{E}_w$ , should be sufficiently strong. Roughly speaking, the magnitude of the wave Lorentz force  $ec^{-1}\mathbf{v} \times \mathbf{B}_w + e\mathbf{E}_w$ , where  $\mathbf{v}$  and  $e$  are particle velocity and charge, and  $c$  the speed of light, should exceed the magnitude background field Lorentz force  $ec^{-1}\mathbf{v} \times \mathbf{B}_0$ . When the projection of the sum of these two forces on the direction of wave phase changing is zero, resonant particles can spend a long time in the resonance. This effect is called *particle trapping* or *capture into resonance*, and it is a unique feature of the nonlinear resonant interaction.

The simplest example of a nonlinear resonance is an electrostatic wave  $\mathbf{B}_w = 0$  propagating in the system without a background field:  $\mathbf{B}_0 = 0$ . In this case,  $\dot{\phi} = (\nabla\phi)\mathbf{v} - \omega = \mathbf{kv} - \omega$ . The corresponding resonant condition,  $\mathbf{kv} = \omega$ , is called the Cherenkov resonant condition: the projection of a particle velocity  $\mathbf{v}$  on the direction of the wavevector  $\mathbf{k}$  is equal to the wave phase velocity  $v_\phi = \omega/k$ . Particles trapped into the Cherenkov resonance propagate with the electrostatic waves [34,35]. If waves propagate in an inhomogeneous plasma, the wave dispersion relation and the conservation of wave frequency [see, e.g., 36] determine the evolution of  $v_\phi$  and thus the change of the particle velocity  $\mathbf{v} = (\mathbf{k}/k)v_\phi$ . This results in an acceleration/deceleration of trapped particles [37–40].

A weak background magnetic field  $\mathbf{B}_0$  alters the resonant interaction with electrostatic waves only if the wave propagates across the field; for field-aligned waves the resonant interaction is not disturbed by the background Lorenz force. For transversely propagating waves, trapping into the Cherenkov resonance requires  $\mathbf{E}_w > c^{-1}\mathbf{v} \times \mathbf{B}_0$  [41,42]. Trapped particles move with the wave while experiencing acceleration in the direction transverse to the background field and wave propagation direction: there is an effective force  $c^{-1}\mathbf{v}_\phi \times \mathbf{B}_0$  acting on particle. Such an acceleration is called the *surfatron* acceleration [43,44].

In systems with a strong background magnetic field, the particle Larmor rotation cannot be significantly disturbed by wave field, but the particle trapping is still possible. In these systems, the particle Larmor rotation has the frequency  $\Omega = e|\mathbf{B}_0|/mc$  where  $e$  and  $m$  are particle charge and mass, and the wave may be in resonance with *one of the harmonics*:  $\omega - k_{\parallel}v_{\parallel} = n\Omega$ . The subscript  $\parallel$  denotes the projection on direction of the background magnetic field:  $(v_{\parallel} = \mathbf{v} \cdot \mathbf{B}_0/|\mathbf{B}_0|)$ , and  $n = 0, \pm 1, \pm 2, \dots$  is an integer number. A particular case with  $n = 0$  is often called the Landau resonance. To trap particles into such a resonance, the wave field should be able to compensate the action of the force, called the mirror force and proportional to the gradient of  $\nabla_{\parallel}|\mathbf{B}_0|$ . Particles trapped into resonance move with the resonant velocity  $v_{\parallel} = (\omega - n\Omega)/k_{\parallel}$  and effectively accelerate in the inhomogeneous ( $\nabla_{\parallel}\mathbf{B}_0 \neq 0$ ) field [45–47].

#### 1.4. Space and laboratory plasma systems with resonant wave-particle interactions

Nonlinear wave-particle resonances play an important role in many near-Earth space plasma systems, schematically shown in Fig. 1. Early in-situ spacecraft observations demonstrated that beyond the ionosphere the near-Earth space was filled by plasma originating from the ionosphere (ionosphere outflow) and from the solar wind. The mean free path for such plasma exceeds the distance between Earth and Sun ( $> 10^8$  km), whereas spatial scales of many plasma systems discovered in near-Earth space do not approach  $10^2 - 10^4$  km. Thus, only the wave-particle interactions can control energy transformation and dissipation in these collisionless systems. Below we describe several examples of such space plasma systems and discuss the importance of wave-particle interaction.

The collisionless solar wind propagating from the Sun does not evolve as an expanding gas, but exhibits a complicated internal dynamics where strong Alfvén, magnetosonic, and electrostatic waves play a critical role in energy exchange between different particle populations [48]. The solar wind temperature decreases with the distance from the Sun significantly slower than it should according to the adiabatic theory of expanding gas. This slowing of cooling is believed to be caused by the interaction of charged particles with Alfvén and whistler wave turbulence dominating in the solar wind magnetic field

**Table 1**

Notation used in the paper.

Symbol	Description
$e$	charge of a particle
$m$	mass of a particle
$\mathbf{B}_0$	background magnetic field
$\Phi$	wave scalar potential amplitude
$\omega$	wave frequency; constant in all applications considered in this review
$\mathbf{k}, k =  \mathbf{k} $	wave number; may depend on spatial coordinates
$\varepsilon$	dimensionless wave amplitude; a small parameter in the systems under consideration
$\Omega, \Omega_0$	dimensionless and dimensional frequency of charged particle oscillations in the system with $\varepsilon = 0$
$\phi$	wave phase
$F(\phi)$	profile of a wave field; for most of applications $F = \sin \phi$
$u$	dimensionless function describing the distribution of wave field in space
$I$	momentum conjugate to $\phi$
$I_{\text{res}}$	$I$ evaluated at the resonance
$P_\phi$	$P_\phi = I - I_{\text{res}}$ ; momentum conjugate to $\phi$
$H$	Hamiltonian of the initial system
$\mathcal{F}$	Hamiltonian after the introduction of conjugate variables $(\phi, I)$
$H_\phi$	a part of Hamiltonian $\mathcal{F}$ describing particle motion in the $(\phi, P_\phi)$ plane
$I_\phi$	the area surrounded by closed particle trajectory in the $(\phi, P_\phi)$ plane (divided by $2\pi$ )
$S_{\text{res}}$	the area surrounded by the separatrix in the $(\phi, P_\phi)$ plane
$v_\phi, v_{\text{res}}$	$v_\phi = \omega/k$ is phase velocity of $\phi$ , and $v_{\text{res}}$ is a dimensionless $v_\phi$
$\Psi$	particle distribution function in the phase space

spectra [e.g., 49,50]. Waves can also be responsible for the formation and dynamics of fine structures. Multiple magnetic field discontinuities observed in the solar wind [e.g., 51–53, and references therein] are formed due to Alfvén waves nonlinear evolution driven by the Landau resonance with ions [e.g., 54,55]. Another example is the electron resonance with strong Langmuir (electrostatic) waves propagating through the inhomogeneous solar wind plasma [56,57]. This nonlinear interaction is responsible for wave evolution and electron acceleration [58,59].

Upon reaching the Earth bow shock, the solar wind transforms from a supersonic to subsonic flow. This transformation and corresponding plasma thermalization are accompanied by the formation of a broad spectrum of electromagnetic waves. Strong electrostatic waves at the bow shock [e.g., 60] trap electrons into the Landau resonance and can significantly change their distributions in the phase space. Electromagnetic whistler and ion cyclotron waves [61,62] trap electrons and ions into the cyclotron resonances [e.g., 63,64], and the corresponding particle acceleration can describe fluxes of high-energy particles observed at the bow shock [e.g., 65–67]. Moreover, the formation and evolution of the Earth bow shock is significantly affected by the nonlinear resonant interaction of ions with electromagnetic waves emitting by the shock [see, e.g., review 68, and references therein].

Shocked solar wind plasma fills the magnetosheath, which is the region between the bow shock and the magnetopause. Magnetopause is a thin boundary separating the solar wind from the magnetospheric plasma. One of the most important questions of the Earth magnetosphere physics is how the magnetosheath plasma penetrates across the magnetopause [see review 69]. In absence of particle collisions and/or magnetopause destruction, the only working mechanism of plasma transport to the magnetosphere is by the wave-particle resonant interaction [e.g., 70]. Abundance of cyclotron [e.g., 71,72] and Alfvén [e.g., 73] waves at the magnetopause supports the scenario of the resonant particle scattering and/or trapping causing the diffusion across the magnetopause [74,75].

Plasma may penetrate into the magnetosphere tail through the magnetopause. Penetrated plasma generates currents flowing in the magnetotail current sheet. Such currents are a significant free energy source, which makes the magnetotail plasma distribution highly unstable. The release of this energy is controlled by reconnections of magnetic field lines. This process transforms magnetic field energy into the charged particle acceleration and heating [e.g., 76–78] and generates various electromagnetic waves [79]. These waves transport some portion of released energy from the reconnection region into the inner magnetosphere [e.g., 80] and the aurora region [e.g., 81,82].

Energy and plasma transported into the inner magnetosphere from the magnetotail play a crucial role in plasma dynamics in the near-Earth environment. Hot ions injected into the inner magnetosphere form the ring current region and generate strong electric currents changing the near-Earth magnetic field [e.g., 20,83]. Ring currents are essentially controlled by the ion resonant trapping and scattering by electromagnetic ion cyclotron waves [e.g., 84, and references therein]. In contrast to ions, injected electrons do not contribute significantly to local electric currents, but generate strong electromagnetic (whistler) waves, that determine the dynamics of the radiation belts [85–87] and accelerate electrons to relativistic energies [22,88].

Released energy, transported into aurora region, fuels aurora electron acceleration and precipitation into the Earth ionosphere. In absence of collisions, this energy absorption is supported by the wave-particle interaction. Currents and magnetohydrodynamic waves, transporting energy to the aurora region, generate strong kinetic Alfvén waves carrying electric fields parallel to the background magnetic field [e.g., 75,89]. These waves resonate with cold electrons and trap them into the Landau resonance, which results in an effective electron acceleration [90–92].

Investigation of space plasma stimulated experimental laboratory simulations of wave generation and resonant charged particle dynamics, which contributed significantly to the understanding of the nonlinear wave-particle resonances. Unlike the spacecraft observations, in laboratory modelling the wave characteristics could be precisely controlled. Among important laboratory simulations are the investigations of the wave generation by plasma beam [e.g., 93,94], the nonlinear wave dynamics [e.g., 95], and energy exchange between particle populations through wave generation and absorption [e.g., 96].

Nonlinear wave-particle resonances observed in space plasma have direct analogies in many laboratory experiments. Strongly nonlinear electron acceleration by intense Langmuir waves in inertial confinement fusion experiments [97] can significantly influence plasma conditions [98]. Appearance of accelerated particle populations in the Free-Electron Laser experiments with Variable Parameter Wigglers [99,100] is described by essentially the same equations as trapping into the cyclotron resonance with electromagnetic waves. Generation or injection of strong waves into mirror machines result in a strong wave-particle interaction and excitation of sideband waves induced by particle trapping [e.g., 101,102]. Electron surface acceleration in the ultraintense laser pulse experiments represents a classical example of electron trapping into the Cherenkov resonance [103].

### 1.5. Review objective and structure

The nonlinear resonance interactions between particles and waves are well described for individual particle trajectories. Using the Hamiltonian mechanics for systems with resonances and introducing a hierarchy of time-scales of particle motion, one can describe particle trapping and scattering for many realistic plasma systems. However, the impact of individual resonant interactions on shaping of particle distribution function as a whole remains not understood. Beyond the diffusive approximation of a weak wave-particle interaction, there is no universal kinetic equation describing a cumulative effect of many nonlinear resonant interactions on the long-term evolution of particle distribution functions. To develop such a new kinetic approach, principal characteristics of the nonlinear resonance processes (the relative number of resonant particles trapped into resonance, average gain of energy in trapping, amplitude of the nonlinear scattering in velocity space) should be evaluated and combined into a generalized kinetic (Fokker-Plank) equation. The main objective of this review is to present a standardized algorithm realising this approach.

The review consists of ten sections. Past the Introduction, in the first part of the review (Sects. 2–5), we present a general theory of scattering on resonance and trapping into resonance (also called capture into resonance) in terms of the theory of adiabatic invariants [104]. We start with main equations and use simple models of physical systems to illustrate the separation of time scales and the introduction of resonance Hamiltonian (Section 2). Then we describe the details of trapping into resonance and illustrate the calculation of probability of trapping (Section 3). Section 4 describes the nonlinear scattering on resonance. Then we discuss effects of trapping and scattering on dynamics of a charged particle ensemble (Section 5), in particular, stochasticization of wave-particle resonances (Section 5.1), relations between trapping and scattering characteristics (Section 5.2), and pathways to a generalized kinetic equation (Section 5.3).

In the second part of the review (Sects. 6–7), we consider different concrete plasma systems where effects of trapping play an important role. These systems differ by the configuration of the background electromagnetic field and/or properties of the waves. Different configurations result in different types of resonances: the Cherenkov resonance for systems with a weak background magnetic field, the Landau resonance for particles interacting with electrostatic waves propagating along a strong background magnetic field, and the cyclotron resonance for particles interacting with electromagnetic waves propagating along a strong background magnetic field. We separate all systems into nonrelativistic and relativistic categories. The principal difference between these two groups is that the period of particle oscillations in a background magnetic field depends on particle energy in relativistic systems, whereas in nonrelativistic systems the period of particle gyrorotation does not depend on energy. Each subsection of (Sections 6–7) discusses one particular physical system. Our objective is to demonstrate that for different electromagnetic fields trapping can be described by the same universal approach described in (Sects. 3–5). In Section 8 we discuss the stability of the nonlinear wave-particle resonance relative to the external electromagnetic field fluctuations and the destruction of the nonlinear resonant interaction. Specifically, resonant sideband fluctuations can easily destroy the nonlinear resonances [17,18,155]. However, even the nonresonant fluctuation can cause particle detraping. In the last two section, we present open questions, discussion, and conclusions.

## 2. Main equations, averaging, and the derivation of the resonance Hamiltonian

Charged particle motion in electromagnetic fields is described by a 3D Hamiltonian possibly depending on time. However, the symmetry of magnetic field configuration can reduce the number of degrees of freedom. Almost all plasma systems considered in this review can be described by Hamiltonian systems with  $1\frac{1}{2}$  degrees of freedom (two conjugate variables  $(x, p_x)$  and time  $t$ ). In dimensionless units, the Hamiltonian of such a system can be written as

$$H = G(x, p_x) + \varepsilon u(x, p_x)F(\phi) \quad (1)$$

where  $G(x, p_x)$  is a Hamiltonian of an unperturbed motion,  $\varepsilon u(x, p_x)$  is an effective amplitude of perturbations ( $|\varepsilon| \ll 1$  and  $|u| \sim 1$  for all  $(x, p_x)$ ), and  $F(\phi)$  describes a profile of perturbation as a function of phase  $\phi$ :

$$\phi = \phi_0 + \int^x k(\tilde{x})d\tilde{x} - \omega t \quad (2)$$

with  $\phi_0$  being an initial phase. Frequency of phase  $\omega$ , and wave number  $k(\tilde{x})$  describe evolution of phase in space and time. Both  $\omega$  and  $k$  are assumed to be large enough (whereas their ratio is about 1) to provide a much faster rate of change of phase  $\phi$  compared with variations of variables  $(x, p_x)$ .

In what follows, all general equations are accompanied by examples obtained for three Hamiltonian systems. The first system describes a linear oscillator in the  $(x, p_x)$  plane (see [Section 6.1](#) with examples of the corresponding physical system):

$$H = \frac{1}{2}p_x^2 + \frac{1}{2}\Omega^2x^2 + \varepsilon u \sin \phi \quad (3)$$

with  $k = \text{const}$ ,  $u = 1$ , and  $\Omega$  is a dimensionless frequency of oscillations in the  $(x, p_x)$  plane.

The second system describes nonlinear oscillator with

$$H = \sqrt{1 + p_x^2 + \Omega^2x^2} + \varepsilon u \sin \phi \quad (4)$$

and  $k = \text{const}$ ,  $u = 1$  (see [Section 7.1](#) with examples of the corresponding physical system).

The third system describes a linear oscillator and perturbations with an inhomogeneous amplitude

$$H = \frac{1}{2}p_x^2 + \frac{1}{2}\Omega^2x^2 + \varepsilon x \sin \phi \quad (5)$$

with  $k = \text{const}$ ,  $u = x$  (see [Section 6.2](#) with examples of the corresponding physical system).

In system (1), the time dependence given by [Eq. \(2\)](#) can be conventionally changed to a new pair of conjugate variables. This change of variables can be performed in two steps. The first step consists of the introduction of a new coordinate  $\psi = \omega t$  and the conjugate momentum  $p_\psi$ . To keep the Hamiltonian form of equations, Hamiltonian (1) should be rewritten as:

$$H_\psi = G(x, p_x) + \varepsilon u(x, p_x)F(\phi) + \omega p_\psi, \quad \phi = \phi_0 + \int^x k(\tilde{x})d\tilde{x} - \psi \quad (6)$$

This transformation is not canonical because number of variables increased: instead of  $1\frac{1}{2}$  degrees of freedom in system (1) we obtained system (6) with 2 degrees of freedom. However, the Hamiltonian equations coincide for both systems. Further in the text, we will skip this step and start with the second step that corresponds to introduction of new variables  $(X, P_x)$ ,  $(\phi, I)$  with the generation function

$$R = I \left( \phi_0 + \int^x k(\tilde{x})d\tilde{x} - \psi \right) + P_x x \quad (7)$$

[Eq. \(7\)](#) gives the following relations between the new and old variables:

$$p_\psi = \frac{\partial R}{\partial \psi} = -I, \quad p_x = \frac{\partial R}{\partial x} = P_x + Ik, \quad X = x \quad (8)$$

The new Hamiltonian takes the form:

$$\mathcal{F} = -\omega I + G(x, P_x + Ik) + \varepsilon u(x, P_x + Ik)F(\phi) \quad (9)$$

where  $k = k(x)$  and we kept the notation  $x$  for  $X$ . Hamiltonian (9) does not depend on time and thus the energy  $h = \mathcal{F}$  is conserved. In terms of Hamiltonian mechanics,  $I$  is a momentum in Hamiltonian (9). Comparing [Eq. \(9\)](#) and [Eq. \(1\)](#), and taking into account the conservation of  $h$ , a change of energy  $H$  in unperturbed system (with  $F = 0$ ) equals to change of  $\omega I$ . In other words, the changes of energy  $H$  of the initial system follow the changes in  $\omega I$ .

Hamiltonian equations for Hamiltonian (9) can be written as:

$$\begin{aligned} \dot{x} &= \frac{\partial \mathcal{F}}{\partial P_x} = \frac{\partial G}{\partial P_x} + \varepsilon \frac{\partial u}{\partial P_x} F \\ \dot{P}_x &= -\frac{\partial \mathcal{F}}{\partial x} = -\frac{\partial G}{\partial x} - \varepsilon \frac{\partial u}{\partial x} F \\ \dot{\phi} &= \frac{\partial \mathcal{F}}{\partial I} = k \frac{\partial G}{\partial P_x} - \omega + \varepsilon k \frac{\partial u}{\partial P_x} F \\ \dot{I} &= -\frac{\partial \mathcal{F}}{\partial \phi} = -\varepsilon u \frac{dF}{d\phi} \end{aligned} \quad (10)$$

These equations show that the rate of change of variables  $(x, P_x)$  is  $\sim 1$  (it does not depend on small parameter  $\varepsilon$ ), the rate of change for  $kI$  is about  $k\varepsilon$  (a product of a small parameter  $\varepsilon$  and a large parameter  $k$ ), and the rate of change of  $\phi$  is of the order of a large parameter  $k$ . We assume that  $\varepsilon k \sim 1$ . In this case, Hamiltonian system (10) contains a fast phase  $\phi$  and slow variables  $(x, P_x)$  and  $I$ . Averaging over the fast phase  $\phi$  gives the following equations of motion:

$$\dot{x} = \frac{\partial G}{\partial P_x} + \varepsilon \frac{\partial u}{\partial P_x} \langle F \rangle, \quad \dot{P}_x = -\frac{\partial G}{\partial x} - \varepsilon \frac{\partial u}{\partial x} \langle F \rangle, \quad \dot{I} = 0 \quad (11)$$

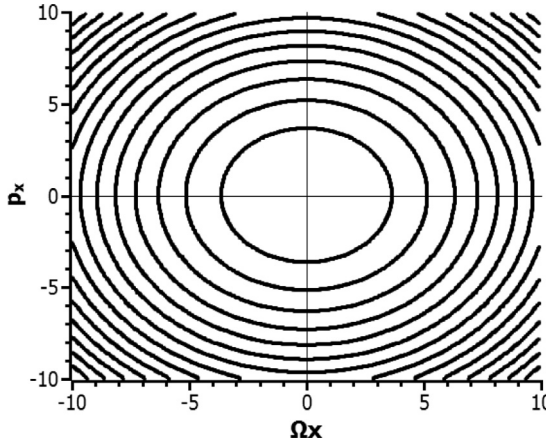


Fig. 2. Phase portraits of systems (3) and (4).

where

$$\langle F \rangle = \lim_{\phi_l \rightarrow \infty} \frac{1}{2\phi_l} \int_{-\phi_l}^{\phi_l} F(\phi) d\phi \quad (12)$$

For periodic perturbations (e.g.,  $F \sim \sin \phi$ ) we have  $\langle F \rangle = 0$ . Moreover, even perturbations with nonzero values of  $\langle F \rangle$  affect the Hamiltonian equations only slightly,  $\sim \varepsilon$ . Therefore,  $I$  can be considered as an adiabatic invariant: it is conserved in the system averaged over  $\phi$  and changes only if separation of time-scales is (the assumption that the phase  $\phi$  is fast) is violated. In other words, the conservation of  $I$  breaks down when  $\dot{\phi} \sim 0$ .

Consider unperturbed system (1) with Hamiltonian  $G(x, P_x)$ . We restrict our consideration to the class of systems where the motion in the  $(x, P_x)$  plane is finite: phase points move along closed trajectories (see and example of characteristic phase portraits in Fig. 2). The perturbation  $\varepsilon u F$  barely deforms trajectories in the  $(x, P_x)$  plane everywhere where the averaging over fast phase  $\phi$  can be performed. This averaging breaks down in the vicinity of the resonance  $\dot{\phi} = 0$ , where the rate of change of the phase drops to zero. In 3D space  $(x, P_x, I)$ , the resonant condition is satisfied on the surface  $I_{\text{res}} = I_{\text{res}}(x, P_x)$ , which can be determined by setting  $\dot{\phi} = 0$  in system (10):

$$k \frac{\partial G}{\partial P_x} - \omega = 0 \quad (13)$$

with  $I_{\text{res}}$  being defined in the zeroth-order approximation (i.e., for  $\varepsilon = 0$ ). For systems (3) and (5), Eq. (13) becomes

$$k(P_x + kI_{\text{res}}) - \omega = 0 \quad (14)$$

The corresponding solution is

$$I_{\text{res}} = \frac{1}{k}(\nu_{\text{res}} - P_x) \quad (15)$$

where  $\nu_{\text{res}} = \omega/k$ . For system (4), Eq. (13) is

$$kI_{\text{res}} = \nu_{\text{res}} \sqrt{1 + (P_x + kI_{\text{res}})^2 + \Omega^2 x^2} - P_x \quad (16)$$

Solution of Eq. (16) is

$$I_{\text{res}} = \frac{1}{k} \left( \frac{\nu_{\text{res}} \sqrt{1 + \Omega^2 x^2}}{\sqrt{1 - \nu_{\text{res}}^2}} - P_x \right) \quad (17)$$

Combination of equation  $I_{\text{res}} = I_{\text{res}}(x, P)$  and unperturbed Hamiltonian (9) defines resonant curves  $P_{\text{res}} = P_{\text{res}}(x)$  in the  $(x, P_x)$  plane or  $p_{x,\text{res}} = p_{x,\text{res}}(x)$  in the  $(x, p_x)$  plane:

$$h = -\omega I_{\text{res}} + G(x, P_{\text{res}} + kI_{\text{res}}) \quad (18)$$

where  $h$  is a conserved energy for Hamiltonian (9). For functions (3) and (5) these curves are

$$P_{\text{res}} = \frac{1}{\nu_{\text{res}}} \left( h + \frac{1}{2} \nu_{\text{res}}^2 - \frac{1}{2} \Omega^2 x^2 \right), \quad p_{x,\text{res}} = \nu_{\text{res}} \quad (19)$$

while for system (4) they are

$$P_{\text{res}} = \frac{1}{\nu_{\text{res}}} \left( h - \sqrt{1 - \nu_{\text{res}}^2} \sqrt{1 + \Omega^2 x^2} \right), \quad p_{x,\text{res}} = \frac{\nu_{\text{res}}}{\sqrt{1 - \nu_{\text{res}}^2}} \sqrt{1 + \Omega^2 x^2} \quad (20)$$

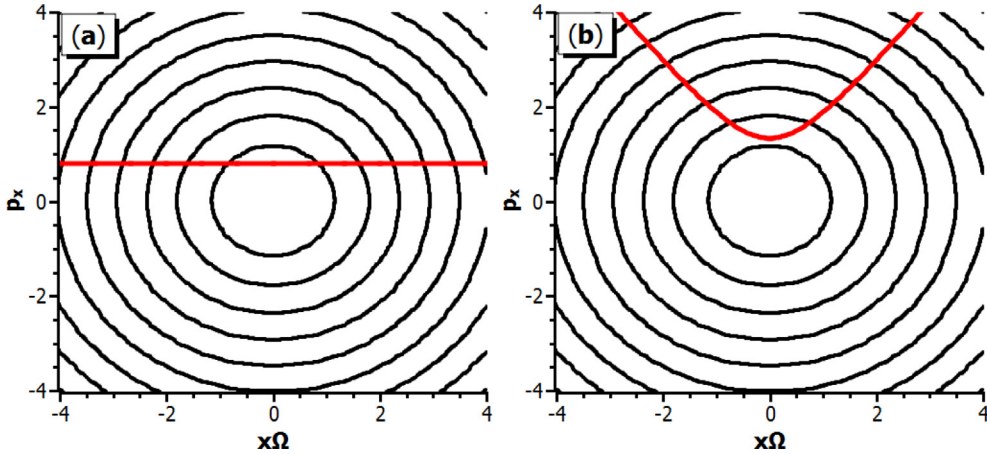


**Fig. 3.** Phase portraits of systems (a)(3) and (b)(4). Red curves are the resonances  $p_x = v_{res}$ (a),  $p_x = P_{res} + kI_{res}$ (b) defined by Eqs. (20), (17).

Fig. 3 shows unperturbed trajectories in the  $(x, p_x)$  plane and the corresponding resonant curves (19) and (20). Closed unperturbed trajectories are crossed by the resonant curve  $p_x = p_{x,res}$  twice. Thus there are two resonance crossings for each period of the unperturbed motion.

Consider a vicinity of the resonance and expand Hamiltonian (9) around  $I - I_{res} = 0$ :

$$\mathcal{F} = -\omega I_{res} + G_{res} + \varepsilon u F(\phi) + \frac{1}{2} \frac{\partial^2 G}{\partial I^2} \Big|_{I=I_{res}} (I - I_{res})^2 \quad (21)$$

where  $G_{res}$  is evaluated at  $I = I_{res}$ . We introduce new variable  $P_\phi = (I - I_{res})$  with the generating function

$$R = (P_\phi + I_{res})\phi + \bar{P}_x x \quad (22)$$

where new conjugate variables  $(\bar{P}_x, \bar{x})$ ,  $(P_\phi, \bar{\phi})$  are

$$\begin{aligned} I &= \frac{\partial R}{\partial \phi} = P_\phi + I_{res} \\ P_x &= \frac{\partial R}{\partial x} = \bar{P}_x + \frac{\partial I_{res}}{\partial x} \phi \\ \bar{\phi} &= \phi, \quad \bar{x} = x - \frac{\partial I_{res}}{\partial \bar{P}_x} \phi \end{aligned} \quad (23)$$

New Hamiltonian takes the form

$$\bar{\mathcal{F}} = -\omega I_{res} + G_{res} \left( \bar{x} - \frac{\partial I_{res}}{\partial \bar{P}_x} \bar{\phi}, \bar{p}_x + \frac{\partial I_{res}}{\partial x} \bar{\phi} \right) + \frac{1}{2} g P_\phi^2 + \varepsilon u F(\bar{\phi}) \quad (24)$$

where

$$g = \frac{\partial^2 G}{\partial I^2} \Big|_{I=I_{res}} \quad (25)$$

In Eq. (24), function  $G_{res}$  depends on  $\bar{x} - (\partial I_{res}/\partial \bar{P}_x) \bar{\phi}$  and  $\bar{p}_x - (\partial I_{res}/\partial x) \bar{\phi}$ . Eq. (8) shows that  $\partial I_{res}/\partial \bar{P}_x \sim 1/k$ ,  $\partial I_{res}/\partial x \sim 1/k$ , therefore these terms can be considered as perturbations for  $\bar{x}$ ,  $\bar{p}_x$  (see also Eqs. (15, 17)). Thus  $G_{res}$  can be expanded as

$$\begin{aligned} G_{res} \left( \bar{x} - \frac{\partial I_{res}}{\partial \bar{P}_x} \bar{\phi}, \bar{p}_x + \frac{\partial I_{res}}{\partial x} \bar{\phi} \right) &\approx G_{res}(\bar{x}, \bar{p}_x) - \frac{\partial I_{res}}{\partial \bar{P}_x} \frac{\partial G_{res}}{\partial \bar{x}} \bar{\phi} + \frac{\partial I_{res}}{\partial x} \frac{\partial G_{res}}{\partial \bar{p}_x} \bar{\phi} \\ &= G_{res}(\bar{x}, \bar{p}_x) + \{I_{res}, G_{res}\} \bar{\phi} \end{aligned} \quad (26)$$

Substituting Eq. (26) into Eq. (24), we obtain

$$\begin{aligned} \bar{\mathcal{F}} &= -\omega I_{res} + G_{res} + \frac{1}{2} g P_\phi^2 - r \bar{\phi} + \varepsilon u F(\bar{\phi}) \\ G_{res} &= G_{res}(x, p_x + kI_{res}(x, p_x)) \end{aligned} \quad (27)$$

where

$$r = \{G_{res}, I_{res}\} = \frac{\partial G_{res}}{\partial x} \frac{\partial I_{res}}{\partial P_x} - \frac{\partial G_{res}}{\partial P_x} \frac{\partial I_{res}}{\partial x} \quad (28)$$

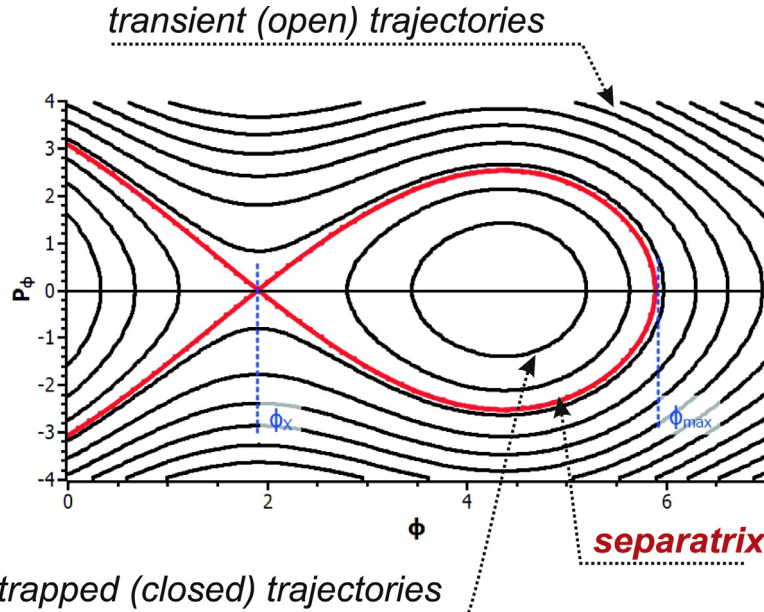


**Fig. 4.** Phase portraits of system (34) for  $|\varepsilon u| > |r|$ . The red line is a separatrix. (For interpretation of the references to colour in this figure legend, the reader is referred to the web version of this article.)

For the sake of simplicity, we omitted the bar over the variables  $\phi$ ,  $p_x$ , and  $x$ . Hamiltonian (27) can be viewed as

$$\bar{\mathcal{F}} = \Lambda + H_\phi \quad (29)$$

Hamiltonian  $\Lambda$  describes the slow motion in the  $(P_x, x)$  plane:

$$\Lambda = -\omega I_{\text{res}} + G_{\text{res}}(x, P_x) \quad (30)$$

and Hamiltonian  $H_\phi$  describes the fast motion in the  $(P_\phi, \phi)$  plane:

$$H_\phi = \frac{1}{2}g(x)P_\phi^2 + \varepsilon u(x)F(\phi) - r(x)\phi \quad (31)$$

Coefficients in Hamiltonian (31) may depend on  $x$  and  $P_x = P_{\text{res}}(x)$  where  $P_{\text{res}}$  is the solution of equation  $\Lambda(x, P_x) = h = \text{const}$  (see, e.g., Eqs. (19), (20), (30)).

For systems (3) and (5) with  $F = \sin \phi$  and  $I_{\text{res}}$  given by Eq. (15), we obtain

$$g = k^2, \quad r = -\frac{\Omega^2}{k}x \quad (32)$$

For system (4) with  $F = \sin \phi$  and  $I_{\text{res}}$  given by Eq. (17), we obtain

$$g = \frac{(1 - \nu_{\text{res}}^2)^{3/2}k^2}{\sqrt{1 + \Omega^2 x^2}} \quad r = -\frac{\Omega^2 x}{k} \frac{1}{\sqrt{1 - \nu_{\text{res}}^2} \sqrt{1 + \Omega^2 x^2}} \quad (33)$$

For Hamiltonians (3), (4), and (5), Eq. (31) can be written as

$$H_\phi = \frac{1}{2}g(x)P_\phi^2 - r(x)\phi + \varepsilon u(x)\sin \phi \quad (34)$$

Hamiltonian (34) is a classical Hamiltonian of a pendulum with torque. A characteristic phase portrait of  $H_\phi$  for  $r > 0$ ,  $|\varepsilon u(x)| > r$  is shown in Fig. 4. There are two types of trajectories: open and closed. The boundary of the region filled with closed trajectories is called the *separatrix*. Phase points moving along closed trajectories oscillate around the line  $P_\phi = 0$ , that defines the resonance  $\dot{\phi} = 0$ .

**Section summary** In the current section we showed that multi-scale systems (systems with fast phase) can be studied using the method of averaging. This method is valid away from the resonances – where the rate of change of a fast variable vanishes. We illustrated a way of locating the resonances. We showed how to expand the Hamiltonian in the vicinity of the resonance, to obtain a Hamiltonian of a nonlinear pendulum. The parameters of the resonance Hamiltonian are defined by the coefficients of the system configuration.

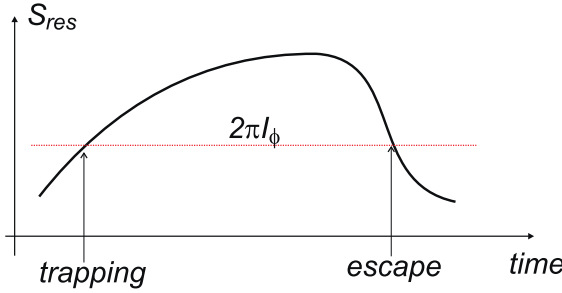


Fig. 5. Schematic view of trapping into resonance and escape from resonance.

### 3. Trapping (capture) into resonance

The phase portrait of a typical Hamiltonian (31) is shown in Fig. 4. The curve demarcating regions filled with closed and open trajectories is called the *separatrix*. Denote by  $S_{\text{res}}$  the area bounded by the separatrix in Fig. 4:

$$S_{\text{res}} = 2 \int_{\phi_x}^{\phi_{\max}} P_\phi \, d\phi \quad (35)$$

If the area  $S_{\text{res}}$  grows along the particle trajectory, new trajectories can be trapped into this region. The trapping corresponds to a change of type of particle motion: trapped particles oscillate around the resonance  $P_\phi = 0$ . Thus, this transition is called *trapping (or capture) into resonance*.

As trapped particles move along the closed trajectories, the corresponding invariant is conserved

$$I_\phi = \frac{1}{2\pi} \oint P_\phi \, d\phi = \frac{1}{\pi} \sqrt{\frac{2}{g}} \int_{\phi_-}^{\phi_+} \sqrt{2H_\phi + r\phi - \varepsilon u \sin \phi} \, d\phi \quad (36)$$

where  $\phi_{\pm}$  are two solutions of the equation  $2H_\phi + r\phi - \varepsilon u \sin \phi = 0$ . The conservation of  $I_\phi$  is a consequence of a separation of time scales between  $(\phi, P_\phi)$  and  $(x, P_x)$ .

At the moment of trapping  $I_\phi = S_{\text{res}}/2\pi$ . In the trapped motion,  $I_\phi = \text{const}$  and  $S_{\text{res}}(x, P_x)$  changes along the resonant trajectory. Thus, as long as the area  $S_{\text{res}}$  grows, the inequality  $I_\phi \leq S_{\text{res}}/2\pi$  does not allow particles to cross the separatrix again and to *escape from resonance*. For the particle to escape from resonance the area  $S_{\text{res}}$  should decrease to its value at the trapping (see a schematics in Fig. 5). Therefore, the  $(x, P_x)$  coordinates of trapping and escape are controlled by the shape of the  $S_{\text{res}}(x, P_x)$  curve. In this section, we describe details of the trapped dynamics.

#### 3.1. Area surrounded by the separatrix

To define the conditions of trapping, we write an expression for the area  $S_{\text{res}}$ :

$$S_{\text{res}} = \oint P_\phi \, d\phi = 2 \sqrt{\frac{2}{g}} \int_{\phi_x}^{\phi_{\max}} \sqrt{H_\phi + r\phi - \varepsilon u F(\phi)} \, d\phi = 2 \sqrt{\frac{2|r|}{g}} \int_{\phi_x}^{\phi_{\max}} \sqrt{(\phi - \phi_x) - a(F(\phi) - F(\phi_x))} \, d\phi \quad (37)$$

where

$$a = \varepsilon u / r \quad (38)$$

Here  $\phi_x$  is the coordinate of the saddle point (i.e., a solution of  $1 - aF'(\phi) = 0$ ),  $\phi_{\max}$  is a solution of  $(\phi - \phi_x) - a(F(\phi) - F(\phi_x)) = 0$  (see Fig. 4). The change of the sign of  $r$  corresponds to changing the direction of integration along  $\phi$  because  $\phi_x$  becomes larger than  $\phi_{\max}$ . In what follows we write the area  $S_{\text{res}}$  as

$$S_{\text{res}} = 2 \sqrt{\frac{2|r|}{g}} \times \begin{cases} f_s(a), & F(\phi) - \text{periodic} \\ \tilde{f}_s(a), & F(\phi) - \text{nonperiodic} \end{cases} \quad (39)$$

For example, for a system with  $F = \sin \phi$ , Eq. (39) takes the form

$$S_{\text{res}} = 2 \sqrt{\frac{2|r|}{g}} \int_{\phi_x}^{\phi_{\max}} \sqrt{(\phi - \phi_x) - a(\sin \phi - \sin \phi_x)} \, d\phi = 2 \sqrt{\frac{2|r|}{g}} f_s(a) \quad (40)$$

The profile of  $f_s(a)$  is shown in Fig. 6. When  $a < 1$ ,  $f_s(a) = 0$ ; when  $a \rightarrow \infty$ , we have  $f_s(a) \rightarrow 8\sqrt{a/2}$  and there is a simple asymptotic expression for  $S_{\text{res}}$ :

$$S_{\text{res}} = 16\sqrt{|\varepsilon u/g|} \quad (41)$$

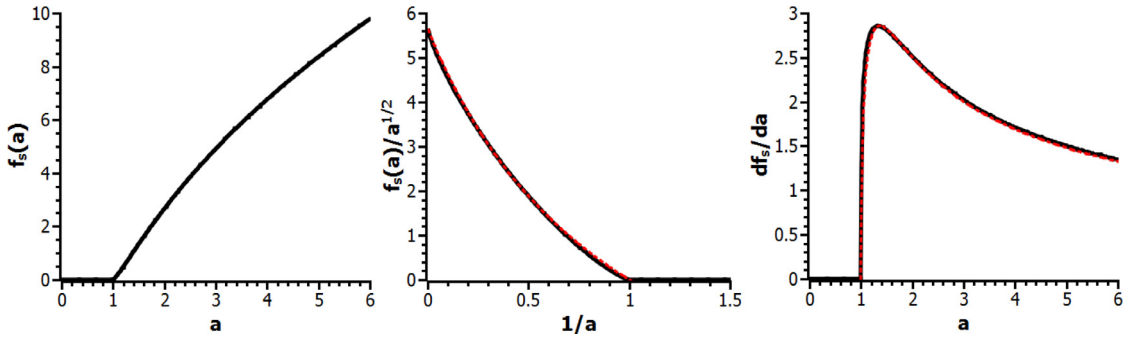


**Fig. 6.** Left panel shows function  $f_s(a)$  given by Eq. (40). Central panel shows  $f_s(a)/\sqrt{a}$  as a function of  $1/a$  and approximation (red dashed curve)  $f_s(a) = 8\sqrt{2a}(a/(1+a) - 1/2)$ . Right panel shows function  $df_s(a)/da$  and approximation (red dashed curve)  $df_s(a)/da \approx C_1\sqrt{a-1}/(a^{1.1} - C_2)$  with  $C_1 \approx 3.917$  and  $C_2 \approx 0.58$ . (For interpretation of the references to colour in this figure legend, the reader is referred to the web version of this article.)

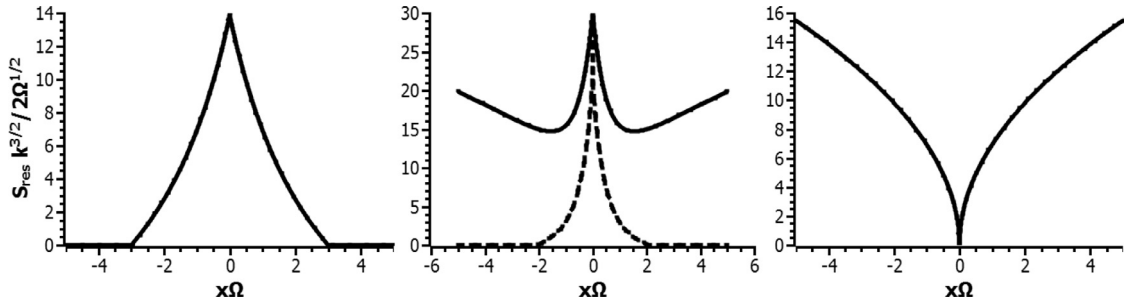


**Fig. 7.** Profiles of  $S_{\text{res}}$  from Eq. (42) (left panel), Eq. (43) (central panel), and Eq. (44) (right panel). System parameters are:  $\varepsilon k/\Omega = -3$ ,  $v_{\text{res}} = 0.8$ . The dashed curve (in central panel) shows  $S_{\text{res}}$  for Eq. (43) with  $\varepsilon k/\Omega < -1/\sqrt{1 - v_{\text{res}}^2}$ .

Function  $f_s(a)$  can be reasonably approximated by  $f_s(a) \approx 8\sqrt{2a}(a/(1+a) - 1/2)$ . However, this approximation is not accurate enough to compute the derivative  $df_s/da$ . For a better fit, see an example in Fig. 6.

Let us consider behavior of  $S_{\text{res}}$  for systems (3)–(5). For system (3),  $u = 1$  and we obtain

$$S_{\text{res}} = \frac{2\Omega}{k^{3/2}} \sqrt{2|x|} f_s(a), \quad a = -\frac{\varepsilon k}{x\Omega^2} \quad (42)$$

Profile of  $S_{\text{res}}(x)$  is shown in Fig. 7 (left panel). The area  $S_{\text{res}}$  differs from zero only for  $|x\Omega| < |\varepsilon k u/\Omega|$  and grows ( $dS_{\text{res}}/dx > 0$ ) for negative  $x$ .

For system (4),  $u = 1$  again and we obtain

$$S_{\text{res}} = \frac{2\Omega}{k^{3/2}(1 - v_{\text{res}}^2)} \sqrt{2|x|} f_s(a), \quad a = -\frac{k\varepsilon\sqrt{1 - v_{\text{res}}^2}\sqrt{1 + \Omega^2 x^2}}{\Omega^2 x} \quad (43)$$

Profile of  $S_{\text{res}}(x)$  is shown in Fig. 7 (central panel). In comparison with  $S_{\text{res}}$  given by Eq. (42), area (43) grows with  $x$  for large enough  $x\Omega$ .

For system (5),  $u = x$  and we obtain

$$S_{\text{res}} = \frac{2\Omega}{k^{3/2}} \sqrt{2|x|} f_s(a), \quad a = -\frac{\varepsilon k}{\Omega^2} = \text{const} \quad (44)$$

A characteristic profile of  $S_{\text{res}}(x)$  is shown in Fig. 7 (right panel). The area  $S_{\text{res}}$  grows for positive  $x$ .

### 3.2. Probability of trapping

The necessary condition for trapping of new particles into resonance at a given location on resonance is the growth of the area  $S_{\text{res}}$  along the resonant trajectories in the slow variables plane,  $(x, P_x)$ . Not all particles passing through the resonance (resonant particles) are trapped into resonance. The fate of a particular particle is defined by a value of phase  $\phi$  near the resonance. This value is defined by the initial (far from the resonance)  $\phi$  and can be individually calculated for each particle. However,  $\phi$  changes fast and even small alternations of the initial particle coordinates can switch the type of motion near the resonance (particle which should not be trapped will be trapped or vice versa). As a result, exactly what particles are to be trapped cannot be realistically predicted. Instead one can compute a relative amount (percentage) of to-be-trapped particles, or, equivalently, the ratio of the phase volume filled by to-be-trapped particles to the entire phase volume filled

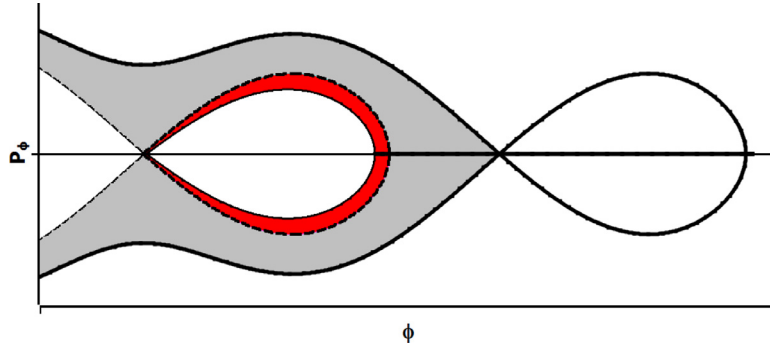


**Fig. 8.** Schematics of the calculation of  $\Pi$ . The red color shows a change of the area  $S_{res}$  over a time  $\sim \Delta t$ , the grey color shows a phase space filled by the transient trajectories. The probability of trapping is equal to the ratio of  $\Delta S_{res}/\Delta t$  to the phase flux through the grey area. (For interpretation of the references to colour in this figure legend, the reader is referred to the web version of this article.)

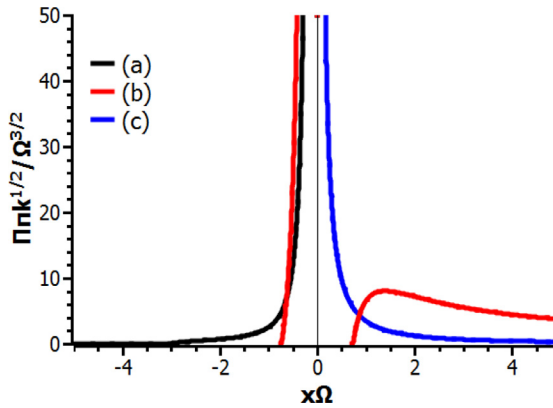


**Fig. 9.** Profiles of  $\Pi$  for Eq. (49)(a), Eq. (50)(b), Eq. (53)(c). System parameters are:  $\varepsilon k/\Omega^2 = -3$ ,  $\nu_{res} = 0.8$ .

by resonant particles. This ratio can be called a probability  $\Pi$  of trapping during a single passage through resonance, [104]. The to-be-trapped phase volume is equal to  $\dot{S}_{res} \Delta t$  where  $\dot{S}_{res}$  is a rate of change of  $S_{res}$ , and  $\Delta t$  is a time interval. The entire phase volume is a product of the phase flux through the resonance and the same  $\Delta t$ . Thus, for  $\Pi$  we have (see [105]):

$$\Pi \approx \frac{\{S_{res}, \Lambda\}}{\{S_{res}, \Lambda\}/2 + \left| \int_0^{2\pi} \dot{P}_\phi d\phi \right|} \quad (45)$$

and  $\Pi = 0$  for  $\dot{S}_{res} < 0$ . Hamiltonian  $\Lambda$  in Eq. (45) is defined by Eq. (30). The calculation of  $\Pi$  is illustrated in Fig. 8. For Hamiltonian (34), Eq. (45) takes the form:

$$\Pi = \frac{2\{S_{res}, \Lambda\}}{\{S_{res}, \Lambda\} + 4\pi|r|} \quad (46)$$

If  $S_{res}$  changes slowly enough ( $\dot{S}_{res} \ll 4\pi|r|$ ), which is the case in almost all systems, we can use approximation

$$\Pi \approx \frac{\{S_{res}, \Lambda\}}{2\pi|r|} \quad (47)$$

For systems (3)–(5) the area  $S_{res}$  depends only on  $x$ . Thus

$$\{S_{res}, \Lambda\} = \frac{\partial S_{res}}{\partial x} \frac{\partial \Lambda}{\partial P_x} = \dot{x} \frac{\partial S_{res}}{\partial x} = P_{res} \frac{\partial S_{res}}{\partial x} \quad (48)$$

For system (3), the area  $S_{res}$  given by Eq. (42),  $r$  given by Eq. (32), and we obtain

$$\Pi \approx \frac{\nu_{res}}{\pi \Omega k^{1/2}} \frac{1}{|x|} \frac{\partial}{\partial x} (\sqrt{2|x|} f_s(a)) \quad (49)$$

Profile of  $\Pi(x)$  is shown in Fig. 9(a): positive probabilities correspond to negative values of  $x$ , where the area  $S_{res}$  increases with  $x$  (compare Figs. 7 and 9(a)).

For system (4),  $S_{\text{res}}$  is given by Eq. (43) and  $r$  is given by Eq. (33):

$$\Pi \approx \frac{1}{\pi \Omega k^{1/2} \sqrt{1 - \nu_{\text{res}}^2}} \frac{\sqrt{1 + \Omega^2 x^2}}{|x|} \frac{\partial}{\partial x} (\sqrt{2|x|} f_s(a)) \quad (50)$$

Profile of  $\Pi(x)$  is shown in Fig. 9(b). Note that for  $|x| \gg 1/\Omega$ , Eq. (43) gives  $a = \text{const}$ :

$$a = \frac{k\epsilon \sqrt{1 - \nu_{\text{res}}^2} \sqrt{1 + \Omega^2 x^2}}{\Omega^2 |x|} \approx \frac{k\epsilon \sqrt{1 - \nu_{\text{res}}^2}}{\Omega} \quad (51)$$

and for  $|a| > 1$  expression (50) takes the form

$$\Pi \approx \frac{f_s(a)}{\sqrt{2\pi} \Omega k^{1/2} \sqrt{1 - \nu_{\text{res}}^2}} \frac{\sqrt{1 + \Omega^2 x^2}}{|x|^{3/2}} \approx \frac{f_s(a)}{\sqrt{2\pi} k^{1/2} \sqrt{1 - \nu_{\text{res}}^2}} \frac{1}{|x|^{1/2}} \quad (52)$$

Eq. (52) shows that  $\Pi$  is always positive for large  $x$ . Thus, new particles can be trapped and trapped particle cannot escape from resonance for large  $x$ .

For system (5), with  $S_{\text{res}}$  given by Eq. (44) and  $r$  is given by Eq. (32):

$$\Pi \approx \frac{f_s(a)}{\pi \Omega k^{1/2}} \frac{1}{|x|} \frac{\partial}{\partial x} (\sqrt{2|x|}) = \frac{f_s(a)}{\sqrt{2\pi} \Omega k^{1/2}} \frac{1}{|x|^{3/2}} \quad (53)$$

where  $a = \epsilon k/\Omega^2 = \text{const}$ . Profile of  $\Pi(x)$  is shown in Fig. 9(c).

### 3.3. Non-periodic perturbations

Eq. (45) describes the probability of particle trapping into resonance with a periodic wave. The important property of the resonance particle interaction with such waves is that *all* the particles crossing the resonance in the slow variable phase plane interact there with the wave, i.e. for all resonant particles the perturbation is described by the same periodic function  $F(\phi)$ . When the wave is non-periodic, the situation is more complicated. Consider a localized wave, for which  $F(\phi) \neq 0$  only over a limited range of  $\phi$ . For such functions, resonant particles crossing the manifold  $\dot{\phi} = 0$  can miss the wave: at the moment of crossing the phase  $\phi$  can be such that  $F = 0$ . Such resonant particles do not interact with waves. Therefore, for non-periodical waves the trapping probability can be meaningfully calculated only for an ensemble of non-periodical waves sufficiently large to support the resonant wave-particle interaction for all resonant particles. To the best of our knowledge there is no example of such calculations.

### 3.4. Dynamics of trapped particles

Motion of trapped particles in the  $(x, P_x)$  plane is described by Hamiltonian (30). Particle momentum in the resonance,  $P_{x,\text{res}}$ , is given by Eq. (18). Substituting Eq. (18) into Eq. (8) we obtain the resonant momentum in initial coordinates  $(x, p_x)$ .

For systems (3) and (5), momentum  $p_{x,\text{res}} = \nu_{\text{res}} = \omega/k$  is conserved, and we obtain that in resonance  $x_{\text{res}} = \int p_{x,\text{res}} dt = \nu_{\text{res}} t + x_0$ . We substitute these expressions into equation for particle energy to get

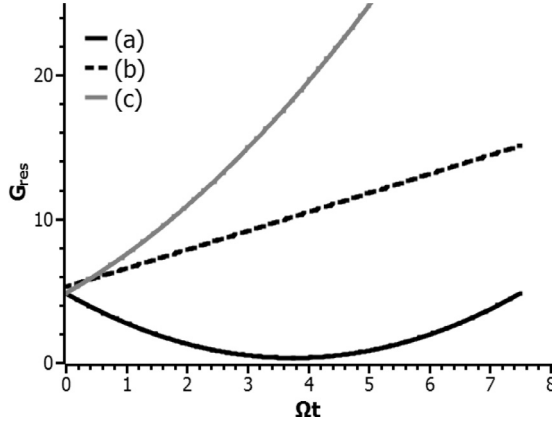
$$G_{\text{res}} = \frac{1}{2} \nu_{\text{res}}^2 + \frac{1}{2} \Omega^2 (\nu_{\text{res}} t + x_0)^2 \quad (54)$$

For system (4), the same procedure is based on Eq. (20) and gives

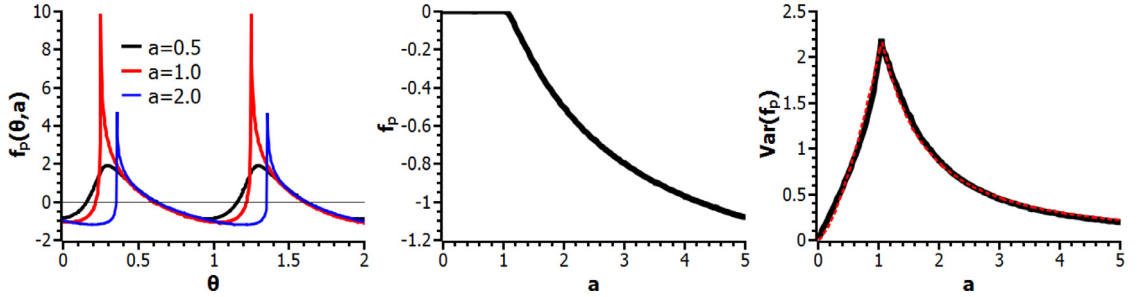
$$G_{\text{res}} = \frac{\sqrt{1 + \Omega^2 (\nu_{\text{res}} t + x_0)^2}}{\sqrt{1 - \nu_{\text{res}}^2}} \quad (55)$$

Fig. 10 illustrates that Eq. (54) can describe both increase and decrease of particle energy. For system (3), trapping is possible only for  $x_{\text{trap}} < 0$  (see Fig. 9(a)) and the energy decreases with time until  $x$  reaches 0. Then the energy starts increasing and reaches the initial value at  $x = -x_{\text{trap}}$ . At that moment, the area  $S_{\text{res}}$  returns to its value at the moment of trapping (see Fig. 7 (left panel)), and the particle escapes from resonance (see Section 6.1 for more details). The situation is different for system (5), where trapping is possible only for positive  $x_{\text{trap}}$  (see Fig. 9(c)). In this case, the energy of trapped particle always increases with time, the area  $S_{\text{res}}$  grows, (see Fig. 7 (right panel)), and trapped particles keep accelerating (see Section 6.2). A similar situation takes place for system (4): trapping is possible for positive  $x_{\text{trap}}$  when both the energy  $G_{\text{res}}$  and the area  $S_{\text{res}}$  grow with time (it follows from Eq. (20) that  $p_{x,\text{res}} > 0$ ), see Figs. 7 (central panel) and 10 (curve b). More details about system (4) can be found in Section 7.1.

**Section summary** In this section we derive a general expression for the probability of trapping,  $\Pi$ , which is a relative measure of resonant particles trapped into resonance for a single resonance crossing. We show that trapped particles change their motion significantly and gain energy moving in the resonance with wave. The trapped dynamics is determined by the evolution of the area surrounded by the separatrix,  $S_{\text{res}}$ .



**Fig. 10.** Profiles of  $G_{\text{res}}$  for Eq. (54) with initial negative  $x_0$  (curve a) and positive  $x_0$  (curve c), and Eq. (55) (curve b). System parameters are:  $\Omega x_0 = -3$ (a),  $\Omega x_0 = 3$ (b),  $\Omega x_0 = 3$ (c),  $v_{\text{res}} = 0.8$ .



**Fig. 11.** Profiles of functions  $f_p(\theta, a)$  (left panel),  $f_p(a) = \langle f_p \rangle$  (central panel),  $\text{Var}(f_p)$  (right panel). Red dashed curves shows approximation: where  $\text{Var}(f_p) = 2a^{3/2}$  for  $|a| < a_*$  and  $\text{Var}(f_p) = 2.4a^{-3/2}$  for  $|a| > a_*$ ,  $a_* \approx 1.06$ .

#### 4. Scattering on resonance

Particles passing through resonance change their energy even in absence of trapping. This effect is called *scattering on resonance*. To describe the energy change for scattered particles, we consider Hamiltonian (9) and write Hamiltonian equation for the momentum  $I$ :

$$I = -\frac{\partial \mathcal{F}}{\partial \phi} = -\varepsilon u(x) \cos \phi \quad (56)$$

where we assumed  $F(\phi) = \sin \phi$  like in Hamiltonian (34). Trajectories of a few scattered, or transient, particles in system (31) are shown in Fig. 4. Any such trajectory consists of two symmetrical parts: phase changes from some initial value to  $\phi^*$  and back. The value of  $\phi^*$  can be obtained from the equation  $P_\phi = 0$  with Hamiltonian (34):

$$-r(x)\phi^* + \varepsilon u(x) \sin \phi^* = H_\phi \quad (57)$$

Therefore, the total change of momentum  $I$  for transient particles can be written as

$$\begin{aligned} \Delta I &= -2 \int_{-\infty}^{t^*} (\varepsilon u \cos \phi) dt = -2 \frac{\varepsilon u}{g} \int_{-\infty}^{\phi^*} \frac{\cos \phi}{P_\phi} d\phi = -\sqrt{\frac{2}{g}} \varepsilon u \int_{-\infty}^{\phi^*} \frac{\cos \phi}{\sqrt{H_\phi + r\phi - \varepsilon u \sin \phi}} d\phi \\ &= -\sqrt{\frac{2}{g}} \varepsilon u \int_{-\infty}^{\phi^*} \frac{\cos \phi}{\sqrt{r(\phi - \phi^*) - \varepsilon u(\sin \phi - \sin \phi^*)}} d\phi = -\sqrt{\frac{2}{g|r|}} \varepsilon u \int_{-\infty}^{\phi^*} \frac{\cos \phi}{\sqrt{2\pi\theta + \phi - a \sin \phi}} d\phi \end{aligned} \quad (58)$$

where we used a notation  $2\pi\theta = a \sin \phi^* - \phi^*$ . Introducing

$$f_p(\theta, a) = \int_{-\infty}^{\phi^*} \frac{\cos \phi}{\sqrt{2\pi\theta + \phi - a \sin \phi}} d\phi \quad (59)$$

we get  $\Delta I = -\sqrt{2/g|r|} \varepsilon u f_p(\theta, a)$ . Function  $f_p(\theta, a)$  is  $2\pi$ -periodic in  $\theta$  and its profile is shown in Fig. 11 for three values of  $a$ . For a particular particle, fast oscillations of  $\phi$  result in a significant change of  $\theta$  even for small changes of the initial energy: two very close initial energies can correspond to very different  $\phi^*$ . Thus, it is convenient to use statistical properties

of  $f_p(\theta, a)$ , which characterize the dynamics of an ensemble of particles with different values of  $\theta$ . Assuming a uniform distribution of  $\theta$  (see a numerical verification of this assumption in [106]), we get

$$\begin{aligned}\langle \Delta I \rangle_\theta &= \int_0^1 \Delta I d\theta = -\sqrt{\frac{2}{g|r|}} \varepsilon u \langle f_p \rangle_\theta \\ \text{Var}(\Delta I) &= \int_0^1 \Delta I^2 d\theta - \langle \Delta I \rangle_\theta^2 = \frac{2}{g|r|} (\varepsilon u)^2 \text{Var}(f_p)\end{aligned}\quad (60)$$

Fig. 11 shows profiles of  $f_p(a) = \langle f_p \rangle_\theta$  and  $\text{Var}(f_p)$ . From now on, we omit  $\langle \dots \rangle_\theta$ , as in the present review, and in almost all of the publications cited here, the function  $f_p(\theta, a)$  is not used. The function  $f_p$  is zero for  $a < 1$ , whereas  $\text{Var}(f_p)$  has a maximum at  $a = 1$  (we can approximate  $\text{Var}(f_p)$  by a simple function shown in Fig. 11).

Eqs. (60) describe changes of momentum  $I$  due to scattering. This momentum is a slowly changing variable in autonomous Hamiltonian (9):  $\mathcal{F}(I, x, P_x) = \text{const}$ . Thus,  $I$  variation results in variation of other slow variables,  $x$  and  $P_x$ : scattering on resonance leads to variations of all slowly varying system variables. Conservation of Hamiltonian  $\mathcal{F}$  results in a direct relation between the momentum change  $\Delta I$  and the energy change  $\Delta h = -\omega \Delta I$ . Thus Eqs. (60) describe particle acceleration/deceleration due to scattering. Similarly, the momentum  $p_x$  is related to  $I$  through the resonant condition:  $k p_x - \omega = (I - I_{\text{res}})g$ . And finally  $\Delta h$  and  $\Delta p_x$  are related via unperturbed Hamiltonian (1):  $\Delta h = (\partial G / \partial p_x)_{\mathcal{F}=\text{const}} \Delta p_x$ .

Hamiltonian equations for Hamiltonian (9) yield  $I - I_{\text{res}} = \dot{\phi}/g$ . As  $\dot{\phi}$  can be defined from Eq. (2), we obtain

$$k p_x - \omega = (I - I_{\text{res}})g \quad (61)$$

Combination of Eqs. (60) and (61) defines  $\Delta p_x$  for scattered particles:

$$\begin{aligned}\langle \Delta p_x \rangle &= \frac{g \langle \Delta I \rangle_\theta}{k} = -\sqrt{\frac{2g}{|r|k^2}} \varepsilon u f_p \\ \text{Var}(\Delta p_x) &= \frac{g^2}{k^2} \text{Var}(\Delta I) = \frac{2g}{|r|k^2} (\varepsilon u)^2 \text{Var}(f_p)\end{aligned}\quad (62)$$

Here  $\Delta p_x$  is essentially a change of  $p_x$  after a passage through resonance (more accurately,  $\Delta p_x$  is a difference between an actual  $p_x$  value after a passage and  $p_x$  at the same time moment in the system without a wave). For systems (3) and (5), Eq. (62) can be written as (see Eq. (32)):

$$\begin{aligned}\langle \Delta p_x \rangle &= -\sqrt{\frac{2}{|x|k}} \frac{k \varepsilon u}{\Omega} f_p \\ \text{Var}(\Delta p_x) &= \frac{2}{|x|k} \left( \frac{k \varepsilon u}{\Omega} \right)^2 \text{Var}(f_p)\end{aligned}\quad (63)$$

where  $u = 1$  for system (3) and  $u = |x|$  for system (5). For system (4), Eq. (62) takes the form (see Eq. (33)):

$$\begin{aligned}\langle \Delta p_x \rangle &= -\left(1 - v_{\text{res}}^2\right)^{3/2} \sqrt{\frac{2}{|x|k}} \frac{k \varepsilon}{\Omega} f_p \\ \text{Var}(\Delta p_x) &= \left(1 - v_{\text{res}}^2\right)^3 \frac{2}{|x|k} \left( \frac{k \varepsilon}{\Omega} \right)^2 \text{Var}(f_p)\end{aligned}\quad (64)$$

Eqs. (62) show that scattering on resonance results in variation of particle momentum (equivalently, in variation of particle energy). For systems with  $a > 1$ , this variation contains both a regular change (drift)  $\langle \Delta p_x \rangle \neq 0$  and diffusive variations. For  $a < 1$ ,  $\langle \Delta p_x \rangle = 0$  and only diffusive variations are present. This diffusion leads to  $p_x \sim \sqrt{\text{Var}(\Delta p_x)} \sim \sqrt{t/k}$  variation with  $\text{Var}(\Delta p_x) \sim 1/k \ll 1$ , whereas regular change  $\langle \Delta p_x \rangle \sim 1/\sqrt{k}$  leads to variation  $p_x \sim t/\sqrt{k}$  [107].

The number of resonant interactions (resonance crossings) for one period of slow variables may be different for different system configurations (slow phase portrait and the shape of the resonance manifold). In terms of the energy (momentum) change due to scattering on resonance, there are two main types of systems with  $a > 1$ . In systems of the first type occurring when there is a certain symmetry of the slow phase portrait, mean changes of energy (momentum) for one period of slow variable oscillations compensate each other. In this case, particle scattering leads to diffusion without drift. In systems of the second type, an asymmetry of the slow variable phase portrait results in the net energy (momentum) change, causing the drift in energy.

**Section summary** In this section we described the energy change of a particle during the scattering on resonance. If the resonant system contains a separatrix ( $S_{\text{res}} \neq 0$ ), there is a finite mean energy change due to scattering, and multiple scatterings lead to a directed acceleration/deceleration of particles. In absence of the separatrix, there is no mean energy change, and the energy change over multiple scatterings is diffusive.

## 5. Evolution of a particle ensemble

This section explains how effects of scattering and trapping can be included into kinetic equations describing the long-time evolution of particle distribution functions in the phase space. In Section 5.1 we consider diffusion due to scattering and demonstrate that for different systems this diffusion can be limited or unlimited. In Section 5.3 we discuss possible approaches to include trapping effects into kinetic equations.

### 5.1. Diffusive scattering and correlations

This subsection discusses diffusion in systems where the average drift due to scattering (see Eq. (58)) is absent. We consider two examples to demonstrate two distinct cases: when diffusion leads to an unlimited acceleration and when the diffusive acceleration is limited. The only significant difference between these quite similar plasma systems is that in the first case we deal with a constant frequency of particle oscillations in absence of wave, and in the second case the frequency depends on particle energy. This difference defines the long-term dynamics of resonant particles. In the system with a constant frequency, at high energies the consecutive scatterings become correlated, and the energy diffusion stops. In the energy-depending frequency, a correlation between two successive resonant interactions is destroyed and the diffusion is unlimited [e.g., 108].

#### 5.1.1. System with a constant frequency

We start with system (5) described by following Hamiltonian (see [109]):

$$\begin{aligned} H &= \frac{1}{2}p_x^2 + \frac{1}{2}\Omega^2x^2 + \varepsilon x \sin \phi \\ \phi &= kx - \omega t \end{aligned} \quad (65)$$

where the frequency of particle oscillations  $\Omega = \text{const}$ . Hamiltonian equations for this system are

$$\begin{aligned} \dot{x} &= p_x \\ \dot{p}_x &\approx -\Omega^2x - \varepsilon kx \cos \phi \end{aligned} \quad (66)$$

In Eq. (66), we omitted the term  $\sim \varepsilon \cos \phi \ll kx \varepsilon \cos \phi$ . The equation for  $\phi$  is

$$\ddot{\phi}/k = -\Omega^2x - \varepsilon kx \cos \phi \quad (67)$$

This equation corresponds to the following Hamiltonian (cf. Eq. (34)):

$$H_\phi = \frac{1}{2}k^2P_\phi^2 + \frac{\Omega^2x}{k}\phi + \varepsilon x \sin \phi \quad (68)$$

where the momentum  $P_\phi = \dot{\phi}/k^2$  is conjugate to  $\phi$ . The derivation of Hamiltonian (68) is totally similar to that of Hamiltonian (34). The variation of particle energy with time is (see Eq. (65))

$$\frac{d}{dt}h = \varepsilon \omega x \cos \phi \quad (69)$$

Thus, for the change of energy for one resonance crossing we have

$$\Delta h = 2\varepsilon \omega x \int_{-\infty}^{t^*} \cos \phi dt = \frac{2\varepsilon \omega |x|}{k^2} \int_{-\infty}^{\phi^*} \frac{\cos \phi}{P_\phi} d\phi = v_{\text{res}} \sqrt{2\varepsilon |x|} \int_{-\infty}^{\phi^*} \frac{\sqrt{a} \cos \phi}{\sqrt{(\phi^* - \phi) + a(\sin \phi^* - \sin \phi)}} d\phi \quad (70)$$

where  $v_{\text{res}} = \omega/k$ ,  $a = k\varepsilon/\Omega^2$ ,  $t^*$  is the moment when a particle crosses the resonance  $\dot{\phi} = 0$  ( $\phi^*$  is a corresponding phase value). The change  $\Delta h$  depends on  $\phi^*$ , and can be treated as a random variable. We consider  $a < 1$ , therefore  $f_p(a) = 0$  (see Section 4).

To analyze how the energy changes with time for an ensemble of particles, we consider the geometry of the motion of the particle. In the leading approximation, a phase point in the  $(\Omega x, p_x)$  plane moves along a Larmor circle with a radius of  $\sqrt{2h}$ . Particles cross the resonance line  $p_x = \dot{x} = v_{\text{res}}$  if  $h > v_{\text{res}}^2/2$ . The time between two consecutive intersections is  $2\arccos(v_{\text{res}}/\sqrt{2h})/\Omega$ . The wave phase gain over this time is

$$\Delta\phi = \int (k\dot{x} - \omega) dt = \frac{2k}{\Omega} \sqrt{2h - v_{\text{res}}^2} - 2\frac{\omega}{\Omega} \arccos(v_{\text{res}}/\sqrt{2h}) \quad (71)$$

When the energy is not too high, this phase gain can be considered as a random variable due to energy changes  $\Delta h$ . Since  $k$  and  $\omega$  are large, a small change in  $h$  leads to a large change in the phase gain. For this reason, the phase values at successive passages through resonance can be treated as independent random variables. Accumulation of multiple energy changes  $\Delta h$  given by Eq. (70) results in diffusion: the sum of random changes  $\Delta h$  is equal to zero, but the variance of  $\Delta h$  is finite. The energy grows until the assumption of independence of  $\Delta\phi$  is valid. However, as the energy increases, the phase gain between successive passages through resonance becomes more deterministic

$$\Delta h \frac{\partial \Delta\phi}{\partial h} \sim h^{-1/4} \rightarrow 0 \quad (72)$$

Therefore, the resonant particle motion becomes regular and the diffusion stops. This result can be independently obtained from the KAM theory [104], which predicts that there is an energy  $h^*$  beyond which the diffusion vanishes. Thus, in systems with constant frequency of unperturbed particle oscillations the diffusion is limited.

### 5.1.2. System with a frequency depending on energy

The second system considered in this subsection is a relativistic analog of system (65). Hamiltonian of this system resembles Hamiltonian (4) but with a more complicated wave amplitude [110]:

$$\begin{aligned} H &= \gamma + \varepsilon x \gamma^{-1} \sin \phi \\ \gamma &= \sqrt{1 + p_x^2 + \Omega^2 x^2} \\ \phi &= kx - \omega t \end{aligned} \quad (73)$$

The factor  $\gamma^{-1}$  comes from the expansion of the initial Hamiltonian for a relativistic particle interacting with an electromagnetic wave [110]. The corresponding Hamiltonian equations can be written as

$$\begin{aligned} \dot{x} &= \frac{p_x}{\gamma} \\ \dot{p}_x &\approx -\frac{\Omega^2}{\gamma} x - \frac{\varepsilon}{\gamma} kx \cos \phi \\ \phi &= kx - \omega t \end{aligned} \quad (74)$$

Frequency of particle oscillations in the  $(x, p_x)$  plane,  $\sim \Omega/\gamma$ , depends on particle energy. Eqs. (33), (34) define  $H_\phi$  near the resonance:

$$\begin{aligned} H_\phi &= \frac{1}{2} g(x) P_\phi^2 + r(x) \phi - \frac{\varepsilon}{\gamma_{\text{res}}} x \sin \phi \\ g &= \frac{(1 - \nu_{\text{res}}^2)^{3/2} k^2}{\sqrt{1 + \Omega^2 x^2}} \\ r &= -\frac{\Omega^2 x}{k} \frac{1}{\sqrt{1 - \nu_{\text{res}}^2} \sqrt{1 + \Omega^2 x^2}} \end{aligned} \quad (75)$$

where  $\nu_{\text{res}} = \omega/k$ , the momentum  $P_\phi = \dot{\phi}/g$  is conjugate to  $\phi$ , and

$$\gamma_{\text{res}} = \frac{\sqrt{1 + \Omega^2 x^2}}{\sqrt{1 - \nu_{\text{res}}^2}} \quad (76)$$

Following (38), we have

$$a = -\frac{\varepsilon x}{\gamma_{\text{res}} r_0 k} = \frac{\varepsilon (1 - \nu_{\text{res}}^2)}{\Omega^2} \quad (77)$$

When  $a < 1$ , the particle energy changes at the resonance due entirely to scattering:  $\langle \Delta h = 0 \rangle$  (see Sect 4), but the dispersion is non-zero. Thus the particle energy diffuses.

According to Hamiltonian (73), the time derivative of energy is

$$\frac{d}{dt} h = \frac{\varepsilon \omega x}{\gamma_{\text{res}}} \cos \phi \quad (78)$$

Taking into account that  $\dot{\phi} = g P_\phi$ , we find for the variation of the energy at one resonance crossing (cf. Eq. (70))

$$\Delta h = \sqrt{\frac{2\varepsilon |x| \omega^2}{g \gamma_{\text{res}}}} \int_{-\infty}^{\phi^*} \frac{\sqrt{a} \cos \phi}{\sqrt{\phi + a \sin \phi - \phi^* - a \sin \phi^*}} d\phi = \frac{\nu_{\text{res}} \sqrt{2\varepsilon |x|}}{\sqrt{1 - \nu_{\text{res}}^2}} \int_{-\infty}^{\phi^*} \frac{\sqrt{a} \cos \phi}{\sqrt{\phi + a \sin \phi - \phi^* - a \sin \phi^*}} d\phi \quad (79)$$

where  $\phi^*$  and  $x$  are the values of  $\phi$ ,  $x$  at the crossing of the resonant surface by an unperturbed trajectory with energy  $h$ . From Hamiltonian equations (74), frequency of particle rotation  $\sim \Omega/\gamma$ . Thus, the time between two successive crossings is of order  $\gamma$ . Integrating equations of motion, the difference of phases at the first and the second resonance crossings is  $\phi_*^{(2)} - \phi_*^{(1)} \sim k\gamma$  (cf. Eq. (71)). Thus, a small variation  $\delta\phi_*^{(1)}$  of the phase  $\phi_*^{(1)}$  results in a variation of the energy change  $\delta(\Delta h) \sim \sqrt{\gamma/k} \delta\phi_*^{(1)}$  at the first resonance crossing. The resulting change  $\delta\phi_*^{(2)}$  is large:

$$\delta\phi_*^{(2)} = \delta(\Delta h) \frac{\partial}{\partial \gamma} (\phi_*^{(2)} - \phi_*^{(1)}) \sim \delta(\Delta h) k \sim \phi_*^{(2)} \sqrt{k\gamma} \gg \phi_*^{(2)} \quad (80)$$

Therefore, the values of phase at successive resonance crossings are statistically independent. Hence, the changes in the particles energy at the resonance produce a diffusive variation of the energy and its unlimited stochastic growth. Which is different from nonrelativistic system (65) where energy diffusion slows down and finally stops at large enough energies.

Two examples (Hamiltonians (65) and (73)) demonstrate the importance of the energy dependence of the frequency of unperturbed particle motion (in absence of waves) for resonant wave-particle interaction. In realistic plasma systems this frequency can rarely be assumed to be constant, but it is the case in many simplified models.

### 5.2. Relation between trapping and scattering

In this subsection we describe the relationship between the average change of momentum on scattering,  $\langle \Delta I \rangle$ , and the probability of trapping,  $\Pi$ . We repeat derivations from [111] and then provide a new expression for  $\langle \Delta I \rangle$ .

Consider Hamiltonian (34):

$$H_\phi = \frac{1}{2} g p_\phi^2 + r\phi - \varepsilon u \sin \phi \quad (81)$$

where the evolution of slow variables  $(x, P_x)$  is described by the Hamiltonian  $\Lambda(x, P_x)$ . The change of the momentum  $I$  due to scattering on resonance is given by Eq. (58):

$$\Delta I = -\sqrt{\frac{2}{g|r|}} \varepsilon u \int_{-\infty}^{\phi^*} \frac{\cos \phi}{\sqrt{h_\phi - \phi + a \sin \phi}} d\phi \quad (82)$$

where  $h_\phi = a \sin \phi^* + \phi^*$ . The average  $\langle \Delta I \rangle$  change is

$$\langle \Delta I \rangle = -\frac{1}{2\pi} \sqrt{\frac{2|r|}{g}} \int_{-\infty}^{\phi^*} d\phi \int_0^{2\pi} \frac{a \cos \phi dh_\phi}{\sqrt{h_\phi - \phi + a \sin \phi}} \quad (83)$$

We introduce  $\tilde{h}_\phi$  as

$$\tilde{h}_\phi = \begin{cases} 0, & \phi < \phi_X \\ \phi - a \sin \phi, & \phi > \phi_X \end{cases} \quad (84)$$

where  $\phi_X$  is a solution of the equations  $a \cos \phi = 1$ ,  $a \sin \phi > 0$ , and  $h_X = -\phi_X + a \sin \phi_X$  (see Fig. 4). Then we separate integral (83) into two parts:

$$\int_{-\infty}^{\phi^*} \int_0^{2\pi} \frac{a \cos \phi dh_\phi d\phi}{\sqrt{h_\phi - \phi + a \sin \phi}} = \int_{-\infty}^{\phi_X+2\pi} \int_{\tilde{h}_\phi+h_X}^{2\pi+h_X} \frac{a \cos \phi dh_\phi d\phi}{\sqrt{h_\phi - \phi + a \sin \phi}} - \int_{\phi_X}^{\phi_{\max}} \int_{\tilde{h}_\phi+h_X}^{h_X} \frac{a \cos \phi dh_\phi d\phi}{\sqrt{h_\phi - \phi + a \sin \phi}} \quad (85)$$

where  $\phi_{\max}$  is a solution of equation  $\phi_X - a \sin \phi_X - \phi + a \sin \phi = 0$ . Then we consider the first integral from Eq. (85):

$$\begin{aligned} \int_{-\infty}^{\phi_X+2\pi} \int_{\tilde{h}_\phi+h_X}^{2\pi+h_X} \frac{a \cos \phi dh_\phi d\phi}{\sqrt{h_\phi - \phi + a \sin \phi}} &= 2 \int_{-\infty}^{\phi_X+2\pi} a \cos \phi \left( \sqrt{2\pi + h_X - \phi + a \sin \phi} - \sqrt{\tilde{h}_\phi + h_X - \phi + a \sin \phi} \right) d\phi \\ &= 2 \int_{-\infty}^{\phi_X} a \cos \phi \left( \sqrt{2\pi + h_X - \phi + a \sin \phi} - \sqrt{h_X - \phi + a \sin \phi} \right) d\phi \\ &\quad + 2 \int_{\phi_X}^{\phi_X+2\pi} a \cos \phi \sqrt{2\pi + h_X - \phi + a \sin \phi} d\phi \\ &= \lim_{N \rightarrow \infty} 2 \int_{\phi_X-2\pi N}^{\phi_X} a \cos \phi \left( \sqrt{2\pi + h_X - \phi + a \sin \phi} - \sqrt{h_X - \phi + a \sin \phi} \right) d\phi \\ &\quad + 2 \int_{\phi_X}^{\phi_X+2\pi} a \cos \phi \sqrt{2\pi + h_X - \phi + a \sin \phi} d\phi \\ &= -2 \int_{\phi_X-2\pi}^{\phi_X} a \cos \phi \sqrt{h_X - \phi + a \sin \phi} d\phi \\ &\quad + 2 \int_{\phi_X}^{\phi_X+2\pi} a \cos \phi \sqrt{2\pi + h_X - \phi + a \sin \phi} d\phi = 0 \end{aligned} \quad (86)$$

where we took into account that integral (82) is periodic over  $h_\phi$  (see Section 4). The second integral in Eq. (85) is

$$\begin{aligned} \int_{\phi_X}^{\phi_{\max}} \int_{\tilde{h}_\phi+h_X}^{h_X} \frac{a \cos \phi dh_\phi d\phi}{\sqrt{h_\phi - \phi + a \sin \phi}} &= 2 \int_{\phi_X}^{\phi_{\max}} a \cos \phi \sqrt{h_X - \phi + a \sin \phi} d\phi \\ &= 2 \int_{\phi_X}^{\phi_{\max}} (a \cos \phi - 1) \sqrt{h_X - \phi + a \sin \phi} d\phi + 2 \int_{\phi_X}^{\phi_{\max}} \sqrt{h_X - \phi + a \sin \phi} d\phi = 2 \int_{\phi_{\max}}^{\phi_X} \sqrt{h_X + \phi - a \sin \phi} d\phi \end{aligned} \quad (87)$$

We substitute Eqs. (86), (87) into Eq. (83)

$$\langle \Delta I \rangle = -\frac{1}{\pi} \sqrt{\frac{2|r|}{g}} \int_{\phi_X}^{\phi_{\max}} \sqrt{(\phi_X - \phi) + a(\sin \phi - \sin \phi_X)} d\phi \quad (88)$$

Comparing Eq. (88) and Eq. (40), we obtain:

$$\langle \Delta I \rangle = -\frac{1}{\pi} \sqrt{\frac{2|r|}{g}} \int_{\phi_X}^{\phi_{\max}} \sqrt{(\phi - \phi_X) - a(\sin \phi - \sin \phi_X)} d\phi = \frac{1}{\pi} \sqrt{\frac{2|r|}{g}} f_s(a) = -\frac{S_{\text{res}}}{2\pi} \quad (89)$$

Thus, the average change of the momentum is proportional to the area  $S_{\text{res}}$ . Comparison of Eq. (40), Eq. (58), and Eq. (89) yields a relation between  $f_s(a)$  and  $f_p(a) = \langle f_p(h_\phi, a) \rangle_{h_\phi}$ :

$$f_p(a) = -2f_s(a)/a \quad (90)$$

Let  $V = \langle \Delta I \rangle$  be a velocity of drift in the momentum space. This velocity depends on slow variables  $(x, P_x)$  along the resonance trajectory, i.e., we can write  $V(x, P_x) = V(x, P_{\text{res}}(x)) = V(x) = V(I_{\text{res}})$  where  $I_{\text{res}} = I_{\text{res}}(x, P_{\text{res}})$  and  $P_{\text{res}}(x)$  are defined by Eqs. (30) and (14). Therefore, we can consider function  $V(I)$  where  $I = I_{\text{res}}$  in the resonance. The gradient  $dV/dt$  along the resonant trajectory is

$$\frac{dV}{dt} = \{V, \Lambda\} = \frac{dV}{dI} \frac{dI}{dt} = \frac{dV}{dI} \{I_{\text{res}}, \Lambda\} = \frac{dV}{dI} r \quad (91)$$

where  $r = \{I_{\text{res}}, \Lambda\}$ , see Eq. (28). Comparing Eq. (89) and Eq. (47), we obtain

$$\frac{dV}{dI} = -\frac{\{S_{\text{res}}, \Lambda\}}{2\pi r} = -\Pi \quad (92)$$

Eq. (92) gives a straightforward relation between probability of trapping  $\Pi$  and velocity of drift  $V$ .

### 5.3. Kinetic equation for trapped and transient particles

Using relation (92) for  $V$  and  $\Pi$ , we will derive an evolution equation for the distribution function of particles interacting with waves. For the sake of simplicity, we focus on a simple but rather general  $1\frac{1}{2}$  degrees of freedom system with the Hamiltonian  $H = G(\tau, I) + \varepsilon u(\tau, I) \cos \phi$ . Here  $(\phi, I)$  are conjugate variables, with  $I$  being the normalized particle momentum. In this system the phase  $\phi$  changes at a rate  $\sim 1$  (much faster than the slow time  $\tau = \varepsilon t$ ). The resonant condition  $\dot{\phi} = \partial G / \partial I = 0$  has a solution  $I = I_{\text{res}}(\tau)$ . Expansion around  $I_{\text{res}}$  gives the following Hamiltonian

$$\mathcal{F} = \Lambda + \frac{1}{2}g(I - I_{\text{res}})^2 + \varepsilon u \cos \phi \quad (93)$$

where  $\Lambda(\tau) = G(\tau, I_{\text{res}}(\tau))$ ,  $g(\tau) = (\partial^2 G / \partial I^2)_{I=I_{\text{res}}}$ ,  $u(\tau) = u(\tau, I_{\text{res}}(\tau))$ . We introduce new variable  $P_\phi = (I - I_{\text{res}})$  (see Eq. (22)) and rewrite the new Hamiltonian  $H_\phi = \mathcal{F} - \Lambda$  as

$$H_\phi = \frac{1}{2}gP_\phi^2 + r\phi + \varepsilon u \cos \phi \quad (94)$$

where  $r = dI_{\text{res}}/dt$  and  $(\phi, P_\phi)$  are conjugate variables.

For the sake of definiteness we consider  $r > 0$  and  $g > 0$ . For  $a(\tau) = \varepsilon u/r > 1$  the phase portrait of Hamiltonian (94) contains a region filled with closed trajectories. The area of this region,  $S_{\text{res}}$ , and the probability of trapping,  $\Pi$ , are both small,  $\sim \sqrt{\varepsilon}$ . Once trapped, particles move in resonance with the wave until the value of  $S_{\text{res}}(\tau)$  returns to its value at the moment of trapping  $\tau_{\text{trap}}$ , Fig. 12. During the trapped motion, the particle momentum  $I$  varies following  $I_{\text{res}}$ , and the particles escape from resonance with larger (or smaller) values of  $I$  (correspondingly with larger (or smaller) values of the energy  $H(I, \tau)$ ). This effect corresponds to the particle acceleration by trapping. Since the duration of trapping can be rather long and variations of  $I$  can be large (both are independent of  $\varepsilon$ ), this process cannot be described as a local diffusion.

Transient particles passing through resonance without being trapped are scattered with a change of momentum  $\Delta I$  given by Eq. (82). Two quantities describe the evolution of a particle distribution  $\Psi(I)$  due to nonlinear and quasi-linear scattering: the velocity of drift  $V = \langle \Delta I \rangle / \tau_0$  and the diffusion coefficient  $D = \langle (\Delta I)^2 \rangle / 2\tau_0$ , where  $\tau_0$  is the time between two successive passages through resonance. This expression for the diffusion coefficient  $D$  coincides with the formula derived previously for a narrow wave spectrum in the quasi-linear theory [108]. Coefficients  $\Pi(\tau)$ ,  $V(\tau)$ ,  $D(\tau)$  can be rewritten as  $\Pi(I)$ ,  $V(I)$ ,  $D(I)$  because  $I = I_{\text{res}}(\tau)$  at resonance.

A trapping/escape event can be considered as a rapid change  $I \rightarrow I'$ , where  $I'$  is defined by equations  $I' = I_{\text{res}}(\tau_{\text{esc}})$ ,  $S_{\text{res}}(\tau_{\text{trap}}) = S_{\text{res}}(\tau_{\text{esc}})$ , see Fig. 12. The functions  $S_{\text{res}}(\tau)$  and  $I_{\text{res}}(\tau)$  can be combined to get  $S_{\text{res}}(I_{\text{res}}) = S_{\text{res}}(I)$  as  $I = I_{\text{res}}$  at the resonance. Using  $D$ ,  $V$ , and  $\Pi/\tau_0$  we can write a Fokker–Planck equation describing the full evolution of the particle distribution function  $\Psi(I)$  due to both scattering and trapping:

$$\frac{\partial \Psi}{\partial t} = \frac{\partial}{\partial I} \left( D \frac{\partial \Psi}{\partial I} \right) - \frac{\partial (V\Psi)}{\partial I} + \int_0^\infty (\Psi(\tilde{I}) Q_{\tilde{I} \rightarrow I} - \Psi(I) Q_{I \rightarrow \tilde{I}}) d\tilde{I} \quad (95)$$

Here  $Q_{I' \rightarrow I}$  is probability of a particle *coming to*  $I$  via trapping, and  $Q_{I \rightarrow I'}$  is probability of a particle *leaving from*  $I$ . For  $I > I_0$ , the area  $S_{\text{res}}$  grows and there is a finite  $Q_{I \rightarrow I'} = (\Pi(I)/\tau_0)\delta(w(I) - I')$ . For  $I < I_0$ , the area  $S_{\text{res}}$  decreases and particles escape from resonance:  $Q_{I' \rightarrow I} = (\Pi(I')/\tau_0)\delta(I - w(I'))$ . In both cases, the input-output function  $w(I')$  gives the value  $I' > I_0$  that particles should have when getting trapped to escape from resonance with  $I < I_0$ . The function  $w$  is defined by the

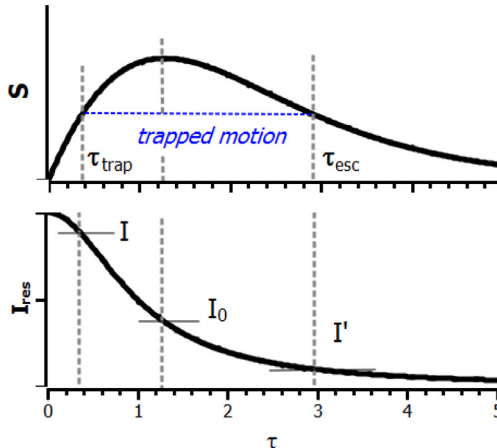


**Fig. 12.** A schematic view of the area  $S_{\text{res}}(\tau)$  and the resonant momentum  $I_{\text{res}}(\tau)$ . A particle is trapped at  $\tau = \tau_{\text{trap}}$  when  $S_{\text{res}}$  grows and  $I = I_{\text{res}}$ . During trapped motion, the momentum varies as  $I_{\text{res}}(\tau)$ . When, at  $\tau = \tau_{\text{esc}}$ ,  $S_{\text{res}}(\tau)$  returns back to  $S_{\text{res}}(\tau_{\text{trap}})$ , the particle escapes from resonance. After the escape, the particle has a momentum  $I_{\text{res}}(\tau_{\text{esc}}) = I'$ . For the sake of simplicity, we consider here systems with a single maximum of  $S_{\text{res}}$  at  $I = I_0$ .

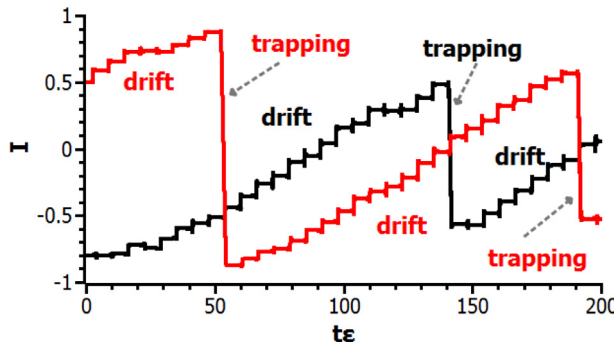


**Fig. 13.** Two test trajectories (shown by black and red lines) for Hamiltonian (93). (For interpretation of the references to colour in this figure legend, the reader is referred to the web version of this article.)

$S_{\text{res}}(I)$  profile, see Fig. 12.  $\Pi(I')$  is the probability of particle trapping at  $I' > I_0$ . The integral operator in Eq. (95) can then be expressed as  $-\Psi(I)\Pi(I)/\tau_0$  for  $I > I_0$  and  $\Psi(I')\Pi(I')|dw/dI'|^{-1}/\tau_0 = (dV/dI)\Psi(I')$  for  $I < I_0$ , where we used

$$\frac{dw(I')}{dI'} = \frac{dI}{dI'} = \frac{dV(I')/dI'}{dV(I)/dI} = -\frac{\Pi(I')/\tau_0}{dV(I)/dI}$$

and  $V(I') = V(I)$  because  $S_{\text{res}}(\tau_{\text{trap}}) = S_{\text{res}}(\tau_{\text{esc}})$ . Using these expressions and Eq. (92), we can rewrite Eq. (95) in its final form

$$\frac{\partial \Psi}{\partial t} = \frac{\partial}{\partial I} \left( D \frac{\partial \Psi}{\partial I} \right) - V \frac{\partial \Psi}{\partial I} - \frac{dV}{dI} (\Psi - \Psi(I')) \Theta(I) \quad (96)$$

where  $I'$  is defined by  $w(I') = I$  and

$$\Theta(I) = \begin{cases} 1, & I < I_0 \\ 0, & I \geq I_0 \end{cases}$$

Eq. (96) is a Fokker–Planck equation generalized to include (1) the drift  $V$  due to the mean change of the nonlinear scattering and (2) nonlocal term ( $\sim \Psi(I) - \Psi(I')$ ) corresponding to the fast transport in phase space due to trapping. The timescale of diffusion is  $\varepsilon^{-1}$  (since  $D \sim \varepsilon$ ), whereas the timescales of drift and trapping-induced transport (determined by  $V$ ,  $dV/dI$ ) are much shorter  $\sim \varepsilon^{-1/2}$ . For systems with small wave amplitudes ( $a < 1$ ),  $V$  and  $dV/dI$  vanish and Eq. (96) reduces to the usual quasi-linear diffusion equation.

To check Eq. (96), we compared its solution with results of numerical integration of the initial system (93). We considered a simple example of Hamiltonian (93) with  $\Lambda = 0$ ,  $g = 1$ ,  $I_{\text{res}} = \sin \tau$ . The function  $B(\tau)$  a periodic function of  $\tau$  with a period  $\tau_0 = 2\pi/\varepsilon$ . It has a single maximum in  $\tau \in [\tau_0/4, 3\tau_0/4]$  and is zero for  $\tau \in [0, \tau_0/4]$ ,  $[3\tau_0/4, \tau_0]$ . The resonant momentum  $I_R$  varies from  $-1$  to  $1$  and all particles pass through resonance over one period  $\tau_0$ . Fig. 13 shows two test trajectories calculated over a long time interval. Particles are trapped at a positive  $I$  and transported to negative  $I$  (in this

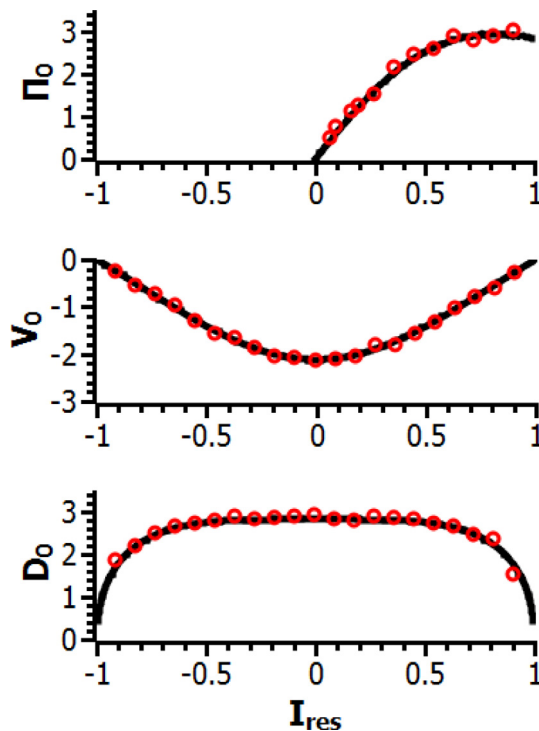


**Fig. 14.** Analytical expressions (black curves) and numerical results (red circles) for  $\Pi_0 = \Pi \tau_0 / \sqrt{\varepsilon}$ ,  $V_0 = V \tau_0 / \sqrt{\varepsilon}$ , and  $D_0 = D \tau_0 / \varepsilon$ . (For interpretation of the references to colour in this figure legend, the reader is referred to the web version of this article.)

system  $I_0 = 0$ ), whereas nonlinear drift  $V$  transports particles back from negative  $I$  to positive  $I$ . Both processes of trapping and drift coexist with the diffusive scattering. Particle behavior shown in Fig. 13 is a typical behavior in plasma systems with nonlinear wave-particle interactions.

For our test system, we calculate  $\Pi$ ,  $V$ , diffusion coefficient  $D$ , and function  $w(I)$ , and express them as functions of  $I = I_R$  (to calculate  $D$  and  $V$  we use the approximations from Fig. 11). To check the analytical formulas for  $\Pi$ ,  $V$ , and  $D$ , we integrated numerically  $10^7$  trajectories with different initial  $I$  and calculated changes  $\Delta I$  over a period  $\tau_0$  that contained a single resonant interaction. The ratio of the number of particles which were trapped into resonance to the total number of particles gives the numerical probability of trapping  $\Pi$ . For untrapped particles, we calculate the average value of  $\Delta I$  and its variance  $\text{Var}(\Delta I)$ . These two functions, depending on the initial  $I$ , are then used to calculate the numerical values of  $V$  and  $D$ . Fig. 14 demonstrates that our analytical expressions quite accurately describe the trapping probability, drift velocity, and diffusion coefficient.

We substituted coefficients  $V$  and  $D$  into Eq. (96) and solved it numerically for a particular initial distribution  $f_0(I)$ . In Fig. 15, this solution is compared with direct numerical simulation of  $10^7$  test particle trajectories for Hamiltonian (93). All expected effects of trapping and scattering are recovered: (1) fast transport of trapped particles from the initial distribution peak at positive  $I$  toward negative  $I$ ; (2) particle nonlinear drift toward positive  $I$ ; and (3) a slower diffusive flattening. Fig. 15 shows that Eq. (96) accurately describes all the major effects of nonlinear as well as quasi-linear wave-particle interactions.

**Section summary** In this section we considered the evolution of particle distribution function due to resonant effects. For systems without the separatrix on the resonance plane, the energy drift is absent and we describe the effect energy diffusion. If the time between two resonance crossings does not depend on particle energy, the diffusive energy gain is limited. For systems with the separatrix, the energy drift due to trapping and nonlinear scattering dominates over the diffusion. Using the relation between trapping probability and scattering amplitude (see Eq. (92)), we derive generalized kinetic equation (96) including both trapping and nonlinear scattering effects.

## 6. Particle acceleration in nonrelativistic plasma systems

In this section we consider several nonrelativistic plasma systems with particle trapping. We start with a simple system where an electrostatic wave propagates across a weak homogeneous magnetic field (Section 6.1). In Section 6.2 we describe a similar system, but instead of an electrostatic wave we consider a strong electromagnetic pulse (solitary wave). In Section 6.3 we consider electrostatic wave resonating with charged particles in the systems with inhomogeneous background magnetic field.

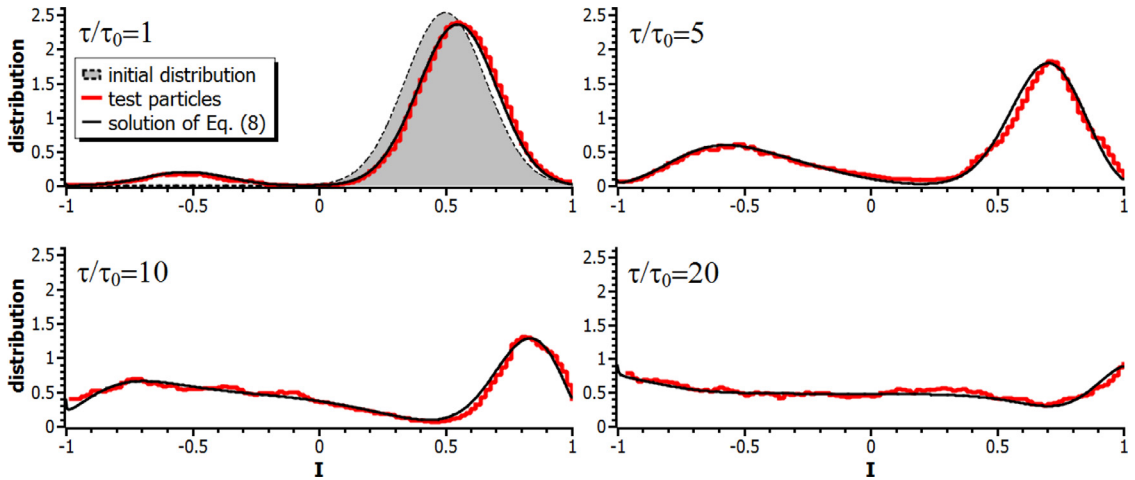


**Fig. 15.** Particle distribution function  $\Psi(I)$  at four moments of time. The initial distribution is displayed in grey, black curves show the numerical solution of generalized Fokker-Planck equation (96), and red curves are obtained from direct numerical integration of Hamiltonian system (93) with  $10^7$  different initial conditions  $(I, \phi)$ . (For interpretation of the references to colour in this figure legend, the reader is referred to the web version of this article.)

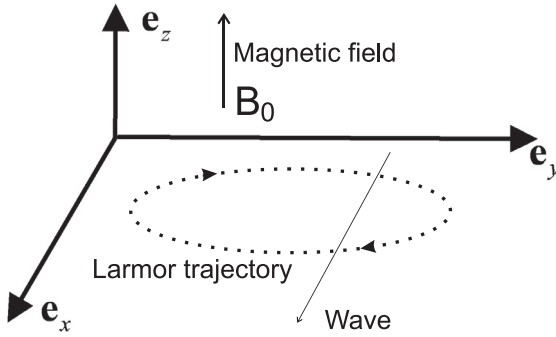


**Fig. 16.** Schematic view of the system configuration.

Trapping is present when the electromagnetic field of the wave generates a force exceeding the Lorentz force of the background magnetic field. In this case the background magnetic field does not control particle motion and particles are effectively *demagnetized*. The Larmor (gyro-) rotation of particles is transformed into motion along the wave electric field and particles are accelerated.

All physical systems considered in this section can be described using a 1D or 2D configuration space. A background magnetic field  $B_0$  is directed along the  $z$ -axis, particles move along  $B_0$  and rotate around  $B_0$  in the  $(x, y)$  plane (see Fig. 16). In the case of an inhomogeneous magnetic field  $B_0(z)$ , the Maxwell equations require the presence of an additional magnetic field component  $B_{0x} = -d(\int B_0(z, \tilde{x})d\tilde{x})/dz$  directed along the  $x$ -axis [112]. The corresponding vector potential still has a single component  $\mathbf{A} = A_y \mathbf{e}_y = (\int B_0(z, \tilde{x})d\tilde{x}) \mathbf{e}_y$ . An external *inductive* electric field  $E_y$  can be included in the Hamiltonian as an additional term  $-c \int E_y(t)dt$  in  $A_y$ , whereas an external *electrostatic* field  $E_z, E_x$  can be described by a scalar potential  $\Phi(x, z, t)$ . Hamiltonian of a particle with a charge  $e$  and mass  $m$  is

$$H = \frac{1}{2m} (p_x^2 + p_z^2) + \frac{1}{2m} \left( p_y - \frac{e}{c} A_y(x, z, t) \right)^2 + e\Phi(x, z, t) \quad (97)$$

Hamiltonian (97) does not depend on  $y$ , and this condition is satisfied in the perturbed system (in the presence of waves) as well. Thus,  $p_y = \text{const}$  and we can set  $p_y = 0$  via time shift (in case of  $E_y \neq 0$ ) or via shift of the origin of  $x$  axis. The Hamiltonian becomes

$$H = \frac{1}{2m} (p_x^2 + p_z^2) + \frac{1}{2m} \left( \frac{e}{c} A_y(x, z, t) \right)^2 + e\Phi(x, z, t) \quad (98)$$

The corresponding Hamiltonian equations are

$$\dot{x} = \frac{\partial H}{\partial p_x} = \frac{1}{m} p_x, \quad \dot{z} = \frac{\partial H}{\partial p_z} = \frac{1}{m} p_z$$

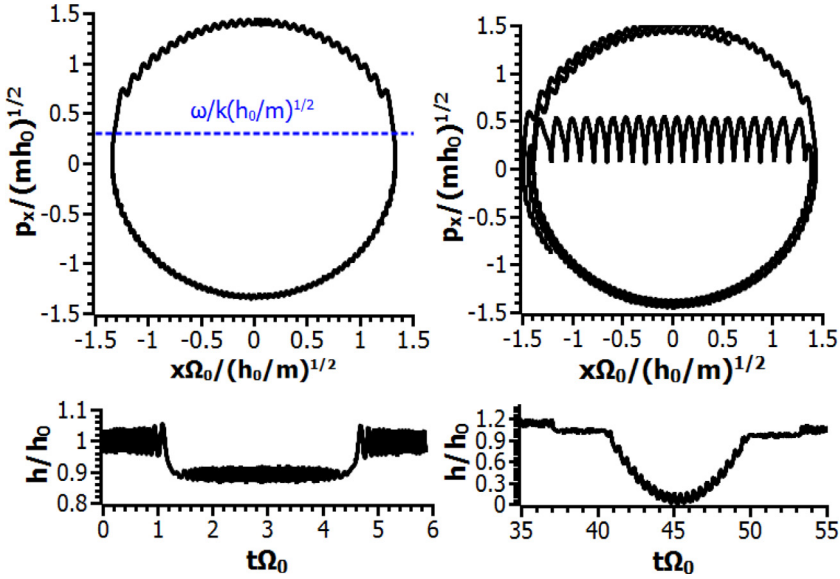


**Fig. 17.** Two particle trajectories of system (101): scattering (left panels) and trapping (right panels) are shown. System parameters are:  $\omega/k\sqrt{h_0/m} = 0.3$ ,  $\omega/\Omega_0 = 100$ , initial energy  $h_0 = 3(\omega/k)^2 m$ .

$$\begin{aligned}\dot{p}_x &= -\frac{\partial H}{\partial x} = \frac{e^2}{mc^2} B_0 A_y - e \frac{\partial \Phi}{\partial x} \\ \dot{p}_z &= -\frac{\partial H}{\partial z} = -\frac{e^2}{mc^2} B_{0x} A_y - e \frac{\partial \Phi}{\partial z}\end{aligned}\quad (99)$$

In case of  $B_0 = \text{const}$ ,  $E_y = 0$ ,  $\Phi = 0$  we obtain  $B_{0x} = 0$ , and the motion along  $z$  is decoupled from the motion in the  $(x, y)$  plane:  $p_z = \text{const}$ . Thus, Eqs. (99) can be rewritten as

$$m\dot{x} = p_x, \quad \dot{p}_x = m\Omega_0^2 x \quad (100)$$

where  $A_y = xB_0$ , and  $\Omega_0 = eB_0/mc$  is the Larmor (gyro-) frequency of particle oscillations around  $B_0$ . These oscillations are those of a linear pendulum.

### 6.1. Electrostatic wave propagating across a weak magnetic field

This subsection discusses a system where particles can be trapped by an electrostatic wave propagating across a sufficiently weak background magnetic field. Weakness of the magnetic field guarantees that gyrorotation is slow enough to consider wave phase as a fast variable. In this case, particles interact with waves through the Cherenkov resonance  $\mathbf{k} \cdot \mathbf{v} = \omega$  where  $\mathbf{v}$  is a particle velocity and  $\mathbf{k}$  is a wavevector. Such a configuration of a background magnetic field and a wave field is a classical problem of plasma physics: the Landau damping in presence of a weak magnetic field [42,113,114]. Some generalisation of results presented in this subsection can be found in [115,116].

Consider a nonrelativistic electron moving in a background uniform magnetic field  $B_0$  and a wave electrostatic field. The wave phase is  $\phi = \phi_0 + kx - \omega t$ , where  $\omega \gg \Omega_0 = eB_0/mc$  and the wave phase velocity  $v_\phi = \omega/k = \text{const}$  is similar to the particle velocity. The corresponding equations of motion are (see Eqs. (100))

$$m\dot{x} = p_x, \quad \dot{p}_x = m\Omega_0^2 x - ek\Phi_0 \cos \phi \quad (101)$$

where  $\Phi_0$  is the amplitude of the scalar potential. Particles may experience both scattering and trapping. The left panel in Fig. 17 shows particle trajectory without trapping. The particle moves around a closed trajectory in the  $(x, p_x)$  plane and crosses the resonance  $p_x = mv_\phi$  twice on one period. At each crossing there is a change of momentum  $p_x$  and energy  $h = p_x^2/2 + \Omega_0^2 x^2/2$ . When  $\Phi_0$  is large enough, this change has nonzero mean and a dispersion (see Section 4). At two consecutive crossings the changes of energy  $h$  have nonzero average values with the opposite signs, and these changes approximately compensate each other (see Fig. 17, left panel). If trapped, a particle leaves a closed trajectory in the  $(x, p_x)$  plane and starts moving along the resonant trajectory  $p_x = mv_\phi$  (see Fig. 17, right panel). Trapping occurs at a negative  $x$  and trapped particles move with a positive  $p_x$ . After trapping particle energy starts decreasing (see description in Section 3). When the trapped particle reaches  $x \sim 0$ , the energy  $h$  and the  $x$  coordinate start increasing and  $h$  returns to the initial value when  $x$  reaches  $-x_{\text{trap}}$ . At this position, the particle escapes from resonance and starts moving along a new closed trajectory in the  $(x, p_x)$  plane (see Fig. 17, right panel).

To consider particle motion near the resonance, we rewrite system (101) in terms of the phase  $\phi$ :

$$\frac{\ddot{\phi}}{k} = \Omega_0^2 \dot{x} - \frac{ek\Phi_0}{m} \cos \phi \quad (102)$$

As  $\omega \gg \Omega_0$ , the phase  $\phi$  changes significantly faster than the variable  $x$ . Thus we can consider  $x$  as a slowly changing parameter and Eq. (102) corresponds to the Hamiltonian:

$$H_\phi = \frac{1}{2} k^2 p_\phi^2 - \Omega_0^2 k^{-1} x \phi + \frac{ek\Phi_0}{m} \sin \phi \quad (103)$$

where  $P_\phi = \dot{\phi}/k^2$  is a momentum conjugate to  $\phi$ . Hamiltonian (103) coincides with the Hamiltonian (34) of a nonlinear pendulum with torque. The area  $S_{\text{res}}$  is shown in the left panel in Fig. 7, and is given by Eq. (42):

$$S_{\text{res}} = \frac{2\Omega_0}{k^{3/2}} \sqrt{2|x|} f_s(a), \quad a = \frac{ek\Phi_0}{m\Omega_0^2|x|} \quad (104)$$

When  $x < 0$ , the area  $S_{\text{res}}$  grows as  $(-x)$  decreases, see Fig. 17, and particle becomes trapped at  $x_{\text{trap}} < 0$ . The trapped particle moves from negative to positive  $x$ . When it reaches the coordinate  $x_{\text{res}} = -x_{\text{trap}}$ , the area  $S_{\text{res}}$  becomes equal to its value at the moment of trapping, and the trapped particle escapes from resonance. As a result of such trapping-escape event, the particle energy does not change more than by the value defined as a resonance width (63):

$$\Delta h = \frac{p_x}{2m} |\langle \Delta p_x \rangle| = \sqrt{\frac{1}{2k|x_{\text{trap}}|}} \frac{ekv_\phi\Phi_0}{\Omega_0} |f_p| = e\Phi_0 \frac{\omega}{\Omega_0} \sqrt{\frac{1}{2k|x_{\text{trap}}|}} |f_p| \quad (105)$$

If the wave amplitude is large enough ( $a \gg 1$  in Eq. (104)), then  $f_p \approx 2f_s/a \approx 8\sqrt{2/a}$  and Eq. (105) takes the form:

$$\Delta h = 8\sqrt{e\Phi_0 v_\phi^2 m} \quad (106)$$

Therefore, the resonance width (and a range of energy variation) is proportional to square root of wave amplitude and the energy of a resonant particle [117,118].

In terms of the energy evolution, scattering of particles on resonance can be considered as a combination of random changes with zero mean (diffusion) and some mean energy change (drift in energy space, see Eq. (64)). The the sign of momentum and energy changes is opposite at  $x_{\text{trap}}$  and  $x_{\text{esc}} = -x_{\text{trap}}$ . As a result, on one period of the Larmor rotation, particles change their energy by values distributed around zero (see Fig. 17). This scattering results in diffusion in energy space (see a detailed description in Section 5). Significant and fast energy change in such a system is possible only if an external force breaks the symmetry of trapping and escape coordinates making  $x_{\text{esc}}$  no longer equal to  $-x_{\text{trap}}$ . In this case, the difference of energies at the moment of trapping and escape is not zero [115].

## 6.2. Front of plasma injection

As shown in the previous subsection, trapping into resonance with an electrostatic wave does not result in the particle acceleration. A situation is different for electromagnetic waves [119,120]. An interesting example of the system with an electromagnetic wave has been recently found in the Earth magnetosphere, where transient reconnection of magnetic field lines runs strong plasma flows [121,122]. Propagating across a weak magnetic field, these flows generate strong electromagnetic perturbations localized near the leading edge of flows. Modern spacecraft observations demonstrate that plasma flows with characteristics configuration of electromagnetic fields are commonly detected in different planetary magnetospheres [123–125] and solar corona [see references in 126]. The leading front of such plasma flows represents the electromagnetic pulse (a strong electromagnetic soliton wave). Charged particles can be trapped into the Cherenkov resonance and accelerated by such a pulse [127,128].

A simple model of a plasma flow front describes a magnetic field directed along the  $z$ -axis and propagating with a constant velocity  $v_\phi$  along the  $x$ -axis:  $B_{z,f} = \delta B_z f(\phi)$ , where  $\delta B_z > B_0$  is an amplitude of the front magnetic field, and  $f(\phi)$  defines the distribution of the front field along the  $x$ -axis [127]. Several more general configurations were considered in [129,130]. Phase  $\phi = \phi_0 + (x - v_\phi t)/L$  depends on the front scale  $L$ , which is usually much smaller than the gyroradius of hot ions observed in planetary magnetospheres. The front electric field is equal to  $E_{y,f} = (v_\phi/c)B_{z,f}$ . The corresponding vector potential is  $A_{y,f} = \delta B_z L \int f(\phi) d\phi = \delta B_z L F(\phi)$ . An example of  $F(\phi)$  profile is shown in Fig. 18(a). Hamiltonian (98) of an ion moving in such an electromagnetic field is

$$H = \frac{1}{2m} p_x^2 + \frac{1}{2m} \frac{e^2}{c^2} (B_0 x + \delta B_z L F(\phi))^2 \quad (107)$$

where we set  $p_z = 0$ , because the Hamiltonian is independent of  $z$ . The Hamiltonian equations are

$$m\dot{x} = p_x, \quad \dot{p}_x = -\frac{1}{m} \frac{e^2}{c^2} (B_0 + \delta B_z f(\phi))(B_0 x + \delta B_z L F(\phi)) \quad (108)$$

Due to smallness of  $L$ , we can omit the term  $\sim L$  and rewrite Eqs. (108) as

$$m\dot{x} = p_x, \quad \dot{p}_x = -m\Omega_0^2 x (1 + b_z f(\phi)) \quad (109)$$

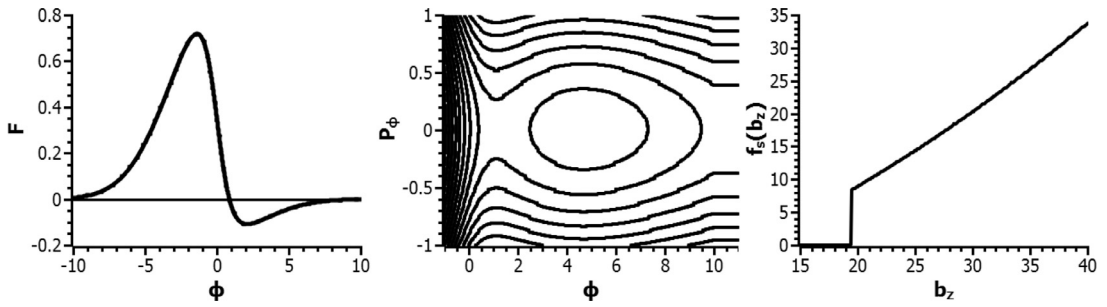


Fig. 18. Function  $F(\phi)$  (left panel), phase portrait of Hamiltonian  $H_\phi$ , Eq. (111) (central panel), function  $\tilde{f}_s(a)$  Eq. (112) (right panel).

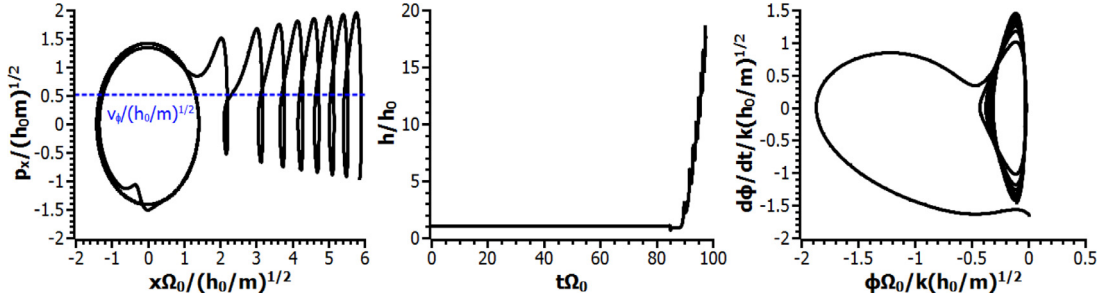


Fig. 19. Numerical integration of system (109). Trajectory in the  $(x, p_x)$  plane (left panel), particle energy as a function of time (central panel), and trajectory in  $(\phi, \dot{\phi})$  (right panel). Parameters are  $\omega/\Omega_0 = 100$ ,  $b_z = 20$ ,  $\omega/k\sqrt{h_0/m} = 0.5$ , initial energy  $h_0 = 3(\omega/k)^2 m$ .

where  $b_z = \delta B_z/B_0$ . The equation for phase  $\phi$  in the vicinity of the resonance  $\dot{\phi} = 0$  can be written as

$$\frac{\ddot{\phi}}{k} = -\Omega_0^2 x(1 + b_z f(\phi)) \quad (110)$$

Due to the fast variation of phase  $\phi$ , we can assume  $x \approx \text{const}$  and obtain a Hamiltonian for Eq. (110):

$$H_\phi = \frac{1}{2}k^2 P_\phi^2 + \Omega_0^2 k^{-1} x(\phi + b_z F(\phi)) \quad (111)$$

where  $P_\phi = \dot{\phi}/k^2$  is a momentum conjugate to  $\phi$ . Hamiltonian (111) is similar to Hamiltonian (34) for system (5) when the amplitude of perturbation and the torque are proportional to slowly changing variable  $x$ . The phase portrait of Hamiltonian (111) is shown in Fig. 18 (central panel). Although the perturbation  $\sim F(\phi)$  is not periodic, within a certain range of  $\phi$  the phase portrait is similar to one shown in Fig. 4.

For Hamiltonian (111), the area surrounded by the separatrix can be written using Eqs. 37–(39):

$$S_{\text{res}} = \frac{2\Omega_0}{k^{3/2}} \sqrt{2|x|} \tilde{f}_s(a), \quad a = b_z$$

$$\tilde{f}_s(a) = \int_{\phi_X}^{\phi_{\text{max}}} \sqrt{(\phi_X - \phi) + a(F(\phi_X) - F(\phi))} d\phi \quad (112)$$

Function  $\tilde{f}_s(a)$  in (112) is independent of  $x$  and depends only on the amplitude of perturbation  $b_z$  (see Fig. 18(right panel)). For  $b_z > 1$ , we have  $\tilde{f}_s \neq 0$  and, thus,  $S_{\text{res}}$  increases with  $x$ . Once trapped, particles cannot leave the region of oscillations around the resonance.

An example of such a trajectory is shown in Fig. 19. The particle rotates around the background magnetic field (closed trajectories in the  $(x, p_x)$  plane) and crosses the resonance curve  $p_x = m\dot{\phi}$  twice on each period of rotation. In contrast with the system shown in Fig. 17, for system (107) the area  $S_{\text{res}}$  increases in resonance for positive  $x$ . Thus trapping happens at the right-hand intersection of trajectory by the resonance curve (see explanation of  $S_{\text{res}}$  behaviour in Section 3). As a result, trapped particles start moving with growing  $x$  (compare Figs. 17 and 19). Energy of a trapped particle increases as  $\sim t^2$  (see Eq. (54)). Trapped oscillations have a decreasing amplitude of  $\phi$  oscillations and increasing amplitude of  $\dot{\phi}$  oscillations (see Fig. 19 (right panel) and [109,131]).

Different profiles of  $f(\phi)$  may appear in concrete models describing particle trapping and acceleration by electromagnetic waves or pulses:  $f(\phi) = \sin \phi$  [109,119],  $f(\phi) = \tanh(\phi)$  [120,132],  $f(\phi) = \phi \exp(-(\phi + \phi_0)^2)$  [127]. Regardless of a specific type of  $f(\phi)$ , trapping into resonance with electromagnetic (as opposite to electrostatic) “wave” results in an unlimited acceleration, as the area  $S_{\text{res}}$  given by Eq. (112) always increases and trapped particles cannot escape from resonance without external perturbations of system (see Section 8).

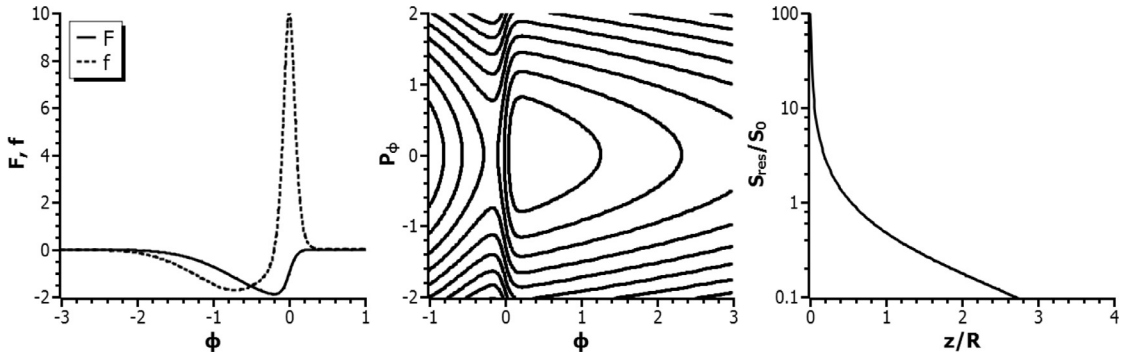


**Fig. 20.** Resonance interaction of particles with electrostatic localized structures. Profiles  $F(\phi)$  and  $f = dF/d\phi$  (left panel). Phase portrait of (121) (central panel). The area  $S_{\text{res}}$  given by Eq. (122) (right panel) with  $S_0 = 2\sqrt{4l_xL^3/Rm}$  and  $e\Phi_0R/2l_xL = 0.5$ .

### 6.3. Nonlinear electrostatic localized structures in inhomogeneous magnetic field

In planetary aurora regions and Earth radiation belts, strong electron beams generate various electrostatic solitary waves, such as double layers or electron holes propagating along a background magnetic field. In an inhomogeneous magnetic field, such structures can trap particles into the Landau resonance and accelerate them to high energies [133,134].

Hamiltonian of electron in a strong inhomogeneous magnetic field and an electrostatic solitary wave field can be written as (see Eq. (98))

$$H = \frac{1}{2m} (p_x^2 + p_z^2) + \frac{1}{2m} \left( \frac{e}{c} B_0(z) x \right)^2 - e\Phi_0 F(\phi) \quad (113)$$

where  $F(\phi)$  defines the shape of a scalar potential (see Fig. 20)(left panel)), and  $\Phi_0$  is an amplitude of a scalar potential. For the sake of simplicity, we assume that wave phase velocity  $v_\phi$  is constant:

$$\phi = (z - v_\phi t)/L \quad (114)$$

The spatial scale of a solitary wave  $L$  is much smaller than a scale of magnetic field inhomogeneity  $B_0(z)$ .

In the absence of perturbations,  $\Phi_0 \sim 0$ , Hamiltonian equations for Hamiltonian (113) are

$$\begin{aligned} \dot{x} &= p_x/m, & \dot{z} &= p_z/m \\ \dot{p}_x &= -m\Omega_0^2(z)x \\ \dot{p}_z &= -m\Omega_0(z)\Omega'_0 x^2 \end{aligned} \quad (115)$$

where  $\Omega_0(z) = eB_0(z)/mc$  and  $\Omega'_0 = \partial\Omega_0/\partial z$ . In a strong background magnetic field the gyrofrequency  $\Omega_0$  is large enough to make oscillations in the  $(x, p_x)$  plane significantly faster than motion in the  $(z, p_z)$  plane. For these fast oscillations we can introduce new conjugate variables  $I_x, \theta$  where  $I_x$  is an adiabatic invariant (see more details in Appendix B):

$$I_x = \frac{1}{2\pi} \oint \sqrt{2mH - p_z^2 - (m\Omega_0(z)x)^2} dx = \frac{2mH - p_z^2}{2m\Omega_0(z)} \quad (116)$$

The new Hamiltonian does not depend on  $\theta$ , therefore  $I_x$  is a constant:

$$H = \frac{1}{2m} p_z^2 + I_x \Omega_0(z) \quad (117)$$

The perturbed Hamiltonian we can be written as

$$H = \frac{1}{2m} p_z^2 + I_x \Omega_0(z) - e\Phi_0 F(\phi) \quad (118)$$

There is an effective potential energy  $I_x \Omega_0(z)$  in Hamiltonian (118). Particle motion in the  $(z, p_z)$  plane is described by equations

$$\dot{z} = p_z/m, \quad \dot{p}_z = -I_x \Omega'_0(z) + \frac{e\Phi_0}{L} F'(\phi) \quad (119)$$

Using definition of phase (114) we can rewrite Eqs. (119) as

$$L^2 \ddot{\phi} = -\frac{I_x L}{m} \Omega'_0(z) + \frac{e\Phi_0}{m} F'(\phi) \quad (120)$$

As the phase  $\phi$  changes much faster than  $z$ , we can integrate Eq. (120) to obtain Hamiltonian

$$H_\phi = \frac{1}{2L^2} P_\phi^2 + \frac{I_x L}{m} \Omega'_0(z) \phi - \frac{e\Phi_0}{m} F(\phi) \quad (121)$$

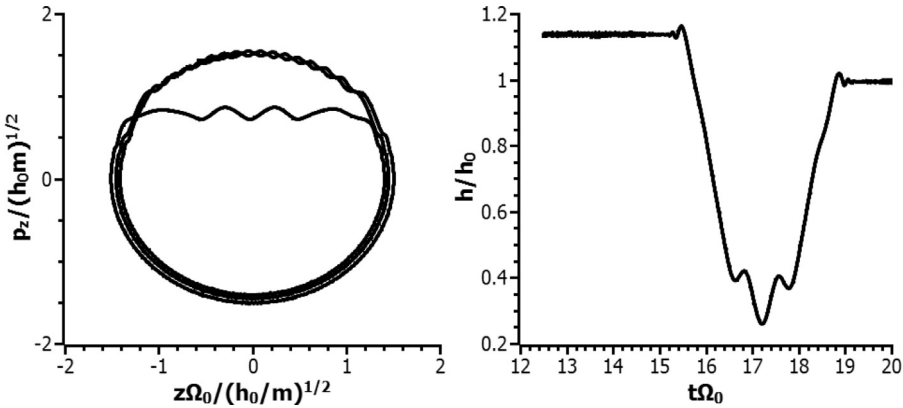


**Fig. 21.** A trajectory and the corresponding energy obtained with numerical integration of (120). Variables are normalised on  $\Omega_0(0)$  and initial energy  $h_0$ . System parameters are:  $v_\phi/\sqrt{h_0/m} = 0.8$ ,  $e\Phi_0 R/L, \Omega_0(0) = 1$ ,  $R\Omega_0(0)/L = 100$ ,  $R\Omega_0(0)/\sqrt{h_0/m} = \sqrt{2}$ . To calculate these trajectories, we chose a simple model of background magnetic field  $B_0 \approx (1 + (z/R)^2)$ .

where  $P_\phi = \dot{\phi}L^2$  is a momentum conjugate to  $\phi$ . In Hamiltonian (121) torque  $\sim \Omega'_0$  is produced by the inhomogeneity of the background magnetic field. Phase portrait of Hamiltonian (121) is shown in Fig. 20 (central panel). For a large enough potential ( $e\Phi_0 > I_x L \Omega'_0$ ), there is a region filled with closed trajectories in the phase plane. Area of this region is defined by Eq. (40):

$$S_{\text{res}} = 2\sqrt{2|\Omega'_0| \frac{I_x L^3}{m}} f_s(a), \quad a = e\Phi_0 / I_x L \Omega'_0 \quad (122)$$

Fig. 20(right panel) shows that  $S_{\text{res}}$  has a maximum at  $z = 0$  (where  $\Omega'_0 = 0$ ) and decrease with  $|z|$ . Thus, particles can be trapped by solitary wave at large  $-z_{\text{trap}}$  where  $S_{\text{res}}$  grows along the resonant trajectory  $\dot{z} = v_\phi > 0$  and they escape from resonance at  $z_{\text{esc}} = -z_{\text{trap}}$ . Corresponding change of particle energy in the resonance is described by Eq. (117) with  $p_z = mv_\phi$  and  $z = z_{\text{trap}} + v_\phi t$ :

$$h = \frac{1}{2}mv_\phi^2 + I_x \Omega_0(z_{\text{trap}} + v_\phi t) \quad (123)$$

The resonant energy decreases for  $z_{\text{trap}} + v_\phi t < 0$  and increases for  $z_{\text{trap}} + v_\phi t > 0$ . Due to the symmetry with respect to the  $z = 0$  plane, there is no net energy gain for a trapping-escape event, like in the system in Section 6.1.

A typical example of particle trajectory is shown in Fig. 21. The particle moves along a closed trajectory in the  $(z, p_z)$  plane and becomes trapped with negative  $z_{\text{trap}}$ . The trapped motion takes the particle from  $z = z_{\text{trap}}$  to  $z = z_{\text{esc}} \approx -z_{\text{trap}} > 0$  almost horizontally in Fig. 21(left panel). Before the particle cross the  $z = 0$  plane, the particle energy decreases, whereas for  $z > 0$  the particle energy increases and reaches approximately the same value as at the moment of trapping.

In realistic space plasma systems such as Earth radiation belts, solitary electrostatic structures are often generated around local minima of magnetic field, defined by  $\Omega'_0 = 0$ . The wave amplitude  $\Phi_0$  depends on  $z$  and increases with  $|z|$ . This condition allows solitary waves to trap and accelerate electrons [135,136].

#### 6.4. Obliquely propagating electromagnetic waves

The obliquity of waves (the presence of a wave number component directed along the background magnetic field) affects the trapped particle motion and leads to particle escape from resonance [106,137]. For the system from Section 6.2 with a periodic wave  $F(\phi) = \sin \phi$  and  $\phi = k_x x + k_z z - \omega t$ , Hamiltonian (107) is

$$H = \frac{1}{2m}(p_x^2 + p_z^2) + \frac{1}{2m} \frac{e^2}{c^2} (B_0 x + \delta B_z k^{-1} \sin \phi)^2 \quad (124)$$

where  $k = \sqrt{k_x^2 + k_z^2}$ . System (124) contains two pairs of conjugate variables  $(x, p_x)$ ,  $(z, p_z)$  and is more complicated than the original system with  $k_z = 0$ . Assuming that the wave amplitude  $\delta B_z = \text{const}$  is much smaller than  $B_0$ , we expand Hamiltonian (124):

$$H = \frac{1}{2m}(p_x^2 + p_z^2) + \frac{1}{2}m\Omega_0^2 x^2 + m\Omega_0^2 \frac{x}{k} b_z \sin \phi \quad (125)$$

where  $\Omega_0 = eB_0/mc = \text{const}$ ,  $b_z = \delta B_z/B_0$ . We introduce  $\phi$  as a new canonical variable using a generating function

$$R = I(k_x x + k_z z - \omega t) + P_x x + P_z z \quad (126)$$

where  $P_x, P_z$  are new momenta, whereas  $x$  and  $z$  remain unchanged. The new Hamiltonian does not depend on  $z$ , thus we can set  $P_z = \text{const} = 0$  to get

$$H = -\omega I + \frac{1}{2m} \left( (P_x + k_x I)^2 + (k_z I)^2 \right) + \frac{1}{2} m \Omega_0^2 x^2 + m \Omega_0^2 \frac{x}{k} b_z \sin \phi \quad (127)$$

The resonance condition  $\dot{\phi} = 0$  can be written as

$$\frac{\partial H}{\partial I} = -\omega + \frac{1}{m} \left( k_x (P_x + k_x I) + k_z^2 I \right) = 0 \quad (128)$$

with the solution

$$I_{\text{res}} = \frac{m k v_\phi - k_x P_x}{k^2} \quad (129)$$

where  $v_\phi = \omega/k = \text{const}$ . We expand Hamiltonian (127) around  $I - I_{\text{res}}$ :

$$\begin{aligned} H &= \Lambda + \frac{1}{2m} k^2 (I - I_{\text{res}})^2 + m \Omega_0^2 \frac{x}{k} b_z \sin \phi, \\ \Lambda &= -\omega I_{\text{res}} + \frac{1}{2m} \left( (P_x + k_x I_{\text{res}})^2 + (k_z I_{\text{res}})^2 \right) + \frac{1}{2} m \Omega_0^2 x^2 \\ &= -\frac{1}{2} m v_\phi^2 + \frac{1}{2m} P_x \left( \frac{k_z^2}{k^2} P_x + 2 m v_\phi \frac{k_x}{k} \right) + \frac{1}{2} m \Omega_0^2 x^2 \end{aligned} \quad (130)$$

We introduce new variable  $P_\phi = I - I_{\text{res}}$  and write  $H - \Lambda$  in the form of Hamiltonian (34)

$$H_\phi = \frac{1}{2m} k^2 P_\phi^2 + m \Omega_0^2 \frac{k_x}{k^2} x \phi + m \Omega_0^2 \frac{x}{k} b_z \sin \phi \quad (131)$$

where  $x$  is a slow variable. It follows from Eq. (40) for  $b_z > k_x/k$  there is a surrounded by the separatrix region with trapped particles. Its area is

$$S_{\text{res}} = 2 \frac{m \Omega_0}{k^2} \sqrt{2 k_x |x|} f_s(a), \quad a = b_z k / k_x \quad (132)$$

When  $S_{\text{res}} \sim \sqrt{|x|}$  grows in the process of motion, particles can be trapped into resonance. In the  $(x, p_x, p_z)$  space, the isoenergetic surface of  $H = h = \text{const}$  is

$$h = \frac{1}{2m} (p_x^2 + p_z^2 + m^2 \Omega_0^2 x^2 - (k m v_\phi / k_z)^2) \quad (133)$$

where  $p_x = P_x + k_x I$  and  $p_z = k_z I - k m v_\phi / k_z$ . This is an ellipsoid centered at the origin ( $x = 0, p_x = 0, p_z = 0$ ). To obtain equation for the resonant plane, we combine Eq. (129) and  $p_z = k_z I - k m v_\phi / k_z$ :

$$\frac{k_x}{k} p_x + \frac{k_z}{k} p_z = 0 \quad (134)$$

The intersection of these two surfaces is a resonant curve  $\mathcal{R}$ . The Larmor rotation in the background magnetic field resides on intersections of the isoenergetic surface and planes  $p_z = \text{const}$ . We use notation  $\mathcal{L}_\alpha$  for the intersection of the isoenergetic sphere and a plane  $p_z = p_z^{(\alpha)} = \text{const}$ .

Characteristic particle motion is shown in Fig. 22. Let initially  $p_z = p_z^{(*)} < 0$  and let  $\mathcal{L}_*$  cross the resonant curve. In the process of Larmor motion the particle repeatedly passes through the resonance. Eventually, at a certain  $p_z = p_z^{(0)}$  close to  $p_z^{(*)}$ , it is trapped into resonance. Of the two points where  $\mathcal{R}$  crosses  $\mathcal{L}_0$ , trapping occurs where  $S_{\text{res}}$  grows, i.e., where  $d|x|/dt > 0$ . Direction of trapped motion on  $\mathcal{R}$  is determined by Hamiltonian  $\Lambda$  (Fig. 22(left panel)). The trapped particle moves along  $\mathcal{R}$  until  $S_{\text{res}}$  returns to its value at the moment of trapping. Upon that return, particle escapes from resonance. It follows from the symmetry with respect to the origin that after the escape the particle moves along another Larmor trajectory  $\mathcal{L}_1$  with  $p_z = p_z^{(1)} = 2 m v_\phi k / k_z - p_z^{(0)}$ . Projections of  $\mathcal{L}_0$  and  $\mathcal{L}_1$  on the  $(x, p_x)$  plane coincide. Hence net change of the particle energy  $E = (p_x^2 + \Omega_0^2 m^2 x^2 + p_z^2)/2m$  due to trapping into resonance is

$$\Delta E = \frac{1}{2m} \Delta(p_z^2) = 2 v_\phi (m v_\phi - p_z^{(0)}) \quad (135)$$

All the energy gain is in the longitudinal component of the momentum. After several of Larmor periods with  $p_z$  close to  $p_z^{(1)}$ , the particle can be trapped into resonance again. This time the trapping occurs at  $x < 0$ , because  $d|x|/dt > 0$  at  $x < 0$  on this part of  $\mathcal{R}$ . After the trapping, the particle moves along the resonant curve and escapes from resonance near  $\mathcal{L}_0$ , thus returning close to its initial energy (Fig. 22 (right panel)).

In the coordinate space, trapped particles move along the wave front. For the first trapping, this motion can be divided into two stages. During the first stage,  $x$  grows with time and particles experience the surfatron acceleration similar to Section 6.2. If  $k_z/k \ll 1$  (i.e.,  $\mathbf{k}$  is almost perpendicular to the background magnetic field), the maximum value of  $|x|$  on the

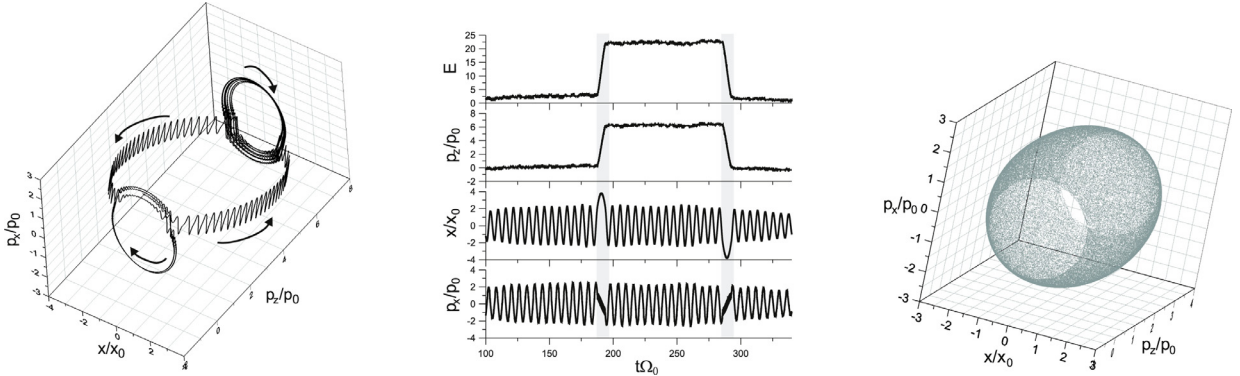


**Fig. 22.** Numerical simulations of Hamiltonian (125). Characteristic trajectory (left panel); energy, coordinate, and momenta (central panel). A stroboscopic map in the  $(x, p_x, p_z)$  space showing multiple scatterings on resonance for Hamiltonian (125) (right panel). Variables are normalized by  $x_0 = \sqrt{h_0/m}/\Omega_0$ ,  $p_0 = \sqrt{h_0 m}$ . The figure is adopted from [137].

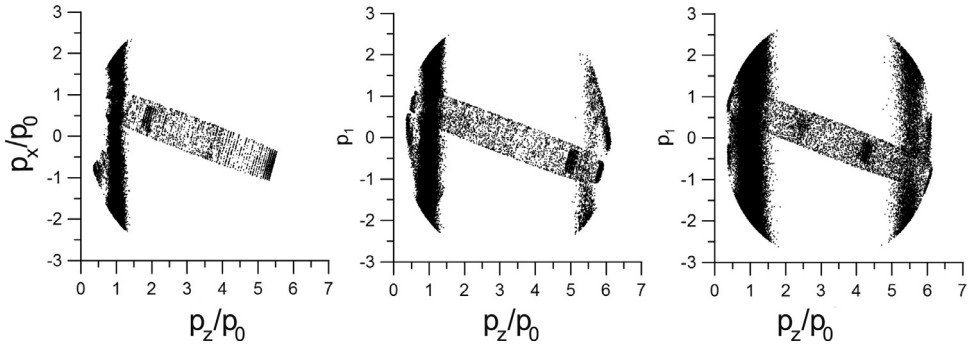


**Fig. 23.** The time evolution of particle distribution in momentum space  $(p_x, p_z)$ . The panels correspond to  $t_1\Omega_0 = 60, 120, 360$ . Variables are normalized on  $x_0 = \sqrt{h_0/m}/\Omega_0$ ,  $p_0 = \sqrt{h_0 m}$ . Figure is adopted from [137].

resonant curve is  $|x|_{max} \approx v_\phi k/\Omega_0 k_z$ , and trapped particles are significantly accelerated. It was shown in Section 6.2, that if  $k_z = 0$  the surfatron acceleration is unlimited (the duration of the first stage is infinite). However, if  $k_z \neq 0$ , the first stage is finite and during the second stage  $x$  decreases to its initial value. The particle gains energy in the  $z$ -direction (motion along the background magnetic field) during both stages:  $p_z$  grows in resonance (see Fig. 22 (central panel, left grey zone)). After escaping from resonance, a particle makes several gyrorotations and becomes trapped again. This second trapping motion corresponds to  $p_z$  decreasing in resonance (see Fig. 22 (central panel, right grey zone)).

Scattering on resonance produces diffusion of the particle energy even when trapping is impossible. A stroboscopic map with a period  $2\pi/\omega$  of a long phase trajectory with multiple scatterings on resonance is shown in Fig. 22 (central panel). The dots uniformly cover a large part of the isoenergetic ellipsoid  $H = h$ . The two regions not covered by dots around the poles correspond to Larmor trajectories that never cross the resonant plane. Motion there is regular.

To investigate the evolution of particle velocity distributions we performed a simulation of  $10^6$  test particles. The initial distribution was uniform in the  $(x, p_x)$  plane and all particles had approximately the same values of  $p_z \sim 0$ . In the  $(p_x, p_z)$  plane, such a distribution looks like a narrow stripe  $p_z \approx \text{const}$ . After a certain time ( $t\Omega_0 \sim 60$ ), the distribution becomes wider in  $p_z$  due to the scattering. Moreover, some particles are trapped; for these particles the  $p_z$ -component of momentum grows with time. Therefore, in the  $(p_x, p_z)$  plane there is a smooth cloud of particles with small  $p_z$  and a stripe of trapped particles (Fig. 23,  $t = t_1$ ). Then some of the trapped particles escape from resonance and fill the region with large  $p_z$  (Fig. 23,  $t = t_2$ ). This region spreads due to the scattering (Fig. 23,  $t = t_3$ ). After a long enough time we observe three groups of particles in the  $(p_x, p_z)$  plane: two groups with a relatively similar number of particles (with small and large  $p_z$ ) and a stripe filled with captured particles.

**Section summary** In this section we considered four nonrelativistic systems containing resonant interaction. Although systems describe significantly different configurations of electromagnetic fields, we show that the same approach can be applied for their description. For each system we derived the resonant Hamiltonian  $H_\phi$  and computed the average change of particle energy due to trapping. These four examples cover a wide range of space plasma systems where the resonant wave-particle interaction plays an important role for charged particle dynamics.

## 7. Particle acceleration in relativistic plasma systems

In this section we discuss three settings with trapping of relativistic particles. In [Section 7.1](#) we describe trapping in the same system as in [Section 6.1](#) but for relativistic particles and show how relativistic effects change the dynamics of trapped particles. Two other subsections discusses charged particle (electron) resonant interaction with whistler waves in inhomogeneous magnetic field, which is a classical problem for near-Earth space plasma physics. We consider two limits: very oblique propagation of a whistler wave relative to the background magnetic field (in this case, the wave is almost electrostatic and can trap electrons into the Landau resonance), and a parallel propagation of a whistler wave, when the wave is purely electromagnetic and can trap electrons into the cyclotron resonance.

As in [Section 6](#), we restrict our consideration to 2D physical systems. Keeping the same configuration of the background magnetic field, as shown in [Fig. 16](#), we obtain a relativistic Hamiltonian (cf. [Eq. \(98\)](#))

$$H = \sqrt{m^2 c^4 + c^2 p_x^2 + c^2 p_z^2 + e^2 A_y^2(x, z)} = mc^2 \gamma \quad (136)$$

The corresponding Hamiltonian equations are

$$\begin{aligned} \dot{x} &= \frac{\partial H}{\partial p_x} = \frac{1}{m\gamma} p_x, \quad \dot{z} = \frac{\partial H}{\partial p_z} = \frac{1}{m\gamma} p_z \\ \dot{p}_x &= -\frac{\partial H}{\partial x} = \frac{e^2}{mc^2\gamma} B_0 A_y \\ \dot{p}_z &= -\frac{\partial H}{\partial z} = -\frac{e^2}{mc^2\gamma} B_{0x} A_y \end{aligned} \quad (137)$$

Comparing [Eqs. \(137\)](#) and [Eqs. \(99\)](#), we obtain for  $B_0 = \text{const}$  (in which case  $B_{0x} = 0$ ) the new gyrofrequency  $\Omega_0/\gamma$  where  $\Omega_0 = eB_0/mc$  is a gyrofrequency in the nonrelativistic ( $\gamma \rightarrow 1$ ) case.

### 7.1. Electrostatic wave propagating across a weak magnetic field

This subsection generalizes results derived in [Section 6.1](#) to relativistic particles. The upper boundary of particle velocity limits the background Lorentz force. If the wave electrostatic field exceeds the maximum Lorentz force, the particle trapped motion (and acceleration) becomes infinitely long [\[44,138,139\]](#). Analysis of similar systems with electromagnetic waves can be found in [\[110,119,140\]](#), and effects of curved magnetic field lines were considered in [\[141\]](#). Effects of the 2-D fronts of waves (curvature of the wave front) were considered [\[142,143\]](#).

A relativistic electron moving in a background uniform magnetic field  $B_0$  and a wave electrostatic field is described by a Hamiltonian

$$\begin{aligned} H &= mc^2 \gamma + e\Phi_0 \sin \phi \\ \gamma &= \sqrt{1 + \left(\frac{p_x}{mc}\right)^2 + \left(\frac{eB_0 x}{mc^2}\right)^2} \end{aligned} \quad (138)$$

where  $\Phi_0$  is an amplitude of the scalar potential,  $\phi = \phi_0 + kx - \omega t$  is a wave phase,  $\omega \gg \Omega_0 = eB_0/mc$ , and  $v_\phi = \omega/k = \text{const} < c$  is a phase velocity. The corresponding Hamiltonian equations are (cf. [Eq. \(101\)](#)):

$$\dot{x} = p_x/m\gamma, \quad \dot{p}_x = -\frac{m\Omega_0^2 x}{\gamma} - ek\Phi_0 \cos \phi \quad (139)$$

Following [Eqs. \(7\)–\(9\)](#), we introduce momentum  $I$  conjugate to  $\phi$  by generating function (cf. [Eq. \(7\)](#))

$$R = I(kx - \omega t) + P_x x \quad (140)$$

where  $(P_x, x), (I, \phi)$  are new variables

$$p_x = \frac{\partial R}{\partial x} = P_x +Ik \quad (141)$$

The new Hamiltonian takes the form (cf. [Eq. \(9\)](#))

$$H = -\omega I + \sqrt{1 + \left(\frac{P_x + kl}{mc}\right)^2 + \left(\frac{eB_0 x}{mc^2}\right)^2} + e\Phi_0 \sin \phi \quad (142)$$

The resonant condition  $\dot{\phi} = 0$  can be written as

$$\frac{\partial H}{\partial I} = -\omega + \frac{k}{\gamma} \left( \frac{P_x + kl}{m} \right) = 0$$

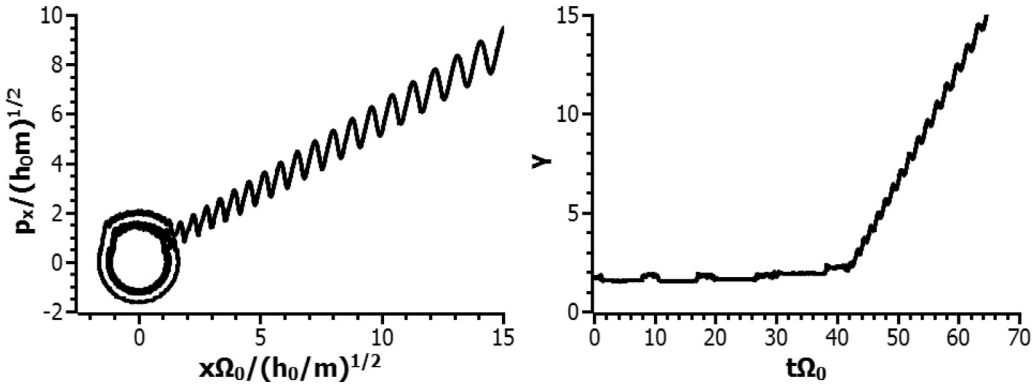


Fig. 24. Trajectory and the corresponding energy from a numerical simulation of (139).

$$\gamma = \sqrt{1 + \left(\frac{P_x + kI}{mc}\right)^2 + \left(\frac{\Omega_0 x}{c}\right)^2} \quad (143)$$

Solution of Eq. (143) is (cf. Eq. (17)):

$$I_{\text{res}} = \frac{1}{k} \left( mc \frac{\nu_{\text{res}} \sqrt{1 + (\Omega_0 x/c)^2}}{\sqrt{1 - \nu_{\text{res}}^2}} - P_x \right) \quad (144)$$

where  $\nu_{\text{res}} = \dot{\phi}/c = \omega/kc = \text{const}$ . Using Eqs. (33), (34) we can write the Hamiltonian near the resonance:

$$\begin{aligned} H_\phi &= \frac{1}{2} g(x) P_\phi^2 - r(x) \phi + e\Phi_0 \sin \phi \\ g &= \frac{\partial^2 H}{\partial I^2} \Big|_{I=I_{\text{res}}} = \frac{(1 - \nu_{\text{res}}^2)^{3/2} mk^2}{\sqrt{1 + (\Omega_0 x/c)^2}} \\ r &= -\frac{\Omega_0^2 mx}{k} \frac{1}{\sqrt{1 - \nu_{\text{res}}^2} \sqrt{1 + (\Omega_0 x/c)^2}} \end{aligned} \quad (145)$$

where  $P_\phi = \dot{\phi}/g$  is a momentum conjugate to the phase  $\phi$ . The area  $S_{\text{res}}$  is defined by Eqs. (40) and (43):

$$S_{\text{res}} = \frac{2}{1 - \nu_{\text{res}}^2} \frac{\Omega_0}{k^2} \sqrt{2k|x|} f_s(a), \quad a = -\frac{ek\Phi_0}{m\Omega_0^2 x} \sqrt{1 - \nu_{\text{res}}^2} \sqrt{1 + (\Omega_0 x/c)^2} \quad (146)$$

For high-energy particles (e.g., for  $\Omega_0 x/c \gg 1$ ) we have

$$a = -\frac{ek\Phi_0}{mc\Omega_0} \sqrt{1 - \nu_{\text{res}}^2} = \text{const} \quad (147)$$

If  $|a| > 1$ ,  $S_{\text{res}}$  grows with  $x$ . This is a crucial difference between the relativistic particle interaction with electrostatic wave and a corresponding nonrelativistic system, where  $S_{\text{res}}$  given by Eq. (104), drops to zero for large  $x$ . Fig. 24 presents an example of a trajectory of a particle that is trapped by the electrostatic wave and does not escape from resonance (cf. Fig. 17). The growth of  $S_{\text{res}}$  for positive  $x$  (see Section 3) results in particle trapping at the right-hand side of the closed trajectory in the  $(x, p_x)$  plane. The trapped particle starts moving along the resonant trajectory

$$p_x = \frac{\nu_{\text{res}}}{\sqrt{1 - \nu_{\text{res}}^2}} \sqrt{1 + (\Omega_0 x/c)^2} \quad (148)$$

with increasing  $x$  and  $p_x$ . The trapped particle energy increases linearly with time  $\gamma = \sqrt{1 + (p_x/mc)^2 + (\Omega_0 x/c)^2} \sim \sqrt{1 + (\Omega_0 t)^2} \sim t$ . This type of acceleration is called *surfatron* acceleration [44,106,138,144,145].

Using Eq. (64) we estimate a change of particle momentum  $p_x$  due to scattering on resonance in the relativistic system (cf. Eq. (105)):

$$\langle \Delta p_x \rangle = -\left(1 - \nu_{\text{res}}^2\right)^{3/2} \sqrt{\frac{2}{k|x|}} \frac{ek\Phi_0}{\Omega_0} f_p \quad (149)$$

The corresponding energy change  $\Delta h$  is

$$\Delta h = \frac{p_x}{m} |\langle \Delta p_x \rangle| = e\Phi_0 \gamma_0 (1 - v_{res}^2)^{3/2} \frac{\omega}{\Omega_0} \sqrt{\frac{2}{k|x_{trap}|}} f_p \quad (150)$$

where  $\gamma_0$  is initial particle energy, and  $x_{trap}$  is a coordinate of resonance, which can be calculated from Hamiltonian (138) with resonant condition  $p_x = \gamma v_{res} m c$ :

$$\Omega_0 |x_{trap}| = c \sqrt{\gamma_0^2 (1 - v_{res}^2) - 1} \quad (151)$$

For a sufficiently large wave amplitude ( $a \gg 1$ ),  $f_p \sim 8\sqrt{2/a}$  and Eq. (150) takes a form

$$\Delta h = 4\gamma_0 \sqrt{e\Phi_0 v_\phi^2 m} \frac{(1 - v_{res}^2)^{5/4}}{(1 + (\Omega_0 x_{trap}/c)^2)^{1/4}} = 4\sqrt{e\Phi_0 \gamma_0 v_\phi^2 m} \left(1 - \frac{v_\phi^2}{c^2}\right) \quad (152)$$

where  $v_\phi = \omega/k = v_{res}c$ . Comparison of Eq. (152) with the analogous expression for nonrelativistic system Eq. (105) shows that there is an additional factor  $\sqrt{\gamma_0}(1 - (v_\phi/c)^2)$ . Therefore the amplitude of energy change and the resonance width in energy space are larger for  $\gamma_0 > 1$  and rapidly decrease when  $v_\phi$  reaches speed of light.

## 7.2. The Landau resonance in an inhomogeneous magnetic field

This subsection generalises results derived in 6.3 for relativistic systems, but instead of localised wave pulses we consider a periodic wave. We consider electron trapping into the Landau resonance with an electrostatic mode of a whistler wave propagating in an inhomogeneous magnetic field [146,147]. Generalization of this system for more sophisticated resonant conditions can be found in [148], effects of curved magnetic field lines were considered in [149,150]. The Hamiltonian of a relativistic electron is (see Eq. (136) and [146,151])

$$H = mc^2\gamma + e\Phi_0 u(z) \sin\phi$$

$$\gamma = \sqrt{1 + \frac{p_x^2 + p_z^2}{m^2 c^2} + \left(\frac{eB_0(z)}{mc^2}x\right)^2} \quad (153)$$

where function  $u(z)$  defines the spatial distribution of the wave field. The general form of wave-phase in this case is

$$\phi = \int k(\tilde{z})d\tilde{z} - \omega t + n\Omega_0 \quad (154)$$

where  $n$  is a resonance number. We focus on the Landau resonance,  $n = 0$ , and consider a strong background magnetic field  $\Omega_0(z) = eB_0(z)/mc > \omega$ . Hamiltonian equations of unperturbed system,  $\Phi_0 \sim 0$ , describe a nonlinear oscillator:

$$\dot{x} = p_x/m\gamma, \quad \dot{p}_x = -\Omega_0^2 x m/\gamma \quad (155)$$

We introduce new variable  $I_x$  (see details in Appendix B):

$$I_x = \frac{1}{2\pi} \oint p_x dx = \frac{mc}{2\pi} \oint \sqrt{\gamma^2 - \frac{p_z^2}{m^2 c^2} - \left(\frac{\Omega_0(z)}{c}x\right)^2} dx = \frac{mc^2}{2\Omega_0(z)} \left(\gamma^2 - 1 - \frac{p_z^2}{m^2 c^2}\right) \quad (156)$$

The Hamiltonian can be written as

$$H = mc^2\gamma + e\Phi_0 u(z) \sin\phi$$

$$\gamma = \sqrt{1 + \frac{p_z^2}{m^2 c^2} + \frac{2\Omega_0(z)I_x}{mc^2}} \quad (157)$$

Here  $I_x$  is a particle magnetic moment and is conserved in the absence of perturbations that depend on  $x$ . We use a generating function  $R$  to introduce the phase  $\phi$  as a new variable (see details in Eqs. (7)–(9)):

$$R = I \left( \int k(\tilde{z})d\tilde{z} - \omega t \right) + P_z z \quad (158)$$

Therefore, the old momentum  $p_z$  is

$$p_z = \frac{\partial R}{\partial z} = P_z + I k(z) \quad (159)$$

In the new variables the Hamiltonian is

$$H = -\omega I + mc^2\gamma + e\Phi_0 u(z) \sin\phi$$

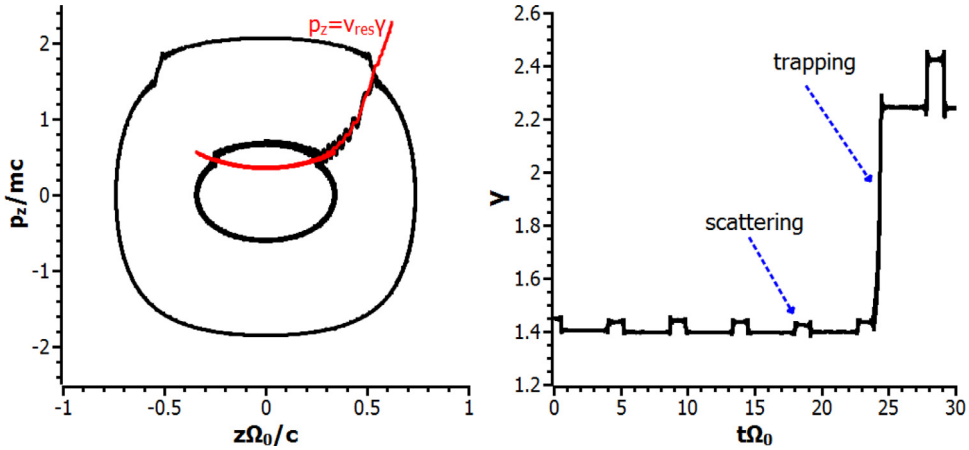


**Fig. 25.** A trajectory and the corresponding energy variation obtained by a numerical integration of (157). Magnetic field is approximated by a dipole field  $B_0(z)$  [112], and  $u(z) = z^2/(z^2 + 0.02)$  function is defined from a whistler wave model [146].

$$\gamma = \sqrt{1 + \frac{(P_z + kI)^2}{m^2 c^2} + Y} \quad Y = \frac{2\Omega_0(z)I_x}{mc^2} \quad (160)$$

Resonant condition  $\dot{\phi} = 0$  for Hamiltonian (160) is given by equation

$$\frac{\partial H}{\partial I} = -\omega + \frac{k}{m\gamma} (P_z + kI) = 0 \quad (161)$$

Solution of Eq. (161) is (cf. Eq. (144)):

$$I_{res} = \frac{1}{k} \left( mc \frac{\nu_{res} \sqrt{1+Y^2}}{\sqrt{1-\nu_{res}^2}} - P_z \right) \quad (162)$$

where  $\nu_{res} = \nu_\phi/c = \omega/k(z)c$  depends on  $z$ . Using Eqs. (33), (34) we can write the Hamiltonian near the resonance as

$$\begin{aligned} H_\phi &= \frac{1}{2}g(x)P_\phi^2 - r(x)\phi + e\Phi_0 u(z) \sin\phi \\ g &= \left. \frac{\partial^2 H}{\partial I^2} \right|_{I=I_{res}} = \frac{(1-\nu_{res}^2)mk^2}{\gamma_{res}} \\ r &= mc^2\{\gamma_{res}, I_{res}\} = -\frac{mc^2 W}{\gamma_{res}(1-\nu_{res}^2)} \\ W &= k^{-1}(YY' + \gamma_{res}^2 \nu_{res} \nu'_{res}), \quad \gamma_{res} = \frac{\sqrt{1+Y}}{\sqrt{1-\nu_{res}^2}} \end{aligned} \quad (163)$$

where  $P_\phi = \dot{\phi}/g$  is a momentum conjugate to the phase  $\phi$ ,  $Y' = (d\Omega_0/dz)I_x/mc^2$ ,  $\nu'_{res} = d\nu_{res}/dz$ . The area  $S_{res}$  is defined by Eqs. (40):

$$S_{res} = \frac{2mc\sqrt{2W}}{(1-\nu_{res}^2)k} f_s(a), \quad a = -\frac{e\Phi_0 u}{mc^2} \frac{\gamma_{res}(1-\nu_{res}^2)}{W} \quad (164)$$

Using Eq. (47) we can write expression for probability of trapping:

$$\Pi \approx \frac{\gamma_{res} \nu_{res} (1-\nu_{res}^2)}{2\pi W} \frac{1}{mc} \frac{\partial S_{res}}{\partial z} \quad (165)$$

Example of a particle trajectory in system (157) is shown in Fig. 25. The particle moves around a closed trajectory in the  $(z, p_z)$  plane. The area  $S_{res}$  grows for positive  $z$ , where the particle becomes trapped and starts accelerating. At some distance from  $z = 0$ ,  $S_{res}$  starts decreasing and the trapped particle escapes from resonance. After leaving the resonance, the particle starts moving along a closed trajectory with a larger radius. The increase of oscillation amplitude in the  $(z, p_z)$  plane corresponds to the increase of particle energy due to the acceleration in trapping.

### 7.3. The cyclotron resonance in an inhomogeneous magnetic field

In this subsection we consider the cyclotron resonance between relativistic electrons ( $\gamma > 2$ ) and a whistler wave propagating along an inhomogeneous magnetic field. The Resonance condition for such systems,  $p_z k/m = \omega\gamma - \Omega$  depends on the gyrofrequency  $\Omega$  [152,153] and is significantly different from the Cherenkov ( $\mathbf{p}\mathbf{k}/m = \omega\gamma$ ) or the Landau ( $p_z k/m = \omega\gamma$ ) resonances.

An electromagnetic whistler wave propagating parallel to the background magnetic field can be described by two components of a vector potential

$$\begin{aligned} A_y &= A \sin \phi, \quad A_x = -A \cos \phi \\ \phi &= \int k(\tilde{z}) d\tilde{z} - \omega t \end{aligned} \quad (166)$$

Hamiltonian (136) is

$$H = \sqrt{m^2 c^4 + p_z^2 c^2 + (cp_x - eA \cos \phi)^2 + (eB_0 x + eA \sin \phi)^2} \quad (167)$$

Assuming that wave energy  $eA$  is much smaller than the particle rest energy  $mc^2$ , we can expand Hamiltonian (167):

$$\begin{aligned} H &= mc^2\gamma + \frac{eA}{\gamma mc} (\Omega_0 mx \sin \phi - p_x \cos \phi) \\ \gamma &= \sqrt{1 + \frac{p_x^2 + p_z^2}{m^2 c^2} + \left(\frac{\Omega_0 x}{c}\right)^2} \end{aligned} \quad (168)$$

where  $\Omega_0(z) = eB_0(z)/mc$ . For unperturbed system ( $A \sim 0$ ) we can introduce a new variable  $I_x$  (see Eq. (156) and Appendix B):

$$I_x = \frac{1}{2\pi} \oint p_x dx = \frac{mc^2}{2\Omega_0} \left( \gamma^2 - 1 - \frac{p_z^2}{m^2 c^2} \right) \quad (169)$$

Coordinates  $(x, p_x)$  can be rewritten using  $I_x$  and a conjugate variable  $\psi$ :

$$x = \sqrt{2I_x/m\Omega_0} \sin \psi, \quad p_x = \sqrt{2I_x m \Omega_0} \cos \psi \quad (170)$$

Substituting Eqs. (170) into Eq. (168) we obtain

$$\begin{aligned} H &= mc^2\gamma - \frac{eA}{\gamma} \sqrt{Y} \cos(\phi + \psi) \\ \gamma &= \sqrt{1 + \frac{p_z^2}{m^2 c^2} + Y}, \quad Y = \frac{2I_x \Omega_0}{mc^2} \end{aligned} \quad (171)$$

Corresponding Hamiltonian equations are

$$\begin{aligned} \dot{I}_x &= -\frac{\partial H}{\partial \psi} = -\frac{eA}{\gamma} \sqrt{Y} \sin(\phi + \psi) \\ \dot{\psi} &= \frac{\partial H}{\partial I_x} = \frac{\Omega_0}{\gamma} - \frac{eA}{2I_x \gamma} \sqrt{Y} \cos(\phi + \psi) \\ \dot{p}_z &= -\frac{\partial H}{\partial z} = -\frac{1}{\gamma} \frac{\Omega'_0}{2\Omega_0} Y - \frac{ekA}{\gamma} \sqrt{Y} \sin(\phi + \psi) - \frac{eA}{\gamma} \frac{\Omega'_0}{2\Omega_0} \sqrt{Y} \cos(\phi + \psi) \\ \dot{z} &= \frac{\partial H}{\partial p_z} = \frac{p_z}{m\gamma} \end{aligned} \quad (172)$$

We use the following generating function to introduce new phase  $\zeta = \phi + \psi$  and conjugate momentum  $I$ :

$$R = I \left( \psi + \int k(\tilde{z}) d\tilde{z} - \omega t \right) + P_z z + \tilde{I}_x \psi \quad (173)$$

where  $(z, P_z)$ ,  $(\psi, \tilde{I}_x)$  are new variables:  $p_z = kI + P_z$ ,  $I_x = I_x + I$ . The new Hamiltonian takes the form:

$$\begin{aligned} H &= -\omega I + mc^2\gamma - \frac{eA}{\gamma} \sqrt{Y} \cos \zeta \\ \gamma &= \sqrt{1 + \frac{(kI + P_z)^2}{m^2 c^2} + Y}, \quad Y = \frac{2(\tilde{I}_x + I)\Omega_0}{mc^2} \end{aligned} \quad (174)$$

Hamiltonian (174) does not depend on  $\psi$  anymore. Thus, the conjugate momentum  $\tilde{I}_x$  is conserved and can be set to zero:  $Y = 2I\Omega_0/mc^2$ . The resonant condition for Hamiltonian (174) becomes

$$\dot{\zeta} = \frac{\partial H}{\partial I} = -\omega + \frac{1}{\gamma} \left( \Omega_0 + k \frac{kl + P_z}{m} \right) = 0 \quad (175)$$

Solution of Eq. (175) is

$$\frac{kl_{\text{res}}}{mc} = \frac{\nu_{\text{res}}}{\sqrt{1 - \nu_{\text{res}}^2}} \sqrt{1 - \left( \frac{\Omega_0}{kc} \right)^2 - 2 \frac{\Omega_0}{kc} \frac{P_z}{mc} - \frac{\Omega_0}{kc} - \frac{P_z}{mc}} \quad (176)$$

where  $\nu_{\text{res}}(z) = \nu_{\phi}(z)/c = \omega/k(z)c$ . The corresponding resonant energy  $\gamma_{\text{res}}$  is

$$\gamma_{\text{res}} = \frac{1}{\sqrt{1 - \nu_{\text{res}}^2}} \sqrt{1 - \left( \frac{\Omega_0}{kc} \right)^2 - 2 \frac{\Omega_0}{kc} \frac{P_z}{mc}} \quad (177)$$

We expand Hamiltonian (174) around the resonance  $I = I_{\text{res}}$ :

$$\begin{aligned} H &= mc^2 \Lambda + \frac{1}{2} (I - I_{\text{res}})^2 - \frac{eA}{\gamma_{\text{res}}} \sqrt{Y_{\text{res}}} \cos \zeta \\ \Lambda &= -\frac{\omega I_{\text{res}}}{mc^2} + \gamma_{\text{res}} = \frac{1}{\nu_{\text{res}}} \left( \frac{\Omega_0}{kc} + \frac{P_z}{mc} \right) \\ Y_{\text{res}} &= \frac{2I_{\text{res}}\Omega_0}{mc^2} = 2 \frac{\Omega_0}{kc} \left( \nu_{\text{res}} \gamma_{\text{res}} - \frac{\Omega_0}{kc} - \frac{P_z}{mc} \right) \\ g &= \left. \frac{\partial^2 \gamma}{\partial I^2} \right|_{I=I_{\text{res}}} = \frac{k^2}{\gamma_{\text{res}} m} (1 - \nu_{\text{res}}^2) \end{aligned} \quad (178)$$

We introduce  $I - I_{\text{res}}$  as a new variable  $P_{\phi} = \dot{\phi}/g$  and rewrite the resonance Hamiltonian as (see Eqs. (33), (34)):

$$\begin{aligned} H_{\phi} &= \frac{1}{2} g P_{\phi}^2 - r \phi - \frac{eA}{\gamma_{\text{res}}} \sqrt{Y_{\text{res}}} \cos \zeta \\ r &= mc^2 \{ \gamma_{\text{res}}, I_{\text{res}} \} = \frac{mc^2 W}{\gamma_{\text{res}} (1 - \nu_{\text{res}}^2)} \\ W &= \frac{1}{k} \left( \nu_{\text{res}}^2 \frac{k'}{k} + \frac{\Omega_0}{kc} \frac{\Omega_0'}{\Omega_0} \frac{P_z}{mc} \right) \end{aligned} \quad (179)$$

where  $\nu_R = \nu_{\text{res}} \gamma_{\text{res}} - \Omega_0/kc = (\omega \gamma_{\text{res}} - \Omega_0)/kc$ . The area  $S_{\text{res}}$  is (see Eq. (40)):

$$S_{\text{res}} = 2 \frac{mc}{1 - \nu_{\text{res}}^2} \frac{1}{k} \sqrt{2|W|} f_s(a), \quad a = -\frac{eA \sqrt{Y_{\text{res}}}}{\gamma_{\text{res}} r} = -\frac{eA}{mc^2} \frac{1 - \nu_{\text{res}}^2}{W} \sqrt{Y_{\text{res}}} \quad (180)$$

In Hamiltonian (179) and Eqs. (180) momentum  $P_z$  equals to the resonant value  $P_{\text{res}}(z)$ , which is defined from unperturbed Hamiltonian (174) with initial energy  $h_{\text{init}}$ :

$$P_{\text{res}} = \frac{mc}{\nu_{\text{res}}} \left( \frac{h_{\text{init}}}{mc^2} - \frac{\Omega_0}{\omega} + \sqrt{1 - \nu_{\text{res}}^2} \sqrt{1 + \left( \frac{\Omega_0}{\omega} \right)^2 - 2 \frac{h_{\text{init}}}{mc^2} \frac{\Omega_0}{\omega}} \right) \quad (181)$$

Substituting (181) to Eq. (177), we obtain  $\gamma_{\text{res}}(z)$  along the trapped trajectory

$$\gamma_{\text{res}} = \frac{1}{\nu_{\text{res}} \sqrt{1 - \nu_{\text{res}}^2}} \left( \frac{\Omega_0}{\omega} \sqrt{1 - \nu_{\text{res}}^2} - \sqrt{1 + \left( \frac{\Omega_0}{\omega} \right)^2 - 2 \frac{\Omega_0}{\omega} \frac{h_{\text{init}}}{mc^2}} \right) \quad (182)$$

A typical particle trajectory for Hamiltonian (171) is shown in Fig. 26. The particle oscillates in the  $(z, p_z)$  plane and becomes trapped with a positive  $z$ . In contrast to the Landau resonance (see Fig. 25), trapping results in a decrease of the radius of particle trajectory in the  $(z, p_z)$  plane. Near  $z \sim 0$  a particle escapes from resonance with a net gain of energy and starts moving along a closed trajectory with a smaller radius.

Using Eq. (47) we have for the probability of trapping:

$$\Pi \approx \frac{\{S_{\text{res}}, \Lambda\}}{2\pi |r|} = \frac{1}{2\pi mc} \frac{\gamma_{\text{res}} (1 - \nu_{\text{res}}^2)}{\nu_{\text{res}} |W|} \left( \frac{\partial S_{\text{res}}}{\partial z} - \frac{\Omega_0'}{\Omega_0} \frac{\Omega_0}{kc} mc \frac{\partial S_{\text{res}}}{\partial P_z} \right) \quad (183)$$

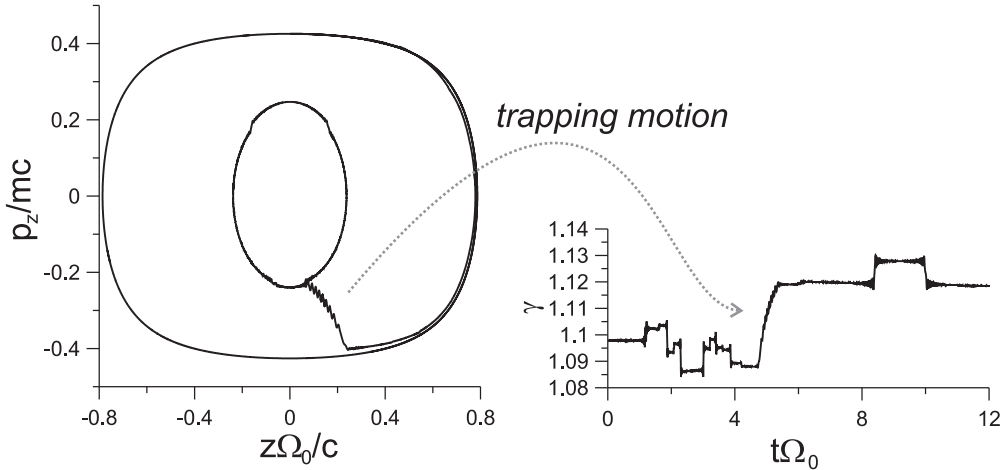


Fig. 26. A trajectory and the corresponding energy variation obtained with a numerical integration of (172).

where  $\Lambda$  is defined by Eq. (178). Eq. (183) shows that probability of trapping in 2D case (when  $S_{\text{res}} = S_{\text{res}}(z, P_z)$ ) is much more complicated than for 1D system (e.g., the Landau resonance considered in 7.2). A detailed investigation and numerical simulations of Eq. (183) were reported in [154].

**Section summary** In this section we considered three relativistic systems with wave-particle resonant interaction. The relativistic effect changes the wave-particle resonance interaction by limiting the Lorentz force acting on particles. This problem is essentially important for description of electron acceleration in the near-Earth plasma environment.

## 8. Stability of trapped particle motion

This section discusses the stability of trapped particle motion in several systems described in Sections 6, 7. Although in this section we consider only effects of an external nonresonant noise resulting in instability of trapped particle motion, the nonlinear resonant interaction can be destroyed by other types of instability. The most important one is the sideband instability leading to spread of wave spectra and stochasticization of trapped particle motion due to resonances with satellite waves [e.g., 17,18,155]. Similar effects of particle motion stochasticization and particle trapping destruction can provide several waves simultaneously resonating with particles [e.g., [131,156,157]]. These effects are not considered in our review but should be analyzed and estimated for any plasma system where nonlinear wave-particle interaction is considered. We start with a general consideration of effects of fluctuations of background magnetic field on trapped particle motion, and then consider one particular system where such fluctuations result in the destruction of the wave-particle resonant interaction.

### 8.1. Destruction of the trapped motion invariant

In this subsection we return to the systems considered in Sections 6.2, 7.1, 7.2 and show how magnetic field fluctuations can destroy the trapped particle motion and cause the diffusive escape of particles from resonance [158,159]. We start with a consideration of general effects of magnetic field fluctuations on behavior of system (34), for which the particle dynamics in the  $(\phi, P_\phi)$  plane has a Hamiltonian

$$H_\phi = \frac{1}{2}g(x)P_\phi^2 - r(x)\phi + \varepsilon u(x) \sin \phi \quad (184)$$

In (184),  $r(x)$ ,  $u(x)$ , and  $g(x)$  are functions of the coordinate along a resonance trajectory. Dynamics in the  $(\phi, P_\phi)$  plane is described by Hamiltonian equations

$$\dot{P}_\phi = r - \varepsilon u \cos \phi, \quad \dot{\phi} = gP_\phi \quad (185)$$

Consider a particle trajectory oscillating near the bottom of the potential well in the  $(\phi, P_\phi)$  plane. At the bottom, the potential energy  $U = \Omega_{tr}^2(\sin \phi - (r/u\varepsilon)\phi)$  (where  $\Omega_{tr} = \sqrt{\varepsilon u}$ ) has a minimum, yielding  $\phi = \phi_0 = \arccos(r/\varepsilon u)$ . Expanding Hamiltonian (184) near  $\phi_0$  we obtain

$$H_\phi = \frac{1}{2}gP_\phi^2 + \frac{1}{2}\Omega_{tr}^2(\phi - \phi_0)^2 + \text{const} \quad (186)$$

Eq. (186) shows that  $g\Omega_{tr}$  is frequency of trapped particle oscillations only at the bottom of the potential well in the  $(\phi - \phi_0, P)$  plane. However, this term can be used to estimate the frequency of oscillations over almost the entire region filled by closed trajectories (except near the separatrix), because the actual frequency depends very weakly on the position

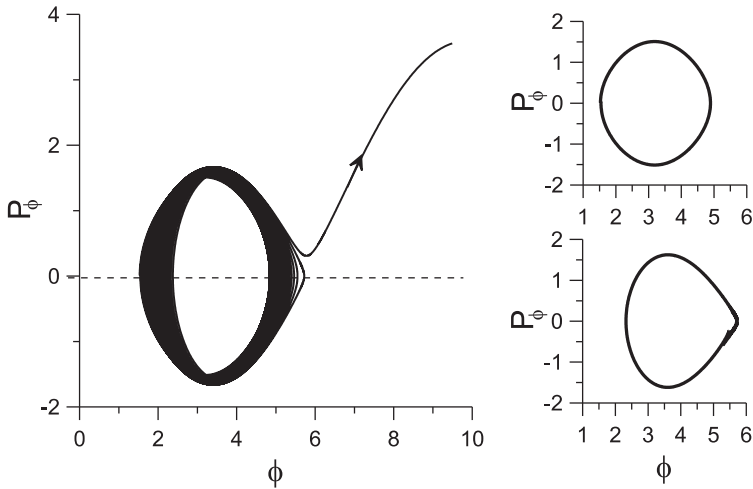


**Fig. 27.** A characteristic particle trajectory in the  $(\phi, P_\phi)$  plane. The right panels show two fragments of the trajectory (at the beginning and just before escape from resonance). The figure is adopted from [159].

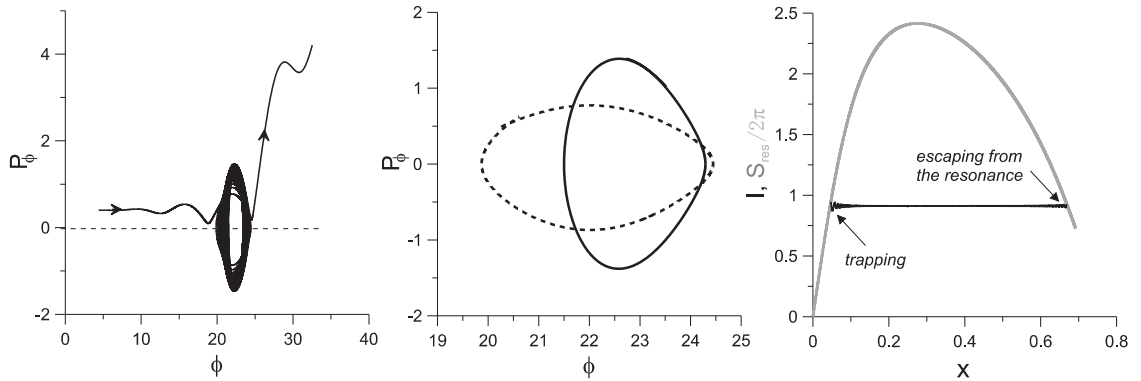


**Fig. 28.** A trapped particle trajectory. The middle panel shows two fragments of the trajectory in the  $(\phi, P_\phi)$  plane: just after trapping (dashed curve) and just before the escape (solid curve).  $I_\phi$  and  $S_{\text{res}}$  profiles are shown in the right panel. The Figure is adopted from [159].

of a particle (see, e.g., [160,161]). The period of trapped particle oscillations,  $2\pi/(g\Omega_{\text{tr}})$ , is small as compared with typical timescales of  $x$  variation.

The periodicity of trapped particle motion in the  $(\phi, P_\phi)$  plane allows us to introduce an action variable  $I_\phi = (2\pi)^{-1} \oint P_\phi d\phi$  (see [162]). In a system with constant  $x$ , the particle trajectory in the  $(\phi, P_\phi)$  plane does not evolve and, thus, the area surrounded by this particle trajectory is conserved exactly. In more realistic cases with slow variations of  $x$ , the action  $I_\phi$  becomes an adiabatic invariant of (184), [104,162], i.e., the area  $2\pi I_\phi$  is conserved to a high degree of accuracy even if the effective potential  $U$  varies with  $x$  (with time). Thus,  $I_\phi$  can be used to characterize a trajectory of trapped particle motion. Consider a solution of Hamiltonian equations (185) for a particle initially trapped at  $x = x_0$ . As  $x > x_0$  slowly changes, the particle motion in the  $(\phi, P_\phi)$  plane is shown in Fig. 27. The action  $I_\phi$  is calculated as

$$I_\phi = \frac{1}{2\pi} \oint P_\phi d\phi = \frac{1}{\pi} \sqrt{\frac{2}{g}} \int_{\phi_1}^{\phi_2} \sqrt{H_\phi + r\phi - \varepsilon u \sin \phi} d\phi \quad (187)$$

where  $\phi_{1,2}$  are roots of the equation  $H_\phi + r\phi - \varepsilon u \sin \phi = 0$ . The variations of parameters  $g$ ,  $r$ , and  $\varepsilon$  result in the observed evolution of the particle trajectory in the  $(\phi, P_\phi)$  plane, but the action  $I_\phi$  is conserved. There are only very small amplitude oscillations of  $I_\phi$ , corresponding to the fact that integral (187) is calculated for a frozen  $x$ , while there are actually small variations of  $x$  within one period of trapped particle oscillations in the  $(\phi, P_\phi)$  plane.

Let us consider a whole cycle of charged particle motion, including particle trapping and escape from resonance. We start the numerical integration at  $x = 0$ , and select a trajectory which becomes trapped (see Fig. 28). We can use the conservation of  $I_\phi$  for trapped particles to determine when a particle enters and escapes from resonance. At the moment of trapping,  $2\pi I_\phi = S_{\text{res}}$  (see Eq. (40)). Thus, the trapped particles escape from resonance when  $S_{\text{res}}$  again becomes equal to  $2\pi I_\phi$ . An example of particle escape from resonance is shown in Fig. 28.

**Figure 28** demonstrate that in the trapped motion the adiabatic invariant  $I_\phi$  is conserved in the original wave-particle system. However, if an additional (external) force inducing variations of  $I_\phi$  is present, then  $2\pi I_\phi$  could become equal to  $S_{\text{res}}$ , leading to particle escape from resonance. In the next section, we consider the effects of such an external force and demonstrate that it may eventually lead to the destruction of the adiabatic invariant  $I_\phi$ .

The magnetic field fluctuations are mostly non-resonant: their frequencies, although of the same order as the main wave frequency, are assumed to differ sufficiently from it. Therefore we can neglect resonant interactions between particles trapped by the main wave and the fluctuations (in contrast to cases considered in [18,157]). Here we consider only fluctuations parallel to the background field line (transverse fluctuations were briefly addressed in [16]). Such fluctuations can be included into the term  $\sim r$  in Hamiltonian (184) as  $\sim r_1 \delta b$  with  $\delta b$  being an amplitude of magnetic field fluctuations. In other words,  $r$  can be expressed as a sum of unperturbed  $r$  and perturbations  $r_1 \delta b$ . The dependence of fluctuations on  $x$  is included into the  $r_1(x)$ . Hamiltonian (184) takes the form

$$H_\phi = \frac{1}{2} g P_\phi^2 - r\phi + \varepsilon u \sin \phi - r_1 \phi \delta b \quad (188)$$

To keep our approach as general as possible, we do not specify the type of fluctuations  $\delta b$  but simply introduce two parameters characterizing it: the timescale  $\tau$  and variance  $\text{Var}(\delta b) = \sigma$ . Magnetic field fluctuations are assumed to be high-frequency, such that  $\tau \Omega_{\text{trg}} \ll 1$ , and both fast variables  $(\phi, P_\phi)$  and slow variable  $x$  change only weakly over one time step (time interval  $\sim \tau$ ) of fluctuations.

As  $\Omega_{\text{trg}} = \partial H_\phi / \partial I_\phi$  (see [162]), we have for the change  $\Delta I_\phi$  on one time step ( $\sim \tau$ ) of fluctuations:

$$\Delta I_\phi = \frac{\Delta H_\phi}{\Omega_{\text{trg}}} = -\frac{r_1 \delta b}{\Omega_{\text{trg}}} \Delta \phi \quad (189)$$

where all functions on the right-hand side of Eq. (189) are evaluated at the same moment within one time step of fluctuations, while  $\Delta \phi$  is the change of  $\phi$  between the beginning and end of this step. This change  $\Delta \phi$  over a small time step  $\tau$  is  $\Delta \phi = g P_\phi \tau$ . Thus, Eq. (189) can be rewritten as

$$\Delta I_\phi = -\frac{r_1 \delta b}{\Omega_{\text{tr}}} P_\phi \tau \quad (190)$$

On the right-hand side of Eq. (190),  $\delta b$  changes much faster than  $P_\phi$ , and both  $\delta b$  and  $P_\phi$  change faster than  $g(x)$ ,  $\Omega_{\text{tr}}(x)$ , or  $r_1(x)$ . One period of particle oscillations in the  $(\phi, P_\phi)$  plane,  $2\pi/g\Omega_{\text{tr}}$ , includes many steps  $\sim \tau$ , but is short enough to keep  $x$  unchanged. Over this period the variance of  $\Delta I_\phi$  is

$$\text{Var}(\Delta I_\phi) = \left( \frac{r_1 \tau}{\Omega_{\text{tr}}} \right)^2 \text{Var}(P_\phi \delta b) \quad (191)$$

We assume that fluctuations  $\delta b$  and variations of  $P_\phi$  are statistically independent and, thus,  $\text{Var}(\delta b P_\phi) = \sigma \text{Var}(P_\phi)$ . The term  $\text{Var}(P_\phi)$  can be considered as a sum of  $M \gg 1$  values of  $P_\phi^2$  calculated within consecutive time steps  $\tau$  (i.e., between successive changes of  $\delta b$ ):

$$\text{Var}(P_\phi) = \frac{1}{M} \sum_{i=0}^M P_{\phi,i}^2 = \frac{\sum_{i=0}^M P_{\phi,i}^2 \tau}{\sum_{i=0}^M \tau} \approx \frac{g \Omega_{\text{tr}}}{2\pi} \oint P_\phi^2 dt = \frac{\Omega_{\text{tr}}}{2\pi} \oint P_\phi d\phi = \Omega_{\text{tr}} I_\phi \quad (192)$$

where we took into account the smallness of  $\tau$ . Substituting Eq. (192) into Eq. (191), we obtain:

$$\text{Var}(\Delta I_\phi) = \frac{(r_1 \tau)^2}{\Omega_{\text{tr}}} I_\phi \sigma \quad (193)$$

The evolution of  $I_\phi$  can be viewed as a random walk. We describe the behavior of an ensemble of such randomly walking trajectories (an ensemble of particles) in terms of the particle distribution function  $\Psi(I_\phi, t)$ : the probability for a particle to have the value of adiabatic invariant in the interval  $(I_\phi - \delta I_\phi/2, I_\phi + \delta I_\phi/2)$  at the time  $t$  is given by  $\Psi(I_\phi, t) \delta I_\phi$ . For this distribution  $\Psi(I_\phi, t)$  we can write a diffusion equation:

$$\frac{\partial \Psi}{\partial t} = \frac{\partial}{\partial I_\phi} \left( D_{II} \frac{\partial \Psi}{\partial I_\phi} \right) \quad (194)$$

In Eq. (185), we introduced the diffusion coefficient  $D_{II} = \text{Var}(\Delta I_\phi)/\tau$ . Switching from  $t$  to  $x$  (via the Hamiltonian equation for system (30)) in Eq. (194) we get:

$$\frac{\partial \Psi}{\partial h} = \frac{\partial}{\partial I_\phi} \left( I_\phi \frac{\partial \Psi}{\partial I_\phi} \right) \quad (195)$$

where  $h = \sigma \tau h_1(x)$  and  $h_1(x)$  is defined by  $x(t)$  solution of Hamiltonian (30).

The boundary of the region filled by trapped trajectories is determined by the (changing along the trajectory) value of the area  $S_{\text{res}}$ . Renormalizing  $i = 2\pi I_\phi / S_{\text{res}}$ , we can rewrite Eq. (195) in a dimensionless form:

$$\frac{\partial \Psi}{\partial K} = \frac{\partial}{\partial i} \left( i \frac{\partial \Psi}{\partial i} \right) \quad (196)$$

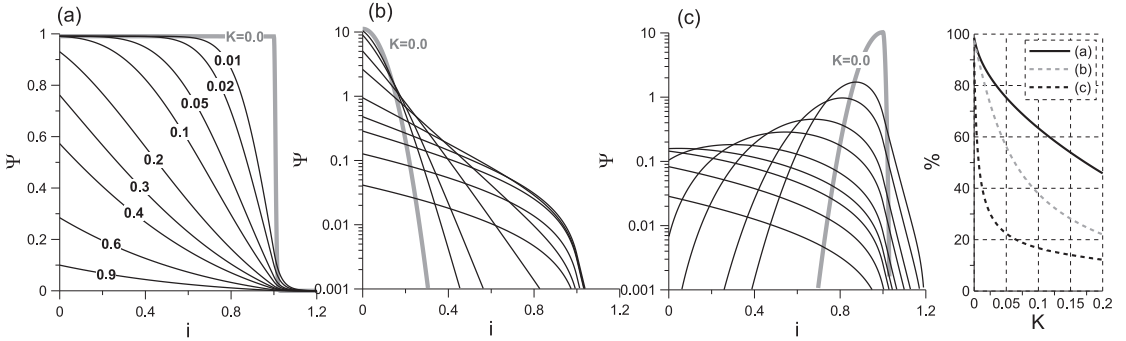


**Fig. 29.** Three examples of the evolution of distributions of trapped particles  $\Psi(i)$ . All particles with  $i > 1$  are assumed to escape from the system within a very short time interval. The right panel shows the evolution of the number of trapped particles for these three examples. Figure is adopted from [159].

where  $K = \sigma \tau h_1(x)/S_{\text{res}}$ . Eq. (196) describes the evolution of the distribution  $\Psi(i)$  of trapped particles. For a given initial distribution, one can calculate the number of particles remaining trapped for a given value of  $K$ . Solutions of Eq. (196) are shown in Fig. 29 for three types of initial distributions: (a) a uniformly filled region of trapped particles, (b) trapped particles originally residing only at the bottom of the potential well, and (c) for only recently trapped particles, with  $i \sim 1$ . The right panel of Fig. 29 shows that in all three cases the number of trapped particles diminishes as  $K$  increases, ultimately decreasing to 50%-20% already for  $K = 0.2$ . Consequently, to estimate the amount of detrapped (escaped) particles in realistic systems, one simply needs to evaluate  $K = \sigma \tau h_1(x)/S_{\text{res}}$ .

## 8.2. Wave-particle resonance in a fluctuating magnetic field

Let us consider particular plasma system with magnetic field fluctuations and demonstrate the applicability of proposed approach. The geometry of the system is the same as in Section 6.2: a background magnetic field  $B_0$  and a random magnetic field  $B_\Gamma(t)$  are directed along the  $z$ -axis, a plane electromagnetic wave (with a frequency  $\omega$  and wave vector  $k$ ) propagates along the  $x$ -axis, particles move in the  $(x, y)$  plane. Equations of motion of a non-relativistic particle (a relativistic analog was considered in [163]) are

$$\begin{aligned} \dot{x} &= v_x, \quad \dot{y} = v_y \\ \dot{v}_x &= \Omega_0 v_y (1 + \Gamma(t) - b_z \sin(\phi)) \\ \dot{v}_y &= -\Omega_0 v_\phi b_z \sin(\phi) - \Omega_0 v_x (1 + \Gamma(t) - b_z \sin(\phi)) \end{aligned} \quad (197)$$

System (197) is equivalent to system (109) with  $v_\phi = \omega/k$  and

$$v_y = -\Omega_0 (x + \Gamma(t) + b_z k^{-1} \cos \phi), \quad v_x = p_x/m \quad (198)$$

The wave amplitude is  $B_z = b_z B_0$ , gyrofrequency is  $\Omega_0 = e B_0 / mc$ , and magnetic field fluctuations are  $B_\Gamma(t) = \Gamma(t) B_0$ . We assume that  $\Gamma(t)$  is a random process with zero mean (a non-zero mean can be included in  $B_0$ ).  $\Gamma(t)$  is constant during the fixed time interval  $\tau$  and when  $t = t_n = \tau n$  ( $n = 1, 2, 3, \dots$ ) the value of  $\Gamma(t)$  changes randomly according to its probability distribution. We also assume that  $k \gg 1$  and the high-frequency fluctuations corresponds to  $\tau \ll 1$ . This means that during one cyclotron gyration a particle experiences many  $\Gamma(t)$  changes. The averaging of Eq. (197) over the fast-oscillating random field corresponds to omitting the terms with  $\Gamma(t)$ . In such a system, the majority of particles moves around the Larmor circles described by Eqs. (100). Over one period of Larmor rotation, most of the particles scatter on resonance. However, some particles can be trapped into resonance. In the absence of the random field  $\Gamma(t)$ , the equations of trapped motion are

$$\dot{v}_y = -\Omega_0 v_\phi, \quad \ddot{\phi} = \Omega_0 k v_y (1 - b_z \sin(\phi)) \quad (199)$$

As  $k \gg 1$ ,  $\phi$  changes much faster than  $v_y$ . The Hamiltonian for the second equation in (199) is

$$H_\phi = \frac{1}{2} k^2 P_\phi^2 - \Omega_0 k^{-1} v_y (\phi + b_z \cos(\phi)) \quad (200)$$

where  $P_\phi = \dot{\phi}/k^2$ . A characteristic frequency of  $\phi$  oscillations is  $\Omega_{\text{tr}} = (|v_y| b_z k)^{1/2}$ .

The trapped motion has an adiabatic invariant,  $I_\phi = (1/2\pi) \oint P_\phi d\phi$ , which is the area under the unperturbed trajectory. The once-trapped particle stays trapped as long as  $2\pi I_\phi$  is smaller than the area  $S_{\text{res}}$ ,

$$S_{\text{res}} = \frac{2\sqrt{\Omega_0 k |v_y|}}{k^2} \int_{\phi_-}^{\phi_+} \sqrt{\phi - \phi_+ + b_z (\cos(\phi) - \cos(\phi_+))} d\phi \quad (201)$$

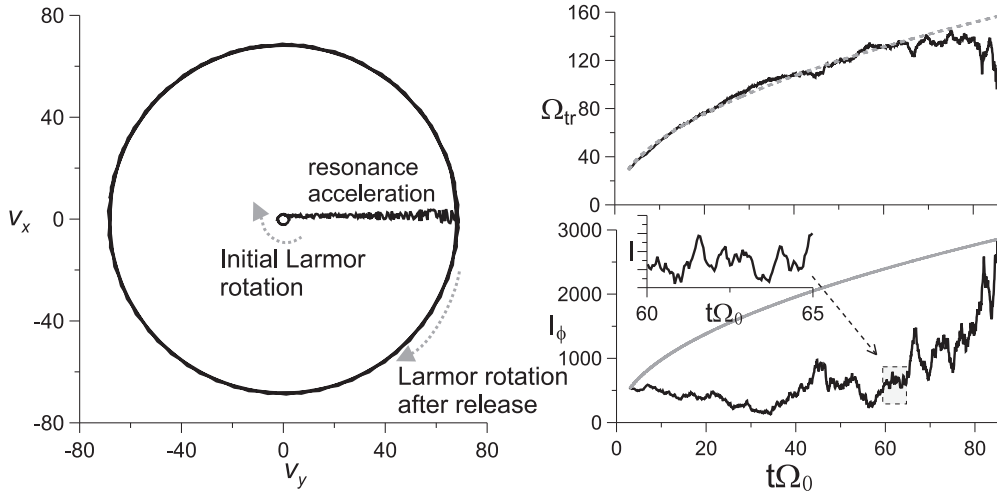


Fig. 30. Capture and release in the presence of fluctuations. Figure is adopted from [158].

where  $\phi_{\pm}$  are solutions of the equation  $\sin\phi = 1/b_z$ . As the particle accelerates in the resonance,  $|v_y| \sim v_\phi t$ , see Eq. (199), and the value of  $S_{\text{res}}$  grows. Together with the conservation of  $I_\phi$  (which is the case in the absence of fluctuations of the magnetic field) the growth of  $S_{\text{res}}$  ensures the permanent trapping.

The particle motion is qualitatively different for different values of  $\Omega_{\text{tr}}\tau$ . We consider the case  $\Omega_{\text{tr}}\tau \ll 1$ . The presence of fast oscillations of the magnetic field does not significantly change the dynamics of particles during the Larmor rotation, but, as we showed above, is important for the resonance motion. Eqs. (199) become

$$\begin{aligned} \dot{v}_y &= -\Omega_0 v_\phi (1 + \Gamma(t)) \\ \ddot{\phi} &= \Omega_0 k v_y (1 - b_z \sin(\phi)) + \Omega_0 k v_y \Gamma(t) \end{aligned} \quad (202)$$

Due to random fluctuations, the value of  $I_\phi$  changes. As  $\Omega_{\text{tr}} = dH_\phi/dI_\phi$  (see [162]), we have (cf. Eq. (190)):

$$(\Delta I_\phi)_n \approx \frac{1}{\Omega_{\text{tr}}} k^2 P_\phi (\Delta P_\phi)_n = \frac{1}{\Omega_{\text{tr}}} P_\phi \tau \Omega_0 k v_y \Gamma(t_n) \quad (203)$$

A typical dynamics of a single particle is illustrated in Fig. 30. The particle is trapped at the rightmost point of the small circle at the center of Fig. 30 (left panel). At the moment of trapping,  $I_\phi = S_{\text{res}}/2\pi$ . Then  $S_{\text{res}}$  starts growing as  $\sim (v_\phi \Omega_0 b_z k t)^{1/2}$  and  $I_\phi$  changes according to Eq. (203). If  $\tau$  is sufficiently small, at the initial stage  $S_{\text{res}}$  grows faster than  $I_\phi$  and particle falls toward the bottom of the potential well during the first few rotations in the  $(\phi, P_\phi)$  plane. While the particle is deep inside the well, its dynamics is quite similar to the dynamics without  $\Gamma(t)$  discussed above. The particle accelerates (the horizontal strip, with the growing width in Fig. 30 (left panel)) and  $\Omega_{\text{tr}}$  grows. In Fig. 30 (right panel), the dashed line is  $\Omega_{\text{tr}} = (v_\phi \Omega_0 b_z k t)^{1/2}$  and the solid line is the numerical value, obtained as the inverse of twice the time between two consecutive crossings of the  $\phi = 0$  line (times  $2\pi$ ). The deviations of the numerical value from the theoretical line are due to the (weak) dependence of  $\Omega_{\text{tr}}$  on  $I_\phi(t)$ , in other words, on the position of the particle inside the separatrix loop. If the particle comes close to the separatrix, the ratio  $2\pi I_\phi(t)/S_{\text{res}}(t)$  increases and  $\Omega_{\text{tr}}(I)$  decreases, which is the most pronounced near  $t\Omega_0 \approx 68$  and at the very right, where the particle comes close to the separatrix and eventually crosses it. However, the dependence of  $\Omega_{\text{tr}}$  on  $I_\phi(t)$  is indeed quite weak: deviations of numerical  $\Omega_{\text{tr}}(t)$  from theoretical curve are much smaller than variations of  $I_\phi(t)$ .

The evolution of  $I_\phi$  can be viewed as random walk (203) with time-dependent statistics of the steps, see Fig. 30(right panel). The inset shows the magnification of a typical interval containing several periods,  $\sim 2\pi/\Omega_{\text{tr}}$ . If in the process of the random walk the value of  $2\pi I_\phi$  exceeds the current value of  $S_{\text{res}}$ , the particle is released from resonance and starts moving along a larger Larmor circle.

To describe evolution of the particle probability distribution  $\Psi(I_\phi, t)$ , we consider Eq. (194) with the diffusion coefficient  $D_{II}(I, t)$  given by the variance of the right hand side of Eq. (203):

$$D_{II} \approx \left( \frac{k v_y \tau \Omega_0}{\Omega_{\text{tr}}} \right)^2 \text{Var}(P_\phi(t_n) \Gamma(t_n)) \quad (204)$$

In Eq. (204) we took into account that random walk (203) has two distinct time scales. The first one is the period of a single rotation in resonance ( $\sim 2\pi/\Omega_{\text{tr}}$ ). The other is the time at which the resonance orbit evolves. Results of numerical simulations presented in Fig. 30 indicate that a typical particle makes many turns before being released from trapping, and

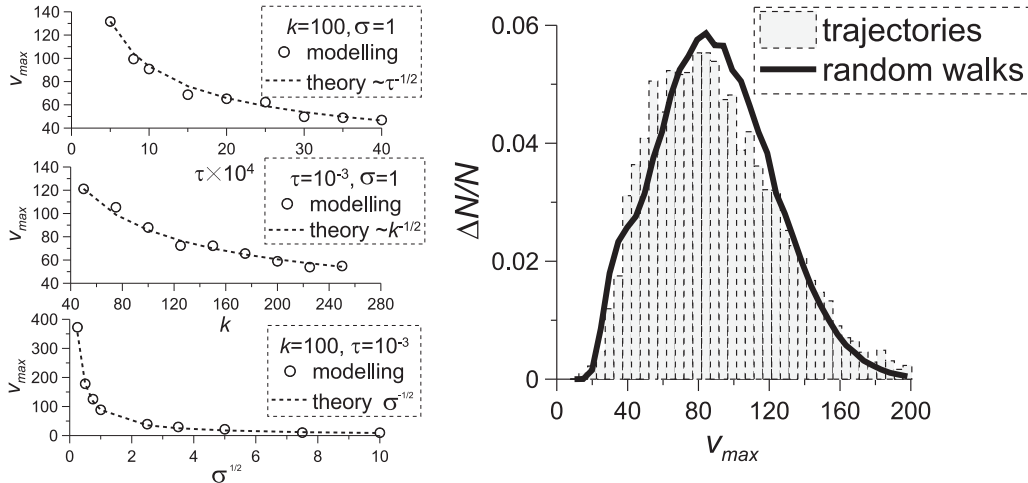


**Fig. 31.** Ensemble average of  $v_{\max}$  as a function of  $k$ ,  $\tau$ , and  $\sigma$  (left panels). The distributions of  $v_{\max}$  (right panel).  $\Delta N$  is the number of particles with  $v_{\max}$  and  $N$  is the total number of particles. Figure is adopted from [158].

for a one period of trapped motion the values of  $\Omega_{tr}$  and  $v_y$  can be considered to be constant. Assuming that  $P_\phi(t_n)$  and  $\Gamma(t_n)$  are uncorrelated and have zero mean, we get (cf. Eqs. (192), (193))

$$D_{II} \approx \left( \frac{v_y \tau \Omega_0}{\Omega_{tr}} \right)^2 \Omega_{tr} I_\phi \sigma \quad (205)$$

where we denoted  $\sigma = \text{Var}(\Gamma(t_n))$ . As it was noted above, we can neglect the dependence of  $\Omega_{tr}$  on  $I_\phi$  (except in the immediate vicinity of the separatrix) and assume  $\Omega_{tr} \sim (|v_y| \Omega_0 b_z k)^{1/2}$ . As  $|v_y| \sim v_\phi \Omega_0 t$ , we get

$$\frac{\partial \Psi}{\partial t} = t^{3/2} D_0 \frac{\partial}{\partial I_\phi} \left( I_\phi \frac{\partial \Psi}{\partial I_\phi} \right), \quad D_0 = \Omega_0^3 \sqrt{\frac{v_\phi^3}{b_z k} \tau \sigma} \quad (206)$$

Introducing a new time,  $t' = (2/5)t^{5/2}$ , we can reduce Eq. (206) to a standard diffusion equation

$$\frac{\partial \Psi}{\partial t'} = D_0 \frac{\partial}{\partial I_\phi} \left( I_\phi \frac{\partial \Psi}{\partial I_\phi} \right) \quad (207)$$

The long-time dynamics of an ensemble of particles can be described as follows: assume the initial distribution,  $\Psi(I_\phi, 0)$ , to be a  $\delta$ -function at a given value of  $I_\phi = I_0$ . The value of  $S_{\text{res}}$  at that moment is  $S_0 = 2\pi I_0$ . After that  $S_{\text{res}}$  starts growing as  $S_{\text{res}} \sim \sqrt{\Omega_0 b_z v_\phi t / k^3} \sim (t')^{1/5}$ . Meanwhile the evolution of  $I_\phi$  can be described as a random walk (203) and  $\Psi(I_\phi, t)$  starts drifting and spreading according to (207). It follows from (207) that on a given trajectory the expected value of  $I_\phi$  grows as  $\sim D_0 t' \sim D_0 t^{5/2}$ . In an asymptotical regime (when  $t \gg 1$ )  $S_{\text{res}}$  grows slower than the expected value of  $I_\phi$ . At a certain moment  $t = t_*$  defined as  $2\pi I_\phi(t_*) = S_{\text{res}}(t_*)$ , the particle is released from trapping. At that moment  $\sqrt{\Omega_0^2 b_z v_\phi t_* / k^3} \sim 2\pi D_0 t_*^{5/2}$ , and the velocity of a particle at the moment of release is

$$v_{\max} = v_\phi \Omega_0 t_* \sim v_\phi \sqrt{\frac{b_z}{2\pi\sigma} \frac{1}{\tau k v_\phi}} \quad (208)$$

We performed a set of numerical simulations for different values of  $k$ ,  $\tau$ , and  $\sigma$ . For each set of parameters, we computed the average value of the maximum velocities achievable in the process of trapping by integrating Eq. (197) for an ensemble of  $10^3$  particles all starting with the initial energy  $h_{\text{init}} = (v_x^2 + v_y^2)/2v_\phi^2 = 2$  (for each particle, the value of the initial angle  $\arctan(v_y/v_x)$  was chosen randomly). For each trajectory we used an individual realization of  $\Gamma(t)$ . We computed the final velocity and averaged it over the ensemble. The results are presented in Fig. 31 (left panels). The symbols are the results of numerical simulations and the curves are obtained from analytic description (208). One can see that the estimates of scaling of  $v_{\max}$  are in a good agreement with the results of the direct numerical modeling.

To verify the PDF-based description (207) and the evolution as random walk (203), we performed two types of numerical simulations. We integrated exact system (197) with  $\omega/\Omega_0 = 100, \sigma = 1, \tau\Omega_0 = 10^{-3}$  for  $10^4$  particles with initial energy  $h_{\text{init}} = 2$  until the release from resonance and computed the distribution of  $v_{\max}$ . We also computed  $10^6$  trajectories as a random walk of  $I_\phi$  using (203) as long as  $I_\phi(t) < S_{\text{res}}(t)/2\pi$ . For each trajectory we obtained its value  $t_*$  such that  $I_\phi(t_*) = S_{\text{res}}(t_*)/2\pi$  and computed  $v_{\max} = v_\phi \Omega_0 t_*$ . Two distributions of  $v_{\max}$  are presented in Fig. 31 (right panel): their similarity shows that the random walk approximation can adequately describe the dynamics of Eq. (197).

**Section summary** In this section we described effects of the background magnetic field fluctuations on wave-particle resonant interaction. We showed that resonant interaction can be destroyed by fluctuations and trapped particles could escape from resonance due to external nonresonant fluctuations. This effect imposes a limit on resonant particle acceleration in realistic space plasma environments.

## 9. Discussion and open questions

### 9.1. Four steps to kinetic equation

The theory of nonlinear resonant wave-particle interaction started from pioneering works of [34,35,164] and rapidly developed into a significant branch of plasma physics [e.g., 165,166]. In last two decades this theory became increasingly important for investigations of space and laboratory plasma systems as advanced measurements of wave signal onboard modern spacecraft [60,167–173] and in laboratory experiments [93–96] pointed at a significantly nonlinear nature of charged particle interaction with many different plasma waves. Although the quasi-linear theory of particle scattering by broad ensembles of low amplitude waves still provides quite a satisfactory explanation of many observed features of the long-term dynamics in various near-Earth plasma systems [e.g., 87,174], more and more often the theory of nonlinear resonances is required to properly describe transient variations of measured charged particle fluxes [e.g., 175,176].

In this review we considered a method construction of universal approach for description of the particle distribution evolution in systems with numerous nonlinear resonances. This approach consists of four main steps

**Averaging and structure of resonance:** Starting from the Hamiltonian for resonant particles in a specific electromagnetic field configuration, obtain expressions for Hamiltonians of slow motion and determine the location of resonance(s) in the phase plane;

**Individual resonance interaction:** Determine the properties of a single resonant interaction (the amplitude of scattering, energy change due to trapping) for a individual particle trajectory;

**Collective properties at multiple crossings:** Average the individual resonant particle properties over a pensemle and multiple resonance interactions to determine collective properties: probability of trapping, velocity of particle drift in energy space, energy drift and diffusion due to scattering;

**Kinetic equation:** Construct a kinetic equation including collective (averaged) properties of resonant interaction;

A kinetic (master) equation derived following these steps is [177]

$$\frac{\partial \Psi}{\partial t} = \int K(\mathbf{v} - \mathbf{v}') \Psi(\mathbf{v}') d\mathbf{v}' \quad (209)$$

with an analytical expression for operator  $K(\mathbf{v}, \mathbf{v}')$ . The derived kinetic equation opens an opportunity to quantify the impact of nonlinear wave-particle interaction on dynamics of particles in various space plasma systems. Although this equation is rather general, there are several questions which should be addressed before for realistic plasma systems.

### 9.2. Open questions

So far the evolution of particle distributions,  $\Psi$ , in the system with the nonlinear wave-particle interaction was described using a simplified test particle approach [e.g., 178,179] or by a numerical construction of an integral operator  $K$  acting on the particle distribution [180,181]. These approaches, when tailored to a particular parameter range, can provide a sufficiently accurate description of the resonant particle dynamics in some plasma systems. However, their accuracy is not sufficient for a description of long-term evolution of  $\Psi$  due to very different scales of resonant particle velocity change in two nonlinear phenomena: scattering and trapping. A small population of particles is trapped and accelerated by intense waves, and an accurate numerical modelling of this population must take a large range of velocities into account. On the other hand, the vast majority of particles are scattered and change their velocities only slightly. Simultaneous consideration of both effects presents a significant challenge for any numerical approach. Moreover, application of numerical approach does not allow controlling the fine relation between scattering and trapping energy (velocity) change, and thus the corresponding numerical results can deviate from the actual  $\Psi$  evolution on long time-scales.

The alternative approach for derivation of Eq. (209), that was demonstrated in Section 5.3, results in a kinetic equation where trapping and scattering effects are balanced. This approach requires a detailed information about the wave-particle nonlinear interactions, such as the probability of trapping and scattering amplitude. In this review we collected results from several of our previous studies to propose a standardized approach. Following this procedure, one can apply the same technique for different configuration of background magnetic field and different wave properties and derive an appropriate kinetic equation for  $\Psi$ . However, we should mention that the approach described in Section 5.3 is not yet finalized. Several important questions remain open:

1. How to generalize Eq. (96) to systems with several frequencies of slow particle motion (i.e., multidimensional systems)?
2. How to include the averaging of the coefficients Eq. (96) over distributions of wave characteristics (e.g., frequency, intensity, etc.)?

3. How to apply Eq. (96) to systems with nonharmonic waves (e.g., localized wave packets)?
4. How to include effects of the resonant interaction destruction due to external resonant and nonresonant noises into Eq. (96)?
5. What are general properties of solutions of Eq. (96)?

Some of these questions are considered in recent publications [182–184], but so far no one of them is solved.

In this review we focused on effects of the nonlinear resonant wave-particle interaction on particle dynamics, and did not discuss the feedback of this dynamics to wave evolution. This approximation is based on the assumption that the acceleration/deceleration of some population of resonant particles occurs at expense of deceleration/acceleration of another resonant population [22,23]. However, for closed plasma systems where the energy exchange between particle populations is not influenced by external energy sources, Eq. (96) should be written for all resonant particles and be supplemented by the second equation for the average wave intensity [like it has been done for quasi-linear models, see, e.g., 166].

## 10. Conclusions

In this review we presented a general approach for analysis of Hamiltonian systems with resonances and discussed several concrete examples where this approach allows us to explain charged particle dynamics and acceleration. We mostly restricted our consideration to dynamics of individual particles and only sketched the construction of general kinetic equations where effects of particle trapping and phase bunching (nonlinear particle scattering) are included in a form of operators acting on particle distribution function. Currently, the analysis of individual particle trajectories can still provide useful information of many plasma system with nonlinear wave-particle interaction. However, the natural next step in the development of this theory be a construction of a universal kinetic equation describing fast particle transport in the phase space due to trapping. This equation should be eventually complemented by equations for wave intensity evolution due to the feedback. Although some approaches for the construction of this self-consistent system of equations can be derived from our review, there are a lot to be done to finalize the kinetic theory of the nonlinear wave-particle interaction.

## Acknowledgements

Work of A.V.A., A.I.N., A.A.V., and I.Y.V. is supported by the Russian Scientific Foundation, Project No. 14-12-00824. This material is based in part upon work supported by the National Science Foundation under Award No. CMMI-1740777 (D.L.V.). Authors are grateful to Dr. D. Mourenas for fruitful discussions and important inputs.

## Appendix A. Conservation of the adiabatic invariant $I_\phi$ and accuracy of integration

In Section 3 we demonstrated that description of trapped particle motion is based on the conservation of adiabatic invariant  $I_\phi$  given by Eq. (36). Relation between this invariant and the area  $S_{\text{res}}$  surrounded by the separatrix determines for how long do trapped particles stay in the resonance before the escape (see scheme in Fig. 5). Therefore, the accuracy of numerical integration of Hamiltonian equations should be sufficient to assure the  $I_\phi$  conservation. Equations of motions contain terms of the different order of small parameter  $\varepsilon$ . To show what terms are important for  $I_\phi$  conservation (see, e.g., the discussion in [185] and references therein), we consider the accuracy of integration of Hamiltonian equations for systems with two pairs of variables and a time-dependent perturbation (e.g., 171).

For the sake of simplicity, we start with a Hamiltonian in a dimensionless form:

$$H = H_0(z, p_z, I_x) + \varepsilon u(z, p_z, I_x) \sin(\phi - n\psi), \quad \phi = \int k(\tilde{z}) d\tilde{z} - \omega t \quad (\text{A.1})$$

where  $\varepsilon \ll 1$ , pairs of conjugate variables are  $(z, p_z)$  and  $(\psi, I_x)$ ; the order of resonance  $n = 0$  (for system (157)) and  $n = -1$  (for system (171)). The corresponding Hamiltonian equation are

$$\begin{aligned} \dot{z} &= \frac{\partial H_0}{\partial p_z} + \varepsilon \frac{\partial u}{\partial p_z} \sin(\phi - n\psi) \\ \dot{p}_z &= -\frac{\partial H_0}{\partial z} + k\varepsilon u \cos(\phi - n\psi) + \varepsilon \frac{\partial u}{\partial z} \sin(\phi - n\psi) \\ \dot{\psi} &= \frac{\partial H_0}{\partial I_x} + \varepsilon \frac{\partial u}{\partial I_x} \sin(\phi - n\psi) \\ \dot{I}_x &= -n\varepsilon u \cos(\phi - n\psi) \end{aligned} \quad (\text{A.2})$$

These equations contain terms independent on  $\varepsilon$ , terms proportional to  $k\varepsilon$ , and terms proportional to  $\varepsilon$ . The later terms are small compared to other terms. However, these small terms are important for accurate system expansion around some resonance. To demonstrate situations when terms  $\sim \varepsilon$  should be taken into account, we consider the resonance  $\phi - n\psi = 0$ . First, we introduce new phase  $\zeta = \phi - n\psi$  and conjugate momentum  $I$  through the generating function:

$$R = I \left( \int k(\tilde{z}) d\tilde{z} - \omega t - n\psi \right) + P_z z + \tilde{I}_x \psi \quad (\text{A.3})$$

New variables are:

$$p_z = kI + P_z, \quad I_x = -nI + \tilde{I}_x, \quad \zeta = \int k(\tilde{z})d\tilde{z} - \omega t - n\psi \quad (\text{A.4})$$

The corresponding Hamiltonian takes the form:

$$H = H_0(z, kI + P_z, -nI + \tilde{I}_x) + \varepsilon u(z, kI + P_z, -nI + \tilde{I}_x) \sin \zeta \quad (\text{A.5})$$

where conjugate variables are  $(z, P_z)$ ,  $(\zeta, I)$ , and  $(\psi, \tilde{I}_x)$ . Hamiltonian (A.5) does not depend on  $\psi$ , and thus  $\tilde{I}_x$  is conserved. We can set  $\tilde{I}_x = 0$  and rewrite Eq. (A.5) as:

$$H = H_0(z, kI + P_z, -nI) + \varepsilon u(z, kI + P_z, -nI) \sin \zeta \quad (\text{A.6})$$

The resonance condition is  $\dot{\zeta} = \partial H_0 / \partial I = 0$  with a solution  $I = I_{\text{res}}(z, P_z)$ . Expanding Hamiltonian (A.6) around  $I - I_{\text{res}} = 0$  we get:

$$\begin{aligned} H &= \Lambda + \frac{1}{2}g(I - I_{\text{res}})^2 + \varepsilon u_{\text{res}} \sin \zeta \\ \Lambda(z, P_z) &= H_0(z, kI_{\text{res}} + P_z, -nI_{\text{res}}) \\ g(z, P_z) &= \partial^2 H_0 / \partial^2 I^2|_{I_{\text{res}}}, \quad u_{\text{res}}(z, P_z) = u(z, kI_{\text{res}} + P_z, -nI_{\text{res}}) \end{aligned} \quad (\text{A.7})$$

Introducing new variable  $P_\phi = (I - I_{\text{res}})$ , we obtain:

$$H = \Lambda + \frac{1}{2}gP_\phi^2 + r\zeta + \varepsilon u_{\text{res}} \sin \zeta, \quad r(z, P_z) = \{\Lambda, I_{\text{res}}\} \quad (\text{A.8})$$

Hamiltonian equation for  $P_\phi$  are

$$\dot{P}_\phi = \frac{\partial H}{\partial \zeta} = -r - \varepsilon u_{\text{res}} \cos \zeta \quad (\text{A.9})$$

Variables  $r, u_{\text{res}}$  change slowly due to a (slow) variation of  $(z, P_z)$ . Eq. (A.9) shows that the accuracy of conservation of  $I_\phi = \int P_\phi d\phi$  is defined by the accuracy of calculation of  $r$  and  $u_{\text{res}}$ . Both functions depend on  $I_{\text{res}}$ , which is defined by the equation  $\dot{\zeta} \partial H_0 / \partial I = 0$ . We rewrite this equation through the initial variables  $p_z, I_x$ . For this reason, we take into account that  $\partial I / \partial p_z = 1/k$  and  $\partial I / \partial I_x = -n$  (see Eq. (A.4)). Thus,  $\partial H_0 / \partial I = 0$  takes the form

$$k \frac{\partial H_0}{\partial p_z} - n \frac{\partial H_0}{\partial I_x} = 0 \quad (\text{A.10})$$

We substitute Eqs. (A.2) to Eq. (A.10):

$$\frac{\partial H_0}{\partial I} = k \left( \dot{z} - \varepsilon \frac{\partial u}{\partial p_z} \sin(\phi - n\psi) \right) - n \left( \dot{\psi} - \varepsilon \frac{\partial u}{\partial I_x} \sin(\phi - n\psi) \right) = 0 \quad (\text{A.11})$$

Eq. (A.11) does not contain terms  $\sim \varepsilon$  only if  $n = 0$  (the Landau resonance, see, e.g., system (157)) and  $\partial u / \partial p_z = 0$ . In this case, to find  $I_{\text{res}}$  we do not need to take into account the second order term  $\sim \varepsilon$  in system (A.2).

For  $n \neq 0$  and/or  $\partial u / \partial p_z \neq 0$ , the accuracy of computation of  $I_{\text{res}}$  depends on terms  $\sim \varepsilon$  and all these terms should be taken into account for a numerical integration of initial system (A.2). This simple example shows that for numerical integration of system (A.2), one should keep all small terms and provide the corresponding accuracy of integration.

## Appendix B. Accuracy of averaging of particle gyrorotation

Through the review, we consider many systems where particles oscillate around a strong background magnetic field. When considering the resonant wave-particle interaction, these fast oscillations should be averaged over. Such an averaging is equivalent to the introduction of a new adiabatic invariant. We use a canonical transformation to perform the averaging. However, for systems with a weakly inhomogeneous background magnetic field, this transformation results in an appearance of new fast oscillating terms in the Hamiltonian equations. In this Appendix we derive expressions for these terms and explain why they can be omitted.

We use a nonrelativistic Hamiltonian, but the same procedure can be performed for relativistic systems:

$$H = \frac{1}{2m} (p_x^2 + p_z^2) + \frac{1}{2}m(\Omega_0(z)x)^2 \quad (\text{B.1})$$

where  $\Omega_0(z) = eB_0(z)/mc$  is a gyrofrequency. In systems with a strong magnetic field, particle gyromotion in the  $(x, p_x)$  plane is much faster than the motion along field lines in the  $(z, p_z)$  plane. This approximation is called *the approximation of a weak magnetic field inhomogeneity* as it is assumed that  $x\partial\Omega_0/\partial z \ll \Omega_0$ . Hamiltonian equations for  $(x, p_x)$  are:

$$\dot{x} = p_x/m, \quad \dot{p}_x = -m\Omega_0^2(z)x \quad (\text{B.2})$$

For frozen  $(z, p_z)$ , a solution of Eqs. (B.2) is:

$$x = \sqrt{\frac{2h_z}{m\Omega_0^2}} \sin \psi, \quad p_x = \sqrt{2h_z m} \cos \psi \quad (\text{B.3})$$

where  $h_z = H - p_z^2/2m$  and  $\dot{\psi} = \Omega_0$ . The corresponding action  $I_x$  can be written as

$$I_x = \frac{1}{2\pi} \oint p_x dx = \frac{2h_z}{\pi\Omega_0} \int_0^\pi \cos^2 \psi d\psi = \frac{h_z}{\Omega_0} \quad (\text{B.4})$$

Thus, Eq. (B.3) can be rewritten as

$$x = \sqrt{\frac{2I_x}{m\Omega_0}} \sin \psi, \quad p_x = \sqrt{2I_x \Omega_0 m} \cos \psi \quad (\text{B.5})$$

We introduce  $(\psi, I_x)$  as new canonical variables using the generating function:

$$\begin{aligned} R(I_x, x; \tilde{p}_z, z) &= \int p_x dx + \tilde{p}_z z = 2I_x \int \cos^2 \psi d\psi + \tilde{p}_z z = I_x(\psi + \sin \psi \cos \psi) + \tilde{p}_z z \\ &= I_x \left( \arcsin \left( x \sqrt{\frac{m\Omega_0}{2I_x}} \right) + x \sqrt{\frac{m\Omega_0}{2I_x}} \sqrt{1 - x^2 \frac{m\Omega_0}{2I_x}} \right) + \tilde{p}_z z \end{aligned} \quad (\text{B.6})$$

The new and old variables are related as

$$\begin{aligned} p_x &= \frac{\partial R}{\partial x} = 2I_x \sqrt{\frac{m\Omega_0}{2I_x}} \sqrt{1 - x^2 \frac{m\Omega_0}{2I_x}} = \sqrt{2I_x m\Omega_0} \cos \psi \\ p_z &= \frac{\partial R}{\partial z} = \tilde{p}_z + \frac{I_x}{\Omega_0} \frac{\partial \Omega_0}{\partial z} x \sqrt{\frac{m\Omega_0}{2I_x}} \sqrt{1 - x^2 \frac{m\Omega_0}{2I_x}} = \tilde{p}_z + I_x \frac{1}{2} \frac{\partial \ln \Omega_0}{\partial z} \sin 2\psi \end{aligned} \quad (\text{B.7})$$

and  $\tilde{z} = z$ . In the new variables the Hamiltonian is

$$\begin{aligned} \tilde{H} &= \frac{1}{2m} \left( \tilde{p}_z + I_x \frac{1}{2} \frac{\partial \ln \Omega_0}{\partial z} \sin 2\psi \right)^2 + I_x \Omega_0 \\ &= \frac{1}{2m} \tilde{p}_z^2 + I_x \Omega_0 + \tilde{p}_z I_x \frac{\partial \ln \Omega_0}{\partial z} \sin 2\psi + \left( I_x \frac{1}{2} \frac{\partial \ln \Omega_0}{\partial z} \right)^2 \sin^2 2\psi \end{aligned} \quad (\text{B.8})$$

There are two fast oscillating terms in (B.8):  $\sim \sin 2\psi$  and  $\sim \sin^2 2\psi$ . Both terms result in oscillations of adiabatic invariant  $I_x$ , as  $\dot{I}_x = -\partial \tilde{H} / \partial \psi$ . Let us consider effects of these two terms separately.

The term  $\sim (\partial \ln \Omega_0 / \partial z) \sin 2\psi$  is small (because the inhomogeneity of the background magnetic field is weak) and oscillates fast around zero. Thus, instead of  $I_x$  we can introduce an improved adiabatic invariant and this procedure removes term  $\sim (\partial \ln \Omega_0 / \partial z) \sin 2\psi$  from the Hamiltonian [104]. The amplitude of the  $\sin^2 2\psi$  term in Hamiltonian (B.8) is  $\sim (\partial \ln \Omega_0 / \partial z)^2$  and much smaller than other terms again because the inhomogeneity of the background magnetic field is weak. For systems with and without wave perturbations this term can be omitted. Therefore, we can rewrite Hamiltonian (B.8) as

$$\tilde{H} = \frac{1}{2m} \tilde{p}_z^2 + I_x \Omega_0(z) \quad (\text{B.9})$$

where  $\tilde{p}_z = p_z$ .

## References

- [1] Pitaevskii LP, Lifshitz EM. Vol. 10: Physical kinetics, course of theoretical physics. New York: Pergamon Press; 1981.
- [2] Galeev A. A., Sudan R. N. Basic plasma physics. 1983.
- [3] Galeev AA, Sudan RN. Handbook of plasma physics. Basic Plasma Phys II 1985;2:7–48.
- [4] Vedenov AA. Theory of a weakly turbulent plasma. Rev Plasma Phys 1967;3(229).
- [5] Vedenov AA, Velikhov E, Sagdeev R. Quasilinear theory of plasma oscillations. Nuclear Fusion Suppl 1962;2. 465475
- [6] Drummond WE, Pines D. Nonlinear stability of plasma oscillations. Nuclear Fusion Suppl 1962;3:1049–58.
- [7] Andronov AA, Trakhtengerts VY. Kinetic instability of the earth's outer radiation belt. Geomag Aeron 1964;4:233–42.
- [8] Kennel CF, Engelmann F. Velocity space diffusion from weak plasma turbulence in a magnetic field. Phys Fluids 1966;9:2377–88. doi:10.1063/1.1761629.
- [9] Lerche I. Quasilinear theory of resonant diffusion in a magneto-active, relativistic plasma. Phys Fluids 11.
- [10] Karpman VI. Nonlinear effects in the ELF waves propagating along the magnetic field in the magnetosphere. Space Sci Rev 1974;16:361–88. doi:10.1007/BF00171564.
- [11] Queau DL, Roux A. Quasi-monochromatic wave-particle interactions in magnetospheric plasmas. Solar Phys. 1987;111:59–80. doi:10.1007/BF00145441.
- [12] Albert JM. Cyclotron resonance in an inhomogeneous magnetic field. Phys Fluids B 1993;5:2744–50. doi:10.1063/1.860715.
- [13] Solovev VV, Shkliar DR. Particle heating by a low-amplitude wave in an inhomogeneous magnetoplasma. Sov Phys JETP 1986;63:272–7.
- [14] Albert JM. Comparison of pitch angle diffusion by turbulent and monochromatic whistler waves. J Geophys Res 2001;106:8477–82. doi:10.1029/2000JA000304.

- [15] Brinca AL. Turbulence effects in the cyclotron resonance of monochromatic whistlers. *Geophys Res Lett* 1978;5:839–42. doi:[10.1029/GL005i010p00839](https://doi.org/10.1029/GL005i010p00839).
- [16] Brinca AL. On the evolution of the geomagnetospheric coherent cyclotron resonance in the midst of noise. *J Geophys Res* 1980;85:4711–14. doi:[10.1029/JA085iA09p04711](https://doi.org/10.1029/JA085iA09p04711).
- [17] Dowden RL. Detrapping by an additional wave of wave-trapped electrons. *J Geophys Res* 1982;87:6237–42. doi:[10.1029/JA087iA08p06237](https://doi.org/10.1029/JA087iA08p06237).
- [18] Nunn D. A nonlinear theory of sideband stability in ducted whistler mode waves. *Planetary Space Science* 1986;34:429–51. doi:[10.1016/0032-0633\(86\)90032-2](https://doi.org/10.1016/0032-0633(86)90032-2).
- [19] Schulz M, Lanzerotti LJ. *Particle diffusion in the radiation belts*. New York: Springer; 1974.
- [20] Lyons LR, Williams DJ. Quantitative aspects of magnetospheric physics. 1984.
- [21] Trakhentzents VY, Rycroft MJ. *Whistler and Alfvén Mode Cyclotron Masers in Space*. Cambridge University Press; 2008.
- [22] Shklyar D, Matsumoto H. Oblique whistler-mode waves in the inhomogeneous magnetospheric plasma: resonant interactions with energetic charged particles. *Surv Geophys* 2009;30:55–104. doi:[10.1007/s10712-009-9061-7](https://doi.org/10.1007/s10712-009-9061-7).
- [23] Shklyar DR. On the nature of pnerzation via resonant wave-particle interaction in the inhomogeneous magnetospheric plasma. *Ann Geophys* 2011;29:1179–88. doi:[10.5194/angeo-29-1179-2011](https://doi.org/10.5194/angeo-29-1179-2011).
- [24] Omura Y, Hikishima M, Katoh Y, Summers D, Yagitani S. Nonlinear mechanisms of lower-band and upper-band VLF chorus emissions in the magnetosphere. *J Geophys Res* 2009;114 7217. doi:[10.1029/2009JA014206](https://doi.org/10.1029/2009JA014206).
- [25] Omura Y, Nunn D, Summers D. Generation processes of whistler mode chorus emissions: current status of nonlinear wave growth theory. In: Summers D, Mann IU, Baker DN, Schulz M, editors. *Dynamics of the Earth's Radiation Belts and Inner Magnetosphere*. American Geophysical Union; 2013. p. 243–54. doi:[10.1029/2012GM001347](https://doi.org/10.1029/2012GM001347).
- [26] Shklyar DR. Energy transfer from lower energy to higher-energy electrons mediated by whistler waves in the radiation belts. *J Geophys Res* 2017;122(1):640–55. doi:[10.1002/2016JA023263](https://doi.org/10.1002/2016JA023263).
- [27] Demekhov AG, Taubenschuss U, Santolik O. Simulation of vlf chorus emissions in the magnetosphere and comparison with themis spacecraft data. *J Geophys Res* 2017 N/a-n/a doi:[10.1002/2016JA023057](https://doi.org/10.1002/2016JA023057).
- [28] Bénisti D. Nonlocal adiabatic theory. i. the action distribution function. *Phys Plasmas* 2017;24(9) 092120. doi:[10.1063/1.4996957](https://doi.org/10.1063/1.4996957) arXiv:[1706.03540](https://arxiv.org/abs/1706.03540).
- [29] Bénisti D. Nonlocal adiabatic theory. II. nonlinear frequency shift on an electron plasma wave in a multidimensional inhomogeneous plasma. *Phys Plasmas* 2017;24(9) 092121. doi:[10.1063/1.4996963](https://doi.org/10.1063/1.4996963).
- [30] Krasovsky VL. Trapped pfect on the velocity of circularly polarized electromagnetic waves in an isotropic plasma. *Phys Lett A* 2010;374:1751–4. doi:[10.1016/j.physleta.2010.02.030](https://doi.org/10.1016/j.physleta.2010.02.030).
- [31] Dodin IY, Fisch NJ. Nonlinear dispersion of stationary waves in collisionless plasmas. *Phys Rev Lett* 2011;107(3) 035005. doi:[10.1103/PhysRevLett.107.035005](https://doi.org/10.1103/PhysRevLett.107.035005) arXiv:[1105.0196](https://arxiv.org/abs/1105.0196).
- [32] Dodin IY, Fisch NJ. Adiabatic nonlinear waves with trapped particles. II. wave dispersion. *Phys Plasmas* 2012;19(1) 012103. doi:[10.1063/1.3662115](https://doi.org/10.1063/1.3662115) arXiv:[1107.3074](https://arxiv.org/abs/1107.3074).
- [33] Tao X, Zonca F, Chen L. Identify the nonlinear wave-particle interaction regime in rising tone chorus generation. *Geophys. Res. Lett.* 2017;44(8):3441–6. doi:[10.1002/2017GL072624](https://doi.org/10.1002/2017GL072624).
- [34] O'Neil T. Collisionless damping of nonlinear plasma oscillations. *Physics of Fluids* 1965;8:2255–62. doi:[10.1063/1.1761193](https://doi.org/10.1063/1.1761193).
- [35] Mazitov RK. Damping of plasma waves. *J Appl Mech Tech Phys* 1965;6:22–5. doi:[10.1007/BF00914365](https://doi.org/10.1007/BF00914365).
- [36] Landau LD, Lifshitz EM. *Electrodynamics of continuous media. Course of Theoretical Physics*, vol. 8. Pergamon Press; 1960.
- [37] Gary SP, Montgomery D, Swift DW. Particle acceleration by electrostatic waves with spatially varying phase velocities. *J Geophys Res* 1968;73:7524–5. doi:[10.1029/JA073i023p07524](https://doi.org/10.1029/JA073i023p07524).
- [38] Laval G, Pellar R. Particle acceleration by electrostatic waves propagating in an inhomogeneous plasma. *J Geophys Res* 1970;75:3255–6. doi:[10.1029/JA075i016p03255](https://doi.org/10.1029/JA075i016p03255).
- [39] Karpman VI, Shklyar DR. Nonlinear damping of potential monochromatic waves in an inhomogeneous plasma. *Sov JETP* 1972;35(500).
- [40] Karpman VI, Istomin JN, Shklyar DR. Particle acceleration by a non-linear langmuir wave in an inhomogeneous plasma. *Phys Lett A* 1975;53:101–2. doi:[10.1016/0375-9601\(75\)90364-3](https://doi.org/10.1016/0375-9601(75)90364-3).
- [41] Sagdeev RZ. *Reviews of plasma physics*, 1st edition, vol. 4. New York: Consultants Bureau; 1966.
- [42] Sagdeev RZ, Shapiro VD. Influence of transverse magnetic field on landau damping. *Soviet J. Exp. Theor. Phys. Letters* 1973;17:279–82.
- [43] Gubchenko VM, Zaitsev VV. On proton and electron acceleration by shock waves during large solar flares. *Sol Phys* 1979;63:337–52. doi:[10.1007/BF00174539](https://doi.org/10.1007/BF00174539).
- [44] Katsouleas T, Dawson JM. Unlimited electron acceleration in laser-driven plasma waves. *Phys Rev Lett* 1983;51:392–5. doi:[10.1103/PhysRevLett.51.846.2](https://doi.org/10.1103/PhysRevLett.51.846.2).
- [45] Nunn D. Wave-particle interactions in electrostatic waves in an inhomogeneous medium. *J Plasma Phys* 1971;6(291). doi:[10.1017/S0022377800006061](https://doi.org/10.1017/S0022377800006061).
- [46] Nunn D. A self-consistent theory of triggered VLF emissions. *Planetary Space Science* 1974;22:349–78. doi:[10.1016/0032-0633\(74\)90070-1](https://doi.org/10.1016/0032-0633(74)90070-1).
- [47] Karpman VI, Istomin JN, Shklyar DR. Nonlinear theory of a quasi-monochromatic whistler mode packet in inhomogeneous plasma. *Plasma Phys* 1974;16:685–703. doi:[10.1088/0032-1028/16/8/001](https://doi.org/10.1088/0032-1028/16/8/001).
- [48] Goldstein ML, Roberts DA, Matthaeus WH. Magnetohydrodynamic turbulence in the solar wind. *ARA&A* 1995;33:283–326. doi:[10.1146/annurev.aa.33.090195.001435](https://doi.org/10.1146/annurev.aa.33.090195.001435).
- [49] Gary SP, Smith CW. Short-wavelength turbulence in the solar wind: linear theory of whistler and kinetic alfvén fluctuations. *J. Geophys. Res.* 2009;114 A12105. doi:[10.1029/2009JA014525](https://doi.org/10.1029/2009JA014525).
- [50] Zhao JS, Voitenko Y, Wu DJ, De Keyser J. Nonlinear generation of kinetic-scale waves by magnetohydrodynamic alfvén waves and nonlocal spectral transport in the solar wind. *Astrophys J* 2014;785(139). doi:[10.1088/0004-637X/785/2/139](https://doi.org/10.1088/0004-637X/785/2/139).
- [51] Neugebauer M. Comment on the abundances of rotational and tangential discontinuities in the solar wind. *J Geophys Res* 2006;111 A04103. doi:[10.1029/2005JA010497](https://doi.org/10.1029/2005JA010497).
- [52] Greco A, Perri S, Servidio S, Yordanova E, Veltri P. The complex structure of magnetic field discontinuities in the turbulent solar wind. *Astrophys J Lett* 2016;823 L239. doi:[10.3847/2041-8205/823/2/L39](https://doi.org/10.3847/2041-8205/823/2/L39) arXiv:[1511.03084](https://arxiv.org/abs/1511.03084).
- [53] Podesta JJ. The most intense current sheets in the high-speed solar wind near 1 AU. *J. Geophys. Res.* 2017;122:2795–823. doi:[10.1002/2016JA023629](https://doi.org/10.1002/2016JA023629).
- [54] Medvedev MV, Shevchenko VI, Diamond PH, Galinsky VL. Fluid models for kinetic effects on coherent nonlinear alfvén waves. II. numerical solutions. *Phys Plasmas* 1997;4:1257–85. doi:[10.1063/1.872356](https://doi.org/10.1063/1.872356). ArXiv:physics/ [9612018](https://arxiv.org/abs/9612018).
- [55] Howes GG. The dynamical generation of current sheets in astrophysical plasma turbulence. *J Geophys Res* 2016;827 L28. doi:[10.3847/2041-8205/827/2/L28](https://doi.org/10.3847/2041-8205/827/2/L28) arXiv:[1607.07465](https://arxiv.org/abs/1607.07465).
- [56] Ergun R.E., Malaspina D.M., Cairns I.H., Goldman M.V., Newman D.L., Robinson P.A., Eriksson S., Bougeret J.L., Briand C., Bale S.D., Cattell C.A., Kellogg P.J., Kaiser M.L. Eigenmode structure in solar-wind langmuir waves. *Phys Rev Lett* 101(5). doi:[10.1103/PhysRevLett.101.051101](https://doi.org/10.1103/PhysRevLett.101.051101)
- [57] Malaspina DM, Newman DL, Wilson III, Goetz K, Kellogg PJ, Kersten K. Electrostatic solitary waves in the solar wind: evidence for instability at solar wind current sheets. *J Geophys Res* 2013;118:591–9. doi:[10.1002/jgra.50102](https://doi.org/10.1002/jgra.50102).
- [58] Kraft C, Volokitin AS, Krasnoselskikh VV. Interaction of energetic particles with waves in strongly inhomogeneous solar wind plasmas. *Astrophys J* 2013;778(111). doi:[10.1088/0004-637X/778/2/111](https://doi.org/10.1088/0004-637X/778/2/111).
- [59] Kraft C, Volokitin AS, Krasnoselskikh VV. Langmuir wave decay in inhomogeneous solar wind plasmas: Simulation results. *Astrophys J* 2015;809(176). doi:[10.1088/0004-637X/809/2/176](https://doi.org/10.1088/0004-637X/809/2/176).

- [60] Bale SD, Kellogg PJ, Larsen DE, Lin RP, Goetz K, Lepping RP. Bipolar electrostatic structures in the shock transition region: evidence of electron phase space holes. *Geophys Res Lett* 1998;25:2929–32. doi:10.1029/98GL02111.
- [61] Balikhin MA, de Wit TD, Alleyne HSCK, Wooliscroft LJC, Walker SN, Krasnoselskikh V, Mier-Jedrzejewicz WAC, Baumjohann W. Experimental determination of the dispersion of waves observed upstream of a quasi-perpendicular shock. *Geophys Res Lett* 1997;24:787–90. doi:10.1029/97GL00671.
- [62] Wilson LB, Koval A, Szabo A, Breneman A, Cattell CA, Goetz K, Kellogg PJ, Kersten K, Kasper JC, Maruca BA, Pulupa M. Electromagnetic waves and electron anisotropies downstream of supercritical interplanetary shocks. *J Geophys Res* 2013;118:5–16. doi:10.1029/2012JA018167. ArXiv: 1207.6429.
- [63] Kuramitsu Y, Krasnoselskikh V. Gyroresonant surfing acceleration. *Phys Rev Lett* 2005;94(3) 031102–+. doi:10.1103/PhysRevLett.94.031102.
- [64] Artemyev AV, Agapitov OV, Krasnoselskikh VV. Cyclotron resonance in plasma flow. *Phys Plasmas* 2013;20(12) 124502. doi:10.1063/1.4853615.
- [65] Kis A, Agapitov O, Krasnoselskikh V, Khotyaintsev YV, Dandouras I, Lemperger I, Wesczergom V. Gyrosurfing acceleration of ions in front of earth's quasi-parallel bow shock. *Astrophys J* 2013;771(4). doi:10.1088/0004-637X/771/1/4.
- [66] Wilson LB, Sibeck DG, Turner DL, Osmane A, Caprioli D, Angelopoulos V. Relativistic electrons produced by foreshock disturbances observed upstream of earth's bow shock. *Phys Rev Lett* 2016;117(21) 215101. doi:10.1103/PhysRevLett.117.215101 arXiv: 1607.02183.
- [67] Oka M, Wilson III, Phan TD, Hull AJ, Amano T, Hoshino M, Argall MR, Contel OL, Agapitov O, Gershman DJ, Khotyaintsev YV, Burch JL, Torbert RB, Pollock C, Dorelli JC, Giles BL, Moore TE, Saito Y, Avanov LA, Paterson W, Ergun RE, Strangeway RJ, Russell CT, Lindqvist PA. Electron scattering by high-frequency whistler waves at earth's bow shock. *Astrophys J Lett* 2017;842 L11. doi:10.3847/2041-8213/aa7759.
- [68] Krasnoselskikh V, Balikhin M, Walker SN, Schwartz S, Sundkvist D, Lobzin V, Gedalin M, Bale SD, Mozer F, Soucek J, Hobara Y, Comisel H. The dynamic quasi-perpendicular shock: cluster discoveries. *Space Sci Rev* 2013;178:535–98. doi:10.1007/s11214-013-9972-y. ArXiv: 1303.0190
- [69] Wing S, Johnson JR, Chaston CC, Echim M, Escoubet CP, Lavraud B, Lemon C, Nykyri K, Otto A, Raeder J, Wang CP. Review of solar wind entry into and transport within the plasma sheet. *Space Sci Rev* 2014;184:33–86. doi:10.1007/s11214-014-0108-9.
- [70] Baumjohann W, Treumann RA. *Basic space plasma physics*. London: Imperial College Press; 1996.
- [71] Panov EV, Büchner J, Fränz M, Korth A, Savin SP, Fornacon KH, Dandouras I, Rème H. CLUSTER Observation of collisionless transport at the magnetopause. *Geophys Res Lett* 2006;33: 15109. doi:10.1029/2006GL026556.
- [72] Yao Y, Chaston CC, Glassmeier KH, Angelopoulos V. Electromagnetic waves on ion gyro-radii scales across the magnetopause. *Geophys. Res. Lett.* *Geophys. Res. Lett.* 2011;38 L09102. doi:10.1029/2011GL047328.
- [73] Chaston CC, Yao Y, Lin N, Salem C, Ueno G. Ion heating by broadband electromagnetic waves in the magnetosheath and across the magnetopause. *J. Geophys. Res.* 2013;118: 5579–91. doi:10.1002/jgra.50506.
- [74] Johnson JR, Cheng CZ. Global structure of mirror modes in the magnetosheath. *J. Geophys. Res.* 1997;102:7179–90. doi:10.1029/96JA03949.
- [75] Chaston CC, Salem C, Bonnell JW, Carlson CW, Ergun RE, Strangeway RJ, McFadden JP. The turbulent alfvénic aurora. *Phys Rev Lett* 2008;100(17) 175003. doi:10.1103/PhysRevLett.100.175003.
- [76] Baker DN, Pulkkinen TI, Angelopoulos V, Baumjohann W, McPherron RL. Neutral line model of substorms: past results and present view. *J. Geophys. Res.* 1996;101:12975–3010. doi:10.1029/95JA03753.
- [77] Angelopoulos V, McFadden JP, Larson D, Carlson CW, Mende SB, Frey H, Phan T, Sibeck DG, Glassmeier K, Auster U, Donovan E, Mann IR, Rae IJ, Russell CT, Runov A, Zhou X, Kepko L. Tail reconnection triggering substorm onset. *Science* 2008;321:931–5. doi:10.1126/science.1160495.
- [78] Paschmann G, Oieroset M, Phan T. In-situ observations of reconnection in space. *Space Sci. Rev.* 2013;178:385–417. doi:10.1007/s11214-012-9957-2.
- [79] Fujimoto M, Shinohara I, Kojima H. Reconnection and waves: a review with a perspective. *Space Sci. Rev.* 2011;160:123–43. doi:10.1007/s11214-011-9807-7.
- [80] Angelopoulos V, Runov A, Zhou XZ, Turner DL, Kiehias SA, Li SS, Shinohara I. Electromagnetic energy conversion at reconnection fronts. *Science* 2013;341:1478–82. doi:10.1126/science.1236992.
- [81] Lysak RL. Electrodynamical coupling of the magnetosphere and ionosphere. *Space Sci. Rev.* 1990;52:33–87. doi:10.1007/BF00704239.
- [82] Birn J, Artemyev AV, Baker DN, Echim M, Hoshino M, Zelenyi LM. Particle acceleration in the magnetotail and aurora. *Space Sci. Rev.* 2012;173 49102. doi:10.1007/s11214-012-9874-4.
- [83] Kivelson M.G., Russell C.T. *Introduction to space physics*. 1995.
- [84] Jordanova VK. *Sources, transport, and losses of energetic particles during geomagnetic storms. The Inner Magnetosphere: Physics and Modeling*, Vol 155 of Washington DC American Geophysical Union Geophysical Monograph Series. Pulkkinen TI, Tsyganenko NA, Friedel RHW, editors; 2005. 9
- [85] Kennel CF, Petschek HE. Limit on stably trapped particle fluxes. *J. Geophys. Res.* 1966;71:1–28.
- [86] Horne RB, Thorne RM, Shprits YY, Meredith NP, Glauert SA, Smith AJ, Kanekal SG, Baker DN, Engebretson MJ, Posch JL, Spasojevic M, Inan US, Pickett JS, Decreau PME. Wave acceleration of electrons in the van allen radiation belts. *Nature* 2005;437:227–30. doi:10.1038/nature03939.
- [87] Thorne RM, Li W, Ni B, Ma Q, Bortnik J, Chen L, Baker DN, Spence HE, Reeves GD, Henderson MG, Kletzing CA, Kurth WS, Hospodarsky GB, Blake JB, Fennell JF, Claudeperre SG, Kanekal SG. Rapid local acceleration of relativistic radiation-belt electrons by magnetospheric chorus. *Nature* 2013;504:411–14. doi:10.1038/nature12889.
- [88] Albert JM, Tao X, Bortnik J. Aspects of nonlinear wave-particle interactions. *Dynamics of the Earth's Radiation Belts and Inner Magnetosphere*, American Geophysical Union. Summers D, Mann IU, Baker DN, Schulz M, editors; 2013. doi: 10.1029/2012GM001324
- [89] Wygant JR, Keiling A, Cattell CA, Lysak RL, Temerin M, Mozer FS, Kletzing CA, Scudder JD, Streltsov V, Lotko W, Russell CT. Evidence for kinetic alfvén waves and parallel electron energization at 4–6  $r_E$  altitudes in the plasma sheet boundary layer. *J. Geophys. Res.* 2002;107 1201. doi:10.1029/2001JA0090113.
- [90] Watt CEJ, Rankin R. Electron trapping in shear alfvén waves that power the aurora. *Phys Rev Lett* 2009;102(4) 045002. doi:10.1103/PhysRevLett.102.045002.
- [91] Damiano PA, Johnson JR, Chaston CC. Ion temperature effects on magnetotail alfvén wave propagation and electron energization. *J. Geophys. Res.* 2015;120:5623–32. doi:10.1002/2015JA021074.
- [92] Artemyev AV, Rankin R, Blanco M. Electron trapping and acceleration by kinetic alfvén waves in the inner magnetosphere. *J. Geophys. Res.* 2015;120(10). doi:10.1002/2015JA021781.
- [93] Starodubtsev M, Kraft C. Resonant cyclotron emission of whistler waves by a modulated electron beam. *Phys Rev Lett* 1999;83:1335–8. doi:10.1103/PhysRevLett.83.1335.
- [94] Compernolle BV, An X, Bortnik J, Thorne RM, Pribyl P, Gekelman W. Excitation of chirping whistler waves in a laboratory plasma. *Phys Rev Lett* 2015;114(24) 245002. doi:10.1103/PhysRevLett.114.245002.
- [95] Tejero EM, Crabtree C, Blackwell DD, Amatucci WE, Mithaiwala M, Ganguli G, Rudakov L. Laboratory studies of nonlinear whistler wave processes in the van allen radiation belts. *Phys Plasmas* 2015;22(9) 091503. doi:10.1063/1.4928944.
- [96] Viktorov ME, Golubev SV, Mansfeld DA, Vodopyanov AV. Excitation of electromagnetic waves in dense plasma during the injection of supersonic plasma flows into magnetic arch. *AIP Conf Proc* 2016;1771(1) 070010. doi:10.1063/1.4964234.
- [97] Bénisti D, Morice O, Gremillet L, Friou A, Lefebvre E. Nonlinear kinetic modeling of stimulated raman scattering in a multidimensional geometrya). *Phys Plasmas* 2012;19(5) 056301. doi:10.1063/1.3693123.
- [98] Dewald EL, Hartemann F, Michel P, Milovich J, Hohenberger M, Pak A, Landen OL, Divol L, Robey HF, Hurricane OA, Döppner T, Albert F, Bachmann B, Meezan NB, MacKinnon AJ, Callahan D, Edwards MJ. Generation and beaming of early hot electrons onto the capsule in laser-driven ignition hohlraums. *Phys Rev Lett* 2016;116(7) 075003. doi:10.1103/PhysRevLett.116.075003.
- [99] Kroll NM, Morton PL, Rosenbluth MN. Free-electron lasers with variable parameter wigglers. *IEEE J Quantum Electron* 1981;17:1436–68. doi:10.1109/JQE.1981.1071285.
- [100] Courant ED, Pellegrini C, Zakowicz W. High-energy inverse free-electron-laser accelerator. *Phys. Rev. A* 1985;32:2813–23. doi:10.1103/PhysRevA.32.2813.

- [101] Clark RW, Swanson DG, Korn P, Sandel F, Robertson S, Wharton CB. High power fundamental and harmonic resonant ion cyclotron heating in a mirror machine. *Physics of Fluids* 1974;17:1322–8. doi:10.1063/1.1694884.
- [102] Jhang H, Lee SG, Kim SS, Park BH, Bak JG. Stabilization of interchange modes in mirror plasmas by a nonlinear rf-plasma wave coupling process. *Phys Rev Lett* 2005;95(3) 035005. doi:10.1103/PhysRevLett.95.035005.
- [103] Nakamura T, Mima K, Sakagami H, Johzaki T. Electron surface acceleration on a solid capillary target inner wall irradiated with ultraintense laser pulses. *Phys Plasmas* 2007;14(5) 053112. doi:10.1063/1.2731383.
- [104] Arnold VI, Kozlov VV, Neishtadt AI. *Mathematical aspects of classical and celestial mechanics*, 3rd edition. *Dynamical Systems III. Encyclopedia of Mathematical Sciences*. New York: Springer-Verlag; 2006.
- [105] Neishtadt A. Passage through a separatrix in a resonance problem with a slowly-varying parameter. *Journal of Applied Mathematics and Mechanics* 1975;39:594–605. doi:10.1016/0021-8928(75)90060-X.
- [106] Itin AP, Neishtadt AI, Vasiliev AA. Captures into resonance and scattering on resonance in dynamics of a charged relativistic particle in magnetic field and electrostatic wave. *Physica D* 2000;141:281–96. doi:10.1016/S0167-2789(00)00039-7.
- [107] Dolgopyat D. *Repulsion from resonances. Memoires De La Societe Mathematique De France*, Vol. 128 of *Memoires De La Societe Mathematique De France*; 2012.
- [108] Albert JM. Diffusion by one wave and by many waves. *J. Geophys. Res.* 2010;115. doi:10.1029/2009JA014732. 0
- [109] Neishtadt AI, Artemyev AV, Zelenyi LM, Vainstein DL. Surfatron acceleration in electromagnetic waves with a low phase velocity. *JETP Lett* 2009;89:441–7. doi:10.1134/S0021364009090045.
- [110] Neishtadt A, Vasiliev A, Artemyev A. Resonance-induced surfatron acceleration of a relativistic particle. *Moscow Mathematical Journal* 2011;11(3):531–45.
- [111] Neishtadt AI. On adiabatic invariance in two-frequency systems, in hamiltonian systems with three or more degrees of freedom. In: Sim C, Dordrecht C, editors. *NATO ASI Series*. Kluwer Acad. Publ. 533; 1999. p. 193–213. doi:10.1063/1.166236.
- [112] Bell TF. The nonlinear gyroresonance interaction between energetic electrons and coherent VLF waves propagating at an arbitrary angle with respect to the earth's magnetic field. *J. Geophys. Res.* 1984;89:905–18. doi:10.1029/JA089iA02p00905.
- [113] Malkov MA, Zaslavskii GM. Wave-particle resonant interaction in a weak magnetic field. *Phys Lett A* 1984;106:257–60. doi:10.1016/0375-9601(84)91022-3.
- [114] Valentini F, Veltri P, Mangeney A. Magnetic-field effects on nonlinear electrostatic-wave landau damping. *Phys. Rev. E* 2005;71(1) 016402. doi:10.1103/PhysRevE.71.016402.
- [115] Vainchtein D, Mezić I. Capture into resonance: a method for efficient control. *Phys Rev Lett* 2004;93(8) 084301. doi:10.1103/PhysRevLett.93.084301.
- [116] Neishtadt AI, Artemyev AV, Zelenyi LM. Regular and chaotic charged particle dynamics in low frequency waves and role of separatrix crossings. *Regular and Chaotic Dynamics* 2010;15:564–74. doi:10.1134/S1560354710040118.
- [117] Karney CFF. Stochastic ion heating by a lower hybrid wave. *Physics of Fluids* 1978;21:1584–99. doi:10.1063/1.862406.
- [118] Karney CFF. Stochastic ion heating by a lower hybrid wave. II. *Physics of Fluids* 1979;22:2188–209. doi:10.1063/1.862512. ArXiv:arXiv:physics/ 0501034
- [119] Takeuchi S, Sakai K, Matsumoto M, Sugihara R. Unlimited acceleration of a charged particle by an electromagnetic wave with a purely transverse electric field. *Phys Lett A* 1987;122:257–61. doi:10.1016/0375-9601(87)90818-8.
- [120] Takeuchi S. New particle accelerations by magnetized plasma shock waves. *Phys Plasmas* 2005;12(10) 102901. doi:10.1063/1.2080520.
- [121] Runov A, Angelopoulos V, Sergeev VA, Glassmeier K, Auster U, McFadden J, Larson D, Mann I. *Global properties of magnetotail current sheet flapping: THEMIS perspectives*. *Ann Geophys* 2009;27:319–28.
- [122] Sitnov MI, Swisdak M, Divin AV. Dipolarization fronts as a signature of transient reconnection in the magnetotail. *J. Geophys. Res.* 2009;114 A04202. doi:10.1029/2008JA013980.
- [123] Runov A, Angelopoulos V, Sitnov MI, Sergeev VA, Bonnell J, McFadden JP, Larson D, Glassmeier K, Auster U. THEMIS Observations of an earthward-propagating dipolarization front. *Geophys. Res. Lett.* 2009;36 L14106. doi:10.1029/2009GL038980.
- [124] Sundberg T, Slavin JA, Boardens SA, Anderson BJ, Korth H, Ho GC, Schriver D, Uritsky VM, Zurbuchen TH, Raines JM, Baker DN, Krimigis SM, McNutt Jr RL, Solomon SC. MESSENGER Observations of dipolarization events in mercury's magnetotail. *J. Geophys. Res.* 2012;117. doi:10.1029/2012JA017756. 0
- [125] Kasahara S, Kronberg EA, Kimura T, Tao C, Badman SV, Masters A, Retinò A, Krupp N, Fujimoto M. Asymmetric distribution of reconnection jet fronts in the jovian nightside magnetosphere. *J. Geophys. Res.* 2013;118:375–84. doi:10.1029/2012JA018130.
- [126] Artemyev AV, Zimbardo G, Ukhorskiy AY, Fujimoto M. Preferential acceleration of heavy ions in the reconnection outflow region. drift and surfatron ion acceleration. *Astron. Astrophys.* 2014;562 A58. doi:10.1051/004-6361/201322462.
- [127] Artemyev AV, Lutsenko VN, Petrukovich AA. Ion resonance acceleration by dipolarization fronts: analytic theory and spacecraft observation.. *Ann Geophys* 2012;30. 317324
- [128] Ukhorskiy AY, Sitnov MI, Merkin VG, Artemyev AV. Rapid acceleration of protons upstream of earthward propagating dipolarization fronts. *J. Geophys. Res.* 2013;118:4952–62. doi:10.1002/jgra.50452.
- [129] Artemyev AV, Kasahara S, Ukhorskiy AY, Fujimoto M. Acceleration of ions in the jupiter magnetotail: role of resonant interaction with dipolarization fronts.. *Planetary Space Science* 2013;82(83):134–48. doi:10.1016/j.pss.2013.04.013.
- [130] Artemyev AV, Vasiliev AA. Resonant ion acceleration by plasma jets: effects of jet breaking and the magnetic-field curvature. *Phys. Rev. E* 2015;91(5) 053104. doi:10.1103/PhysRevE.91.053104.
- [131] Artemyev AV, Neishtadt AI, Zelenyi LM, Vainchtein DL. Adiabatic description of capture into resonance and surfatron acceleration of charged particles by electromagnetic waves. *Chaos* 2010;20(4) 043128. doi:10.1063/1.3518360.
- [132] Zhou X, Angelopoulos V, Sergeev VA, Runov A. Accelerated ions ahead of earthward propagating dipolarization fronts. *J. Geophys. Res.* 2010;115 A00103. doi:10.1029/2010JA015481.
- [133] Mozer FS, Agapitov O, Krasnoselskikh V, Lejosne S, Reeves GD, Roth I. Direct observation of radiation-belt electron acceleration from electron-volt energies to megavolts by nonlinear whistlers. *Phys Rev Lett* 2014;113(3) 035001. doi:10.1103/PhysRevLett.113.035001.
- [134] Artemyev AV, Agapitov O, Mozer F, Krasnoselskikh V. Thermal electron acceleration by localized bursts of electric field in the radiation belts. *Geophys. Res. Lett.* 2014;41 57345739. doi:10.1002/2014GL061248.
- [135] Mozer FS, Agapitov O, Artemyev A, Drake JF, Krasnoselskikh V, Lejosne S, Vasko I. Time domain structures: what and where they are, what they do, and how they are made. *Geophys. Res. Lett.* 2015;42 36273638. doi:10.1002/2015GL063946.
- [136] Vasko IY, Agapitov OV, Mozer FS, Artemyev AV. Thermal electron acceleration by electric field spikes in the outer radiation belt: generation of field-aligned pitch angle distributions. *J. Geophys. Res.* 2015;120:8616–32. doi:10.1002/2015JA021644.
- [137] Vasiliev A, Neishtadt A, Artemyev A. Nonlinear dynamics of charged particles in an oblique electromagnetic wave. *Phys Lett A* 2011;375:3075–9. doi:10.1016/j.physleta.2011.06.055.
- [138] Neishtadt AI, Petrovichev BA, Chernikov AA. *Prntraint into unlimited acceleration*. *Soviet Journal of Plasma Physics* 1989;15:1021–3.
- [139] Chernikov AA, Schmidt G, Neishtadt AI. Unlimited particle acceleration by waves in a magnetic field. *Phys Rev Lett* 1992;68:1507–10. doi:10.1103/PhysRevLett.68.1507.
- [140] Itin AP. Trapping and scattering of a relativistic charged particle by resonance in a magnetic field and an electromagnetic wave. *Plasma Phys Rep* 2002;28:592–603. doi:10.1134/1.1494058.
- [141] Vainchtein DL, Rovinsky EV, Zelenyi LM, Neishtadt AI. Resonances and particle stochasticization in nonhomogeneous electromagnetic fields. *Journal of NonLinear Science* 2004;14:173–205. doi:10.1007/s00332-003-0576-7.
- [142] Bulanov SV, Sakharov AS. Acceleration of particles captured by a strong potential wave with a curved wave front in a magnetic field. *Soviet Journal of Experimental and Theoretical Physics Letters* 1986;44:543–6.

- [143] Bulanov SV, Krasnoselskikh V. Particle acceleration in expanding and moving shocks. *Magnetic Fields and Solar Processes*, vol 448. ESA Special Publication; 1999. 1047
- [144] Erokhin NS, Moiseev SS, Sagdeev RZ. Relativistic surfing in inhomogeneous plasma and the origin of energetic cosmic-rays. *Soviet Astronomy Letters* 1989;15(1).
- [145] Erokhin AN, Erokhin NS, Milant'ev VP. Trapping of high-energy electrons into regime of surfatron acceleration by electromagnetic waves in space plasma. *Plasma Phys Rep* 2012;38:396–406. doi:10.1134/S1063780X12040022.
- [146] Artemyev A, Krasnoselskikh V, Agapitov O, Mourenas D, Rolland G. Non-diffusive resonant acceleration of electrons in the radiation belts.. *Phys Plasmas* 2012;19 122901. doi:10.1063/1.4769726.
- [147] Osmane A, Hamza AM. Relativistic surfatron process for landau resonant electrons in radiation belts. *Nonlinear Process Geophys* 2014;21:115–25. doi:10.5194/npg-21-115-2014. ArXiv: 1402.1691
- [148] Artemyev AV, Vasiliev AA, Mourenas D, Agapitov O, Krasnoselskikh V. Nonlinear electron acceleration by oblique whistler waves: landau resonance vs. cyclotron resonance.. *Phys Plasmas* 2013;20 122901. doi:10.1063/1.4836595.
- [149] Vainchtein DL, Vasiliev AA, Neishtadt AI. Electron dynamics in a parabolic magnetic field in the presence of an electrostatic wave. *Plasma Phys Rep* 2009;35:1021–31. doi:10.1134/S1063780X09120046.
- [150] Neishtadt A, Vainchtein D, Vasiliev A. Dynamics of electrons in a parabolic magnetic field perturbed by an electromagnetic wave. *Plasma Phys Controlled Fusion* 2011;53(8) 085014. doi:10.1088/0741-3335/53/8/085014.
- [151] Artemyev A, Agapitov O, Mourenas D, Krasnoselskikh V, Shastun V, Mozer F. Oblique whistler-mode waves in the earth's inner magnetosphere: energy distribution, origins, and role in radiation belt dynamics. *Space Sci Rev* 2016;200:261–355. doi:10.1007/s11214-016-0252-5.
- [152] Omura Y, Furuya N, Summers D. Relativistic turning acceleration of resonant electrons by coherent whistler mode waves in a dipole magnetic field. *J. Geophys. Res.* 2007;112 6236. doi:10.1029/2006JA012243.
- [153] Summers D, Omura Y. Ultra-relativistic acceleration of electrons in planetary magnetospheres. *Geophys. Res. Lett.* 2007;34 24205. doi:10.1029/2007GL032226.
- [154] Artemyev AV, Vasiliev AA, Mourenas D, Neishtadt AI, Agapitov OV, Krasnoselskikh V. Probability of relativistic electron trapping by parallel and oblique whistler-mode waves in earth's radiation belts. *Phys. Plasmas* 2015;22(11) 112903. doi:10.1063/1.4935842.
- [155] Zaslavskii GM, Filonenko NN. *Stochastic instability of trapped particles and conditions of applicability of the quasi-linear approximation*. Soviet Journal of Experimental and Theoretical Physics 1968;27(851).
- [156] Zaslavsky A, Krafft C, Gorbunov L, Volokitin A. Wave-particle interaction at double resonance. *Phys. Rev. E* 2008;77(5) 056407. doi:10.1103/PhysRevE.77.056407.
- [157] Shklyar DR, Zimbardo G. Particle dynamics in the field of two waves in a magnetoplasma. *Plasma Phys Controlled Fusion* 2014;56(9) 095002. doi:10.1088/0741-3335/56/9/095002.
- [158] Artemyev A, Vainchtein D, Neishtadt A, Zelenyi L. Resonant acceleration of charged particles in the presence of random fluctuations. *Phys. Rev. E* 2011;84(4) 046213. doi:10.1103/PhysRevE.84.046213.
- [159] Artemyev AV, Mourenas D, Agapitov OV, Vainchtein DL, Mozer FS, Krasnoselskikh VV. Stability of relativistic electron trapping by strong whistler or electromagnetic ion cyclotron waves. *Phys. Plasmas* 2015;22 082901. doi:10.1063/1.4927774.
- [160] Albert JM. Gyroresonant interactions of radiation belt particles with a monochromatic electromagnetic wave. *J. Geophys. Res.* 2000;105 21191. doi:10.1029/2000JA000008.
- [161] Ukhorskiy AY, Sitnov MI. Dynamics of radiation belt particles. *Space Sci. Rev.* 2013;179:545–78. doi:10.1007/s11214-012-9938-5.
- [162] Landau LD, Lifshitz EM. *Mechanics. Course of Theoretical Physics*, vol. 1. Oxford: Pergamon; 1988.
- [163] Artemyev A, Vainchtein D, Neishtadt A, Zelenyi L. Stability of relativistic surfatron acceleration. *Phys. Rev. E* 2014;89(4) 043106. doi:10.1103/PhysRevE.89.043106.
- [164] Bernstein IB, Greene JM, Kruskal MD. Exact nonlinear plasma oscillations. *Physical Review* 1957;108:546–50. doi:10.1103/PhysRev.108.546.
- [165] Karpman V.I., Cap F.P. Non-linear waves in dispersive media. 1975.
- [166] Galeev AA, Sagdeev RZ. *Nonlinear plasma theory. Reviews of Plasma Physics*, vol 7; 1979. Vol. 7 of *Reviews of Plasma Physics*, p. 1
- [167] Matsumoto H, Kojima H, Miyatake T, Omura Y, Okada M, Nagano I, Tsutsui M. Electrotastic solitary waves (ESW) in the magnetotail: BEN wave forms observed by GEOTAIL. *Geophys. Res. Lett.* 1994;21:2915–18. doi:10.1029/94GL01284.
- [168] Ergun RE, Carlson CW, McFadden JP, Mozer FS, Delory GT, Peria W, Chaston CC, Temerin M, Roth I, Muschietti L, Elphic R, Strangeway R, Pfaff R, Cattell CA, Klumpp D, Shelley E, Peterson W, Moebius E, Kistler L. FAST Satellite observations of large-amplitude solitary structures. *Geophys. Res. Lett.* 1998;25:2041–4. doi:10.1029/98GL00636.
- [169] Cattell C, Wygant JR, Goetz K, Kersten K, Kellogg PJ, von Rosenvinge T, Bale SD, Roth I, Temerin M, Hudson MK, Mewaldt RA, Wiedenbeck M, Maksimovic M, Ergun R, Acuna M, Russell CT. Discovery of very large amplitude whistler-mode waves in earth's radiation belts. *Geophys. Res. Lett.* 2008;35 1105. doi:10.1029/2007GL032009.
- [170] Cully CM, Bonnell JW, Ergun RE. THEMIS Observations of long-lived regions of large-amplitude whistler waves in the inner magnetosphere. *Geophys. Res. Lett.* 2008;35(17). doi:10.1029/2008GL033643.
- [171] Balikhin MA, Shprits YY, Walker SN, Chen L, Cornilleau-Wehrlin N, Dandouras I, Santolik O, Carr C, Yearby KH, Weiss B. Observations of discrete harmonics emerging from equatorial noise. *Nat Commun* 2015;6(7703). doi:10.1038/ncomms8703.
- [172] Wilder FD, Ergun RE, Goodrich KA, Goldman MV, Newman DL, Malaspina DM, Jaynes AN, Schwartz SJ, Trattner KJ, Burch JL, Argall MR, Torbert RB, Lindqvist PA, Marklund G, Contel OL, Mirioni L, Khotyaintsev YV, Strangeway RJ, Russell CT, Pollock CJ, Giles BL, Plaschke F, Magnes W, Eriksson S, Stawarz JE, Sturmer AP, Holmes JC. Observations of whistler mode waves with nonlinear parallel electric fields near the dayside magnetic reconnection separatrix by the magnetospheric multiscale mission. *Geophys. Res. Lett.* 2016;43:5909–17. doi:10.1002/2016GL069473.
- [173] Mozer FS, Agapitov OA, Artemyev A, Burch JL, Ergun RE, Giles BL, Mourenas D, Torbert RB, Phan TD, Vasko I. Magnetospheric multiscale satellite observations of parallel electron acceleration in magnetic field reconnection by fermi reflection from time domain structures. *Phys Rev Lett* 2016;116(14) 145101. doi:10.1103/PhysRevLett.116.145101.
- [174] Thorne RM, Ni B, Tao X, Horne RB, Meredith NP. Scattering by chorus waves as the dominant cause of diffuse auroral precipitation. *Nature* 2010;467:943–6. doi:10.1038/nature09467.
- [175] Agapitov OV, Artemyev AV, Mourenas D, Mozer FS, Krasnoselskikh V. Nonlinear local parallel acceleration of electrons through landau trapping by oblique whistler mode waves in the outer radiation belt. *Geophys. Res. Lett.* 2015;42(10). doi:10.1002/2015GL066887.
- [176] Foster JC, Erickson PJ, Omura Y, Baker DN, Kletzing CA, Claudepiere SG. Van allen probes observations of prompt mev radiation belt electron acceleration in nonlinear interactions with vlf chorus. *Journal of Geophysical Research: Space Physics* 2017;122(1):324–39. doi:10.1002/2016JA023429.
- [177] Kampen N.G.V. *Stochastic processes in physics and chemistry*, 3rd edition, north holland. 2003.
- [178] Bortnik J, Thorne RM, Inan US. Nonlinear interaction of energetic electrons with large amplitude chorus. *Geophys. Res. Lett.* 2008;35(21102). doi:10.1029/2008GL035500.
- [179] Mozer FS, Artemyev A, Agapitov OV, Mourenas D, Vasko I. Near-relativistic electron acceleration by landau trapping in time domain structures. *Geophys. Res. Lett.* 2016;43:508–14. doi:10.1002/2015GL067316.
- [180] Omura Y, Miyashita Y, Yoshikawa M, Summers D, Hikishima M, Ebihara Y, Kubota Y. Formation process of relativistic electron flux through interaction with chorus emissions in the earth's inner magnetosphere. *J. Geophys. Res.* 2015;120:9545–62. doi:10.1002/2015JA021563.
- [181] Hsieh YK, Omura Y. Study of wave-particle interactions for whistler mode waves at oblique angles by utilizing the gyroaveraging method. *Radio Sci* 2017;52(10):1268–81 2017RS006245. doi:10.1002/2017RS006245.
- [182] Artemyev AV, Neishtadt AI, Vasiliev AA, Mourenas D. Probabilistic approach to nonlinear wave-particle resonant interaction. *Phys. Rev. E* 2017;95(2) 023204. doi:10.1103/PhysRevE.95.023204.

- [183] Artemyev A.V., Neishtadt A.I., Vasiliev A.A., Mourenas D. Kinetic equation for systems with resonant captures and scatterings. ArXiv e-prints [1710.04489](https://arxiv.org/abs/1710.04489).
- [184] Leoncini X., Vasiliev A., Artemyev A. Resonance controlled transport in phase space. *Physica D* <http://www.sciencedirect.com/science/article/pii/S0167278917302877>. doi:[10.1016/j.physd.2017.09.010](https://doi.org/10.1016/j.physd.2017.09.010).
- [185] Li J., Bortnik J., Xie L., Pu Z., Chen L., Ni B., Tao X., Thorne RM, Fu S., Yao Z., Guo R. Comparison of formulas for resonant interactions between energetic electrons and oblique whistler-mode waves. *Phys Plasmas* 2015;22(5) 052902. doi:[10.1063/1.4914852](https://doi.org/10.1063/1.4914852).